UNIVERSITY OF CALIFORNIA,
IRVINE

Integrative Approaches to Utilizing the Zebrafish Model for Cardiovascular Studies and Drug Screening

DISSERTATION

submitted in partial satisfaction of the requirements
for the degree of

DOCTOR OF PHILOSOPHY

in Biomedical Engineering

by

Jimmy Zhang

Dissertation Committee:
Professor Hung Cao, Chair
Professor James Brody
Professor Arash Kheradvar

2023

DEDICATION

This thesis is dedicated to my family for their continued support, love, and encouragement.

TABLE OF CONTENTS

LIST OF FIGURES

LIST OF TABLES

ACKNOWLEDGMENTS

First, I would like to extend my deepest gratitude to my advisor and mentor, Prof. Hung Cao, for his support and guidance in my development as a researcher. I also want to thank Prof. Cao for this experience to conduct research within his group and for the numerous words of encouragement he has provided throughout this arduous yet rewarding journey. I would like to give thanks to my collaborators, Prof. Xiaolei Xu and Prof. Juhyun Lee, for their guidance and support throughout my work. I would like to acknowledge and thank my committee members Prof. James Brody and Prof. Arash Kheradvar for their advice and support.

I would like to acknowledge the funding resources who have supported me through my research journey: the National Science Foundation (Grants 1936519 and 1917105) and the National Institutes of Health (Grants R44OD024874, HL081753, and HL107304). I would also like to thank Elsevier for permission to include chapter 4 of this dissertation, which is a reprint of the material as it appears in [6]. The co-authors listed in this publication are Tai Le, Anh Hung Nguyen, Ramses Seferino Trigo Torres, Khuong Vo, Nikil Dutt, Juhyun Lee, Yonghe Ding, Xiaolei Xu, Michael P.H. Lau, and Hung Cao.

This research endeavor would not have been possible without the support of the HERO Lab group. Special thanks to Dr. Anh Hung Nguyen, who has provided countless amounts of guidance, feedback, and support around the clock. I am also grateful to my fellow lab members not only for their advice and support but also their energy and enthusiasm, which have inspired me to strive for my best effort every day. I am especially grateful to my fellow lab member, Ramses Trigo Torres, for his unfaltering support and inspiring comments both in and out of lab. His contributions have been an integral part of my work, and the insightful conversations we had during our experiments have helped more grow as a researcher and as a person.

Lastly, I would be remiss in not thanking my family, especially my father John, my mother Vivian, and my sister Vicki for their valuable words of encouragement and relentless patience over the years, and to motivate me to push forward even during the tough times. It would have been impossible for me to complete my studies without their unwavering love and support.

VITA

Jimmy Zhang

EDUCATION

Doctor of Philosophy in Biomedical Engineering **2023**
University of California, Irvine *Irvine, CA*

Master of Engineering in Bioengineering **2018**
University of Maryland, College Park *College Park, MD*

Bachelor of Science in Bioengineering **2017**
University of Maryland, College Park *College Park, MD*

RESEARCH EXPERIENCE

Graduate Research Assistant **2018–2022**
University of California, Irvine *Irvine, California*

Graduate Research Assistant **2017–2018**
University of Maryland, College Park *College Park, Maryland*

TEACHING EXPERIENCE

Teaching Assistant (Quantitative Physiology) **2023–2023**
University of California, Irvine *Irvine, California*

REFEREED JOURNAL PUBLICATIONS

Intravascular sensors to assess unstable plaques and their compositions: a review **2019**
Progress in Biomedical Engineering

A novel wireless ECG system for prolonged monitoring of multiple zebrafish for heart disease and drug screening studies **2022**
Biosensors and Bioelectronics

Microelectrode array membranes to simultaneously assess cardiac and neurological signals of xenopus laevis under chemical exposures and environmental changes **2022**
Biosensors and Bioelectronics

Towards Multiplexed and Multimodal Biosensor Platforms in Real-Time Monitoring of Metabolic Disorders **2022**
Sensors

REFEREED CONFERENCE PUBLICATIONS

Continuous Electrocardiogram Monitoring in Zebrafish with Prolonged Mild Anesthesia **2020**
42nd Annual International Conference of the IEEE Engineering in Medicine & Biology Society

Methamphetamine Abuse: Investigating Zebrafish Cardiophysiology After Drug Treatment **2020**
2020 Biomedical Engineering Society Annual Meeting

A Novel Approach to Establishing a Hypoxic Zebrafish Model for Cardiovascular Applications **2022**
2022 Biomedical Engineering Society Annual Meeting

A Novel Wireless ECG System for Prolonged Monitoring of Multiple Zebrafish for Heart Disease and Drug Screening Studies **2022**
2022 Biomedical Engineering Society Annual Meeting

Cardiotoxic Effects of Acute Methamphetamine Exposure Associated with Electrophysiological and Cardiac Index in Larval Zebrafish **2022**
2022 Biomedical Engineering Society Annual Meeting

ABSTRACT OF THE DISSERTATION

Integrative Approaches to Utilizing the Zebrafish Model for Cardiovascular Studies and Drug Screening

By

Jimmy Zhang

Doctor of Philosophy in Biomedical Engineering

University of California, Irvine, 2023

Professor Hung Cao, Chair

Cardiovascular diseases remain the leading cause of death worldwide, necessitating research to tackle the multitude of pathologies within the cardiovascular system. The zebrafish model (*Danio rerio*) is an intriguing animal model for cardiovascular research because of its similar homology to humans, ample genomic knowledge with orthologous genes, ease of maintenance, and regenerative capability. Therefore, the zebrafish model is applicable for various cardiovascular pathologies, including drug response, electrophysiological analysis, genetic characterization, and strategies for future cardiac treatments. The work outlined in this dissertation presents several of these applications. An ECG (electrocardiogram) system suitable for elucidating drug response and genetic function was developed, and validation was performed to demonstrate the capability of the system, including dose-response experiments and phenotyping mutations pertinent to electrophysiology. An in-depth analysis of how methamphetamine may affect abnormal electrophysiological phenotypes was conducted, and an underlying genetic mechanism for causing such abnormalities was proposed. Finally, a system was developed to investigate how inducing hypoxia, the condition of low oxygen concentration, may modulate the hypoxia genetic pathway. This carries implication on elucidating the intrinsic regeneration process in zebrafish. Overall, the work presented in this dissertation provides contribution in promoting the zebrafish model in the multifactorial

facets of cardiovascular diseases and drug screening.

Chapter 1

Motivation

1.1 The Widespread Epidemic of Cardiovascular Diseases

Despite numerous efforts to understand and treat cardiovascular diseases (CVDs), they are still the leading cause of death in the US and worldwide. In the most recent report from the American Heart Association (AHA), cardiovascular diseases were responsible for almost 860,000 deaths in the US. Overall, CVDs accounted for approximately $351.2 billion in costs [7]. In the European Nation, CVDs were responsible for roughly 40% of all deaths [8]. While the efforts of treating CVDs were well documented in developed nations, statistics indicate that 80% of worldwide CVD related deaths were located in developing nations [9]. Studies have extensively outlined the risk factors associated with the etiology of CVDs. These include uncontrollable factors such as age, sex, and race, as well as controllable factors such as blood pressure, cholesterol levels, and smoking [10]. Indeed, preventative treatments have been devised to mitigate the controllable risk factors, which include dietary modifications, exercise implementation, surgical intervention, and medication to restore physiological blood

pressure and/or cholesterol levels [11].

However, current treatments are limited in their efficacy. While issues caused by social disparities and deficiencies in the prevention or modification of cardiovascular risk factors were mentioned, a major concern that is not readily addressed is the long-term prognosis of CVDs, such as the prevalence of recurring cardiovascular events [12, 13]. Generally, medications such as statins and beta-blockers are prescribed after palliative intervention to improve patient outcomes, but these procedures do not encompass the multifaceted nature of CVDs and might even create additional problems of their own [14, 15]. For example, research has determined that beta-blockers could induce side effects such as hypotension, bradycardia, and cardiogenic shock [16]. Therefore, more attention should be focused towards resolving cardiovascular issues from multiple perspectives.

For example, the fundamental definition of myocardial infarction is the ischemic myocardial damage that occurs due to obstruction of blood flow in one or multiple coronary blood vessels. However, this simple definition is an oversimplification of the multifactorial nature of its pathology. The American Heart Association has published extensive guidelines for diagnosing myocardial infarction, which includes formulating myocardial infarctions into multiple categories based on etiologies and outlining various symptoms including cardiac troponin detection for tissue injury, ischemic ECG changes (*i.e.,* ST segment deviations, pathological Q waves), and wall motion abnormality revealed by echocardiography [17]. Additionally, this universal definition has been updated multiple times, highlighting not only the progress of cardiovascular research but also the need for more clarification on the multifaceted nature of myocardial infarctions. Other cardiovascular diseases present similar issues, and these diseases tend to be interdependent, further stressing the need to analyze the multifactorial nature of cardiovascular diseases.

1.2 Contributions and Impact

This doctoral work sought to utilize the zebrafish model to investigate multiple cardiovascular pathologies. The zebrafish model possesses several advantages, including similar homology to humans, genetic orthologues present in humans and zebrafish, and the relative ease of maintenance. In order to leverage those advantages, various modalities were developed and experiments were completed to provide a further understanding into some specific applications as listed below:

- Fabrication of an ECG system to acquire signals from zebrafish for extended drug dose-response testing and genetic functional analysis of mutation in the gene *SCN5A* relevant to cardiac electrophysiology. See Chapter 4 and the journal paper []
- In-depth analysis into the effects of methamphetamine on cardiac electrophysiological dysfunction. See Chapter 5 and the journal paper [].
- Development of a system to induce physical hypoxia as an alternative to elucidating the mechanism of the underlying hypoxia pathway in the context of regeneration. See Chapter 6

1.3 Dissertation Outline

The overarching objective of the work outlined in this dissertation is to promote the use of the zebrafish model for a spectrum of cardiovascular research, which is multifactorial and complex in nature. The dissertation is divided into the following chapters. **Chapter 2** highlights the current literature regarding the use of animal models pertinent to cardiovascular research. The chapter also explains the advantages of using the zebrafish model in this field of research.

In **Chapter 3**, the concept of ECG (electrocardiogram) is reviewed and elaborated, as it constitutes a major portion of the work outlined in the dissertation. The chapter describes the invention of ECG, the underlying mechanisms and uses of the ECG for cardiovascular diagnosis. The chapter concludes with a discussion of ECG acquisition in the zebrafish model.

Chapter 4 presents the work completed on developing an ECG system for various zebrafish cardiovascular studies, including extended measurement for drug dose-response analysis and the characterization of the specific mutation *Tg(SCN5A-D1275N* pertinent in arrhythmic diseases.

To elaborate on the effect of drugs on cardiac electrophysiology, an in-depth study on the effects of methamphetamine is conducted, outlined in **Chapter 5**. Electrophysiological abnormalities are reported, and the underlying mechanisms to these abnormalities, such as the GPCR pathway, are investigated.

In **Chapter 6** a system for inducing hypoxia in zebrafish is developed. This is constructed as an alternative to current approaches in analyzing the related hypoxia signaling pathway, which has been shown to regulate physiological processes including the regeneration process. The physical hypoxia system modulates the time-dependent process of wound healing, which may have a profound effect on downstream regeneration.

Chapter 7 summarises the findings in the works outlined in this dissertation, including notable discoveries from each work. Future works are also presented.

Chapter 2

Animal Models in Cardiovascular Research

2.1 Introduction

This chapter will review animal models used in cardiovascular research. Specifically, common animal models will be reviewed, and an in-depth discussion on the zebrafish model will be provided. Advantages, disadvantages, and notable cardiovascular applications will be discussed.

2.2 Common Models for Research

The most common animal models utilized in cardiovascular research are mammalian models, including mice, rats, pigs, and other large animal models. These models are widely chosen as the preferred models because of their similar features in anatomy, physiology, and disease pathology, especially in regards to the cardiovascular system [18]. Furthermore, researchers

have developed various genetic engineering tools for small mammalian models, which were popularized in mutant studies [19]. Numerous research approaches involving these animal models utilized a combination of treatment procedures, such as drugs and mechanical injury, followed by genetic analysis. A common strategy was to produce mutant lines in order to analyze how a specific gene would influence the wound healing or regeneration process after physically inducing injury (*i.e.*,, LAD ligation) [20]. These studies elucidated which molecular pathways may be the most influential for treating cardiovascular diseases. Mammalian models are also prevalent in drug discovery and screening studies, as the aforementioned qualities also promote them as the most suitable substitutes for human drug testing [21]. However, it is important to note that mammalian models, even mice and rats, can be challenging to use due to their size, degree of maintenance, and relative lack of fecundity [22]. As a result, alternative animal models should be explored.

2.3 Why Zebrafish?

Zebrafish (*Danio rerio*) is a small freshwater fish originally found in South Asia with a myriad of qualities suitable for biological research. First utilized in the 1950s, the zebrafish model was mainly applied in toxicology-related studies associated with drugs or natural contaminants [23, 24, 25]. However, recent advances in genetics boosted the popularity of the zebrafish, as the sequencing of the zebrafish genome revealed remarkable similarities with human genome. Additional similarities such as morphology and physiology further promoted the animal model, and the intrinsic ability to regenerate certain organs such as the heart and brain provided intrigue for future applications, as illustrated in figure 2.1 These unique abilities allow zebrafish to become a valuable vertebrate model crucial to driving future cardiovascular research for the treatment of cardiovascular diseases. The importance of the zebrafish model was not widely recognized until 1981, when pioneering molecular biologist

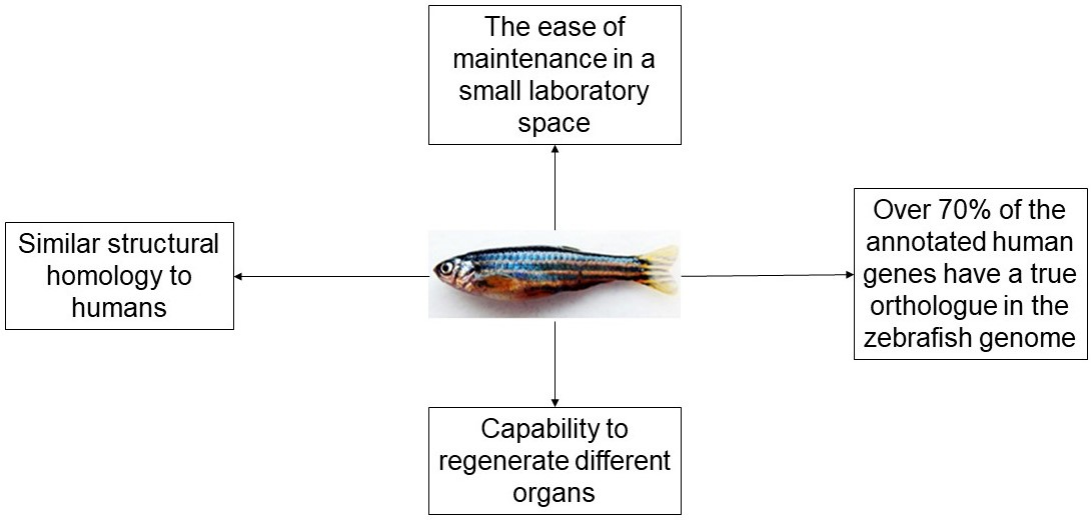

Figure 2.1: Notable features of the zebrafish model pertinent to cardiovascular, drug screening, and genetic studies. Adapted from [1] under the CC-BY license.

George Streisinger published his work on developing homozygous clones of zebrafish [26]. Initially fascinated by the rapid development of zebrafish embryos, Streisinger formulated the clones to analyze mutations relevant to neuronal development, the overarching goal of his research. In his manuscript, he cited several advantages of zebrafish embryos, including the rapid generation time of 3-4 months, the ability to producing many eggs at a time, the small size allowing for easy maintenance, and the transparent egg sac for easy observation into the morphological development of the embryos. After this initial documentation, several other researchers garnered interest, especially from those who had previously worked other developmental animal models such as fruit flies [27]. The breadth of knowledge surrounding zebrafish genetics has expanded since then. The zebrafish genome sequencing project commenced in 2001, and results have yielded that approximately 70% of the human genes in the reference genome have at least one associated zebrafish orthologue, suggesting that the zebrafish model is a comparable model for analyzing human-associated genetics and diseases [28]. Consequently, zebrafish research has increased dramatically, as over 1300 laboratories worldwide have utilized zebrafish in numerous studies, according to the ZFIN database in 2019 [27].

Trait	**Mammals**	**Zebrafish**	**Invertebrates (*i.e., Drosophila, C. elegans*)**
Morphological Homology (to Humans)	High	Medium	Low
Fecundity	Low	Medium	High
Size	Large (>5 cm)	Medium (∼3-5 cm)	Small (<1 cm)
Maintenance and Ethics	High	Medium	Low (No Regulatory Approval)
Experimental Duration/Lifespan	Long (>1.5 years)	Medium (∼1 year)	Short (<1 month)
Maturation Duration	Long (>2-3 months)	Long (∼3 months)	Short (<3 days)

Table 2.1: Comparison of traits between mammalian, zebrafish, and invertebrate models for cardiovascular/genetic research

Throughout the last few decades, zebrafish have proved to be one of the main animal models that can provide significant advantages surrounding cardiovascular research and disease causality [29, 30]. Zebrafish as a cardiovascular model for human cardiac pathologies has given us knowledge surrounding the architecture of the mechanisms of regeneration and development of the heart up to the molecular level [29]. The zebrafish serves as an adequate model to study the complexities of cardiovascular development and disease, as depicted in figure 2.2 [31]. The main benefits surrounding zebrafish as a cardiac model include their small size, rapid embryonic development, optical transparency of embryos, high genetic homology with humans, and the ability to have transgenic models [32]. They also provide many additional advantages over other mammalian models for elucidation of vertebrate development and organogenesis [33]. In direct comparison to the mouse model, zebrafish can regenerate their heart indefinitely if the injury does not exceed ¿25% for area of injury, as opposed to intrinsic mouse cardiac regeneration only lasting around 7 days after birth [34]. The ze-

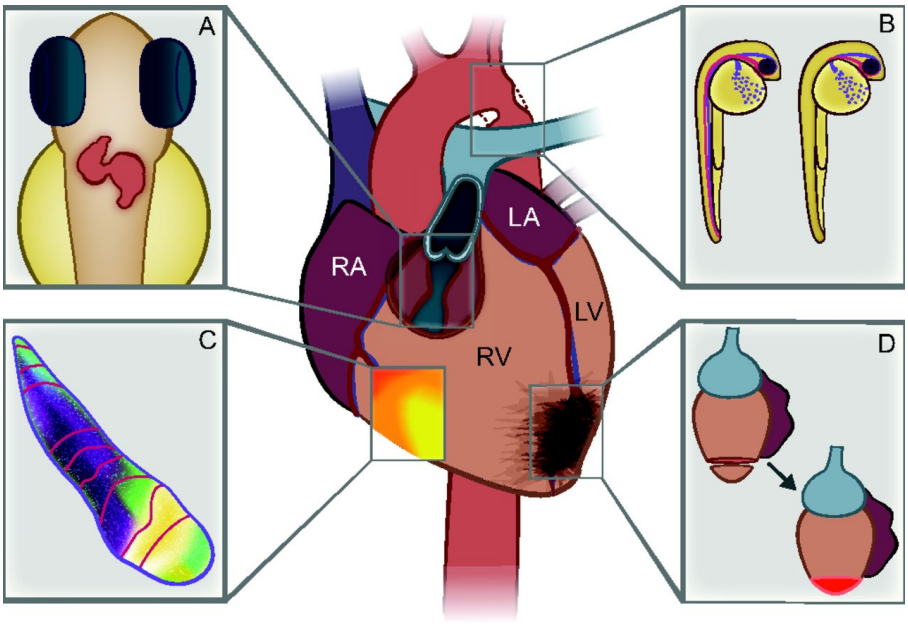

Figure 2.2: Zebrafish as a model for current cardiovascular studies. The human heart is illustrated in the center with chambers labelled RA=right atrium, LA=left atrium, RV=right ventricle, LV=left ventricle. Each section labelled A-D represents a specific application of the zebrafish model. (A) illustrates that despite having only 2 distinct chambers, zebrafish can be a model for cardiac development due to similiarities to that in humans. (B) illustrates that potential of zebrafish for mutational studies, important for congenital heart defects. (C) illustrates voltage mapping performed on zebrafish, which is integral for arrhythmic studies. (D) illustrates the capability of heart regeneration, which may be useful in uncovering treatments for certain cardiac diseases. Reproduced from [2] under the CC-BY license.

brafish model has proven to be one of most popular animal models for regenerative studies. Researchers first analyzed this remarkable ability of regeneration through fin amputation, which helped establish the current framework of understanding the regenerative capabilities in zebrafish. After injury, the injured site is covered by epidermal tissue, and a regenerative blastema, a heterogeneous collection of cells that compose the preliminary tissue for regeneration, is formed in the site to facilitate wound healing [35]. This process is analogous to the wound healing process found in humans and mammals [36]. With the advent of genetic engineering tools, studies were performed to analyze the genes that are most influential to the regenerative process. Those genes originated from embryonic morphogenic pathways, so the understanding was that this regenerative activity may be connected to processes com-

monly found during embryonic development [37]. In addition, these studies yielded results that cells were capable of dedifferentiating and redifferentiating into appropriate cell types most suitable for regeneration, seen in the study by Singh *et al.,* where fin osteoblasts would regenerate even when all resident osteoblasts were previously ablated [38]. These principles also apply for zebrafish heart regeneration. Research by Kikuchi *et al.,* determined that the zebrafish heart regenerated through the proliferation of cardiomyocytes expressing *gata4*, a gene crucial to embryonic heart development [39]. Additionally, the study by Jopling *et al.,* found that the cardiomyocytes dedifferentiated during the regeneration process, which was indicated by the disappearance of muscle fiber structure [40]. However, more research will need to be conducted to clarify the complex mechanism driving this process, including the specific regeneration pathways and the method of induction during wound healing and regeneration. Additionally, the zebrafish model is still relevant for drug testing and discov-

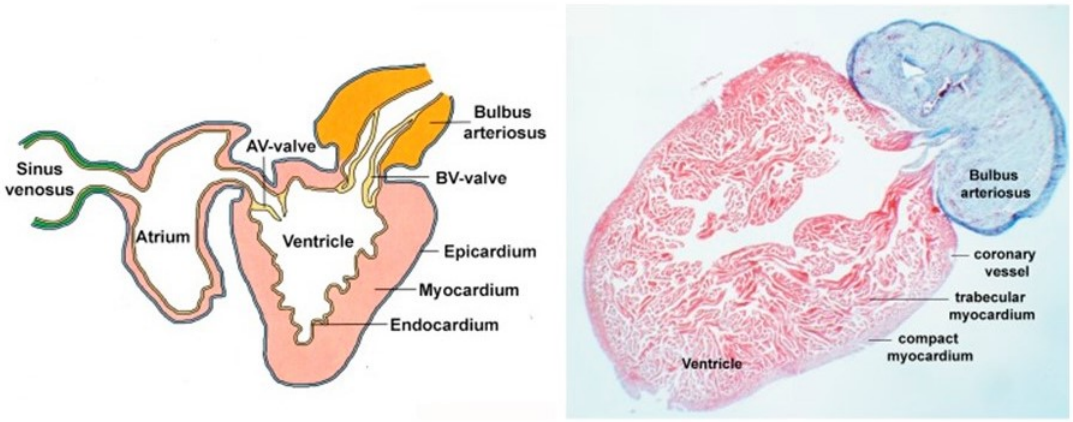

Figure 2.3: Illustration of the zebrafish heart. Left: The zebrafish heart consists of only one atrium and one ventricle. The sinus venosus, analogous to the vena cava in humans, is collects blood prior to the atrium. The bulbus arteriosus, analogous to the aorta in humans, receives blood pumped from the ventricle. Right: Trichrome-stained section of zebrafish cardiac tissue, where myocardial tissue is stained in red, and non-myocardial tissue is stained in blue. Notably, the compact myocardium is thin in zebrafish tissue, which may be vital in regeneration and conduction. Reproduced from [3] under the CC-BY license.

ery studies, stemming from their first use in research for toxicology studies. The zebrafish model serves as a middle ground for balancing ease of experimentation and translatability

for human drug discovery. Compared to conventional mammalian models such as mice and rats, zebrafish possess relatively high fecundity and low maintenance, attributes that are more conducive for high-throughput drug screening [41]. Compared to common invertebrate models such as *Drosophila* and *C. elegans*, zebrafish possess more similar morphology and physiology to those in humans. While researchers have called into question the validity of using animal models for human applications, studies have demonstrated that the zebrafish model displays similar qualities to those in humans. For example, receptors that serve as common drug targets such as the glucocorticoid receptor share remarkable structural homogeneity of up to 90% between zebrafish and human variants [42]. Once again, this can be attributed to the relative similarity between human and zebrafish genomes. Researchers have also tested if administering certain drugs to zebrafish produced similar effects. Milan *et al.,* conducted a drug screen to analyze whether the zebrafish would exhibit changes in heart rate [43]. The results documented that of the 23 drugs known to disrupt the repolarization of the heart in humans, 22 of them induced a similar effect in zebrafish, which displayed as signs of bradycardia. Similar morphology would be another attributing factor to the rise of the zebrafish model in drug discovery. Genetically engineering zebrafish lines have become relatively straightforward, and researchers have utilized this capability to determine zebrafish morphological features and their development. Works by de Pater *et al.,* and Lazic *et al.,* demonstrated that zebrafish heart development occurred in two separate phases analogous to the two heart fields found during human heart development [44, 45]. Additionally, orthologous genetic pathways govern the heart development of both species, signifying the potential applicability of the zebrafish model for assessing drug functionalities [2]. Thus, the zebrafish model remained one of the most popular animal models for drug screening, especially for cardiovascular studies.

2.4 Summary

In this chapter, the animal models utilized in cardiovascular research were discussed. The most common animal models utilized for cardiovascular research included mammalian models such as mice and rats primarily due to their similar homology to humans. However, maintenance and cost for these models are high, and the experimental duration tend to be long. With the advent of genetic technologies, invertebrates such as *Drosophila* and *C. elegans* are used to analyze specific genetic pathways due to their rapid development and high fecundity. Their drawback is the lack of homology to humans, rendering results to be difficult to translate for human practice. The zebrafish model offers an intriguing alternative as a suitable model, as it provides a compromise between the two aforementioned extremities. Additionally, zebrafish are capable of regenerating organs, specifically the heart, which enables them to be investigated for possible cardiovascular treatments. Therefore, zebrafish have grown increasingly popular in cardiovascular research today.

Chapter 3

History and Usage of the Electrocardiogram (ECG)

3.1 Introduction

Cardiac electrophysiology remains one of the most aspects to maintaining proper cardiac function. It is defined by the initiation and propagation of the electrical signals within the heart, ensuring proper contraction of the different chambers of the heart in order to maintain blood circulation. In humans, this cascade of signals is known to be orchestrated by the network of cardiac nodal cells found throughout the heart, as shown in figure 3.1. This mini neurological system found within the heart originates its signals from a set of pacemaker cells, named for their spontaneous initiation of the electrical signals [46]. From the pacemaker cells, the signal permeates the atria of the heart, allowing the atria to contract, pushing blood into the ventricles. Following atrial contraction, the signal travels through the atrioventricular (AV) node, which briefly delays the signal to ensure that all blood has left the atria and into the ventricles [47]. Once the signal passes through AV node, it travels along

the bundle branches in the ventricles, which then branches into individual Purkinje fibers to cover the entire ventricular wall. At this point, the ventricles contract to pump blood out of the heart into systemic or pulmonary circulation. As seen from this brief description of blood circulation throughout the heart, maintaining proper signal rhythm is crucial for normal cardiac function. Disruptions within this heart rhythm would easily hamper cardiac function and contribute to numerous cardiovascular diseases. This chapter will provide a brief overview into the development of the electrocardiogram (ECG), which is used to detect heart rhythm. This chapter will also provide a discussion into the various applications of ECG in cardiovascular diseases, as well as how ECG has been utilized in cardiovascular research, with a focus on the zebrafish model.

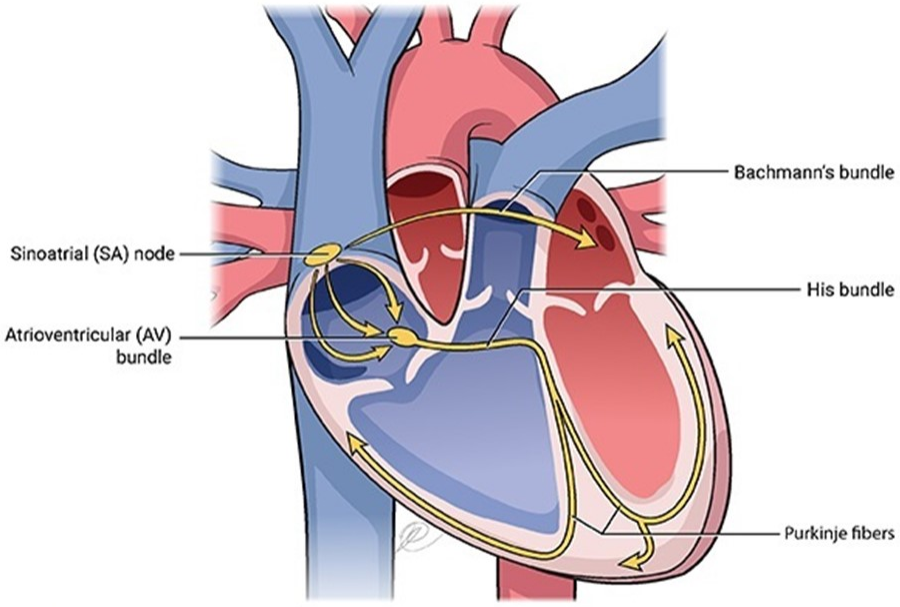

Figure 3.1: Illustration of human cardiac nodal system. The SA node, found within the right atrial wall, initiates the cardiac conduction. After spreading through the atria, the conduction signal passes through the AV node between the atrium and ventricle. The signal propagates through the His bundle and the Purkinje fibers throughout the ventricles. Source: US National Library of Medicine

3.2 Invention and Characteristics of ECG

The first detection of cardiac electrical signals came in 1842, when Dr. Matteucci first documented the occurrence of electrical currents accompanying each heartbeat [48]. Later works determined that these spikes in electrical activity occur before ventricular contraction and were triphasic in nature [49]. Those discoveries served as inspiration for Dr. Willem Einthoven, who coined the set of letters (PQRST) to define the various deflections in the electrical signal [50]. Additionally, Einthoven developed the first prototype of the electrocardiograph, utilizing only three electrodes instead of the conventional five-electrode setup used at that time. Einthoven optimized the setup by eliminating the electrodes deemed to provide the lowest output yield, and the final three-electrode setup consisted of placing electrodes in three limbs on the body: the right arm, the left arm, and the left leg. The placement of these electrodes became the bedrock of Einthoven's Triangle, a diagram used to describe the various leads in ECG today [51].

Einthoven's Triangle is illustrated as an imaginary triangle delineated by vertices at the limbs where the electrodes are placed [52]. The heart is located approximately in the center of the triangle, representing the source of electrical signals which the triangle is based around. Based on these assumptions, the edges of Einthoven's Triangle represent the three limb leads. Lead I is portrayed as going from right arm to left arm; lead II is portrayed as going from right arm to left leg; and lead III is portrayed as left arm to left leg. Each one of these leads captures the single averaged electrical dipole of the heart within the same direction depicted in the lead, and the resultant electrocardiogram displays the deflections seen in each of the three directions in an attempt to understand the multi-dimensional propagation of electrical activity. Later research added additional leads, such as the augmented leads and precordial leads, to provide additional electrical dipoles for analysis. Electrocardiograms capture the progression of cardiac cycles depicted through electrical activity. As defined by Einthoven, an instance of the ECG cycle is primarily denoted by the presence of the 5 deflections, or

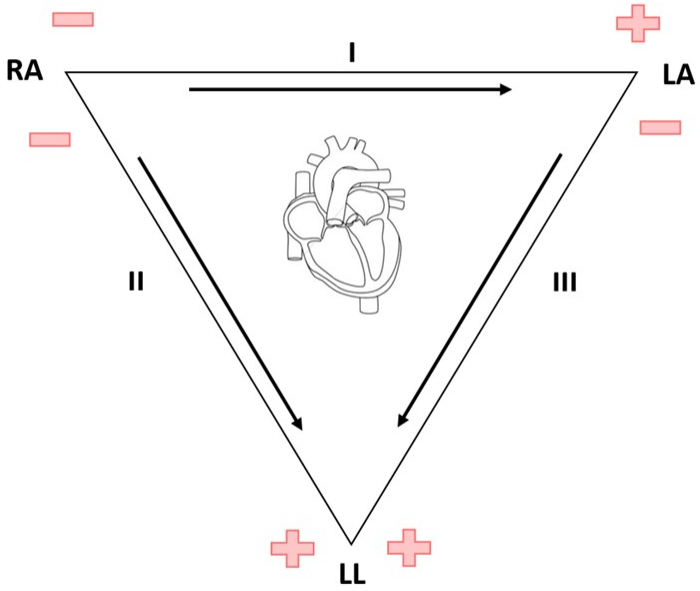

Figure 3.2: Representation of Einthoven's Triangle. The triangle is delineated by three electrodes positioned at right arm (RA), left arm (LA), and left leg (LL). The limb leads, designated by I, II, and III on the edges of the triangle, dictate the direction of the lead, and the resultant signals correspond to the conduction produced in the direction of the lead. Credit: The Student Physiologist

waveforms, labelled as PQRST [53]. Each of the waveforms represents a particular step of cardiac muscle contraction and signal propagation. The P wave is produced by the pacemaker cells and indicates the depolarization of the atria. (As the signal travels through a particular portion of cardiac tissue, the tissue experiences a sudden depolarization of the membrane. The cardiac tissue returns to the resting state after the general phase of repolarization.) The combination of the Q, R, and S waves, also termed as the QRS complex, is produced by the AV node and depicts ventricular depolarization. The T wave is defined as the period of ventricular repolarization. The heart returns to its resting state after the T wave and is prepared for the initiation of the next ECG cycle. As stated before, aberrations along this cycle represent the presence of a condition. Determining the location of the abnormality along the cycle as well as the leads where this abnormality exists may help determine the

cause and nature of the condition.

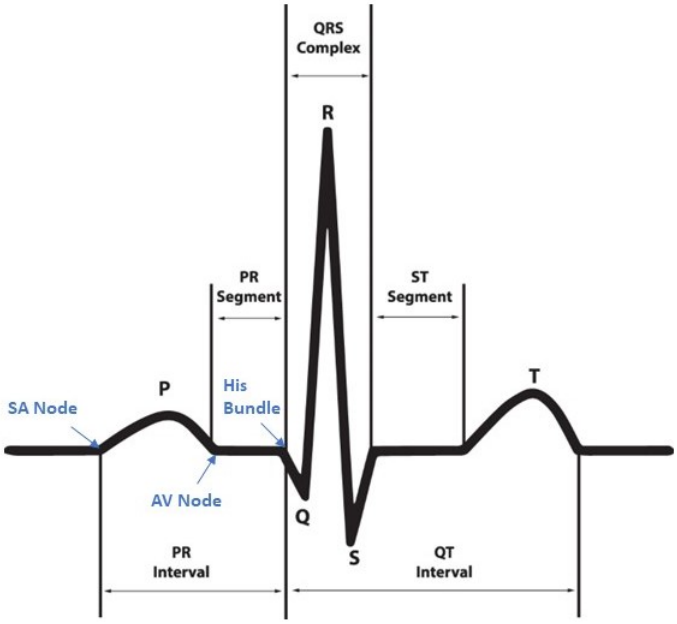

Figure 3.3: Representative ECG recording. The figure illustrates one full cycle of cardiac conduction from the depolarization phase in the SA node to repolarization. Each deflection, or wave, as shown on the figure is labelled by PQRST. Relevant intervals outlined by the waves are also depicted on the figure. Blue labels indicate where the conduction signal is located within the heart at the period defined in the ECG cycle. Adapted from [4] under the CC-BY license.

3.3 Applications of ECG

Since the first acquisition of the ECG, clinicians have quickly adopted the technology for cardiological assessments, realizing that cardiac electrophysiology play an integral role in the diagnoses of cardiovascular diseases. Arrhythmia, or the presence of cardiac rhythm abnormalities, has been characterized as a symptom of these diseases. Numerous ECG changes have been associated with common diseases, such as ST segment elevation and T wave alterations for coronary artery disease and myocardial infarction. The presence of a prolonged QT interval has been labelled as a sign of ventricular arrhythmias [54]. Indeed,

ECG still remains the gold standard for detecting aberrations in heart rhythm and a mainstay for cardiovascular diagnostics in general, despite the introduction of advanced tools such as echocardiography and magnetic resonance.

ECG may also be used as a diagnostic of drug cardiotoxicity. Numerous drugs have been determined to induce detrimental ECG changes. Overdosing of beta-blockers, anti-depressants, anti-psychotics, among others, may cause arrhythmic effects which can be precursors for more severe diseases [55]. The widespread use of opioids and other illicit drugs have also demonstrated their propensity to alter ECG characteristics, further highlighting their deleterious effects [56]. ECG remains an invaluable tool for not only determining known drug cardiotoxicities but also discovering new cardiotoxic effects from current and novel drugs.

3.4 Zebrafish ECG Analysis

As the zebrafish model became increasing popular in cardiovascular research, scientists began to study the underlying electrophysiology within the zebrafish heart. Despite being anatomically simpler than the human heart, the zebrafish heart still outputs an ECG that is remarkably similar to that in humans. Specifically, zebrafish ECG still retains the same PQRST waveforms seen in human ECG [57]. The zebrafish and human heart rate are similar compared to that in mice, the most popular animal model [58]. Analogously, the QT interval between zebrafish and humans is also comparable. Due to these similarities, the zebrafish model has been established as an intriguing model for drug studies, especially those with cardiovascular implications. Combined with the ability to develop specific mutant lines, the zebrafish model is ideal for drug screening, toxicology, and determining novel mechanisms of action [42]. For example, the use of glucocorticoids may reduce the symptoms of prolonged QT syndrome induced by mutations in the potassium ion channel [59].

Despite notable similarities between zebrafish and human ECG, researchers have determined significant differences that may impact the initial setup and interpretation of results. Zhao et al. documented that ECG leads for zebrafish have to be reversed in polarity compared to human ECG leads [60]. (For example, the zebrafish equivalent of lead II, referred to as reverse lead II, places the negative electrode close to the abdomen (equivalent to the left leg) and the positive electrode slightly anterior to the heart. This is opposite to human ECG electrode placement.) This suggests that the zebrafish have a different depolarization and repolarization gradient than humans. Thus, this difference has to be considered during electrode placement for zebrafish ECG acquisition.

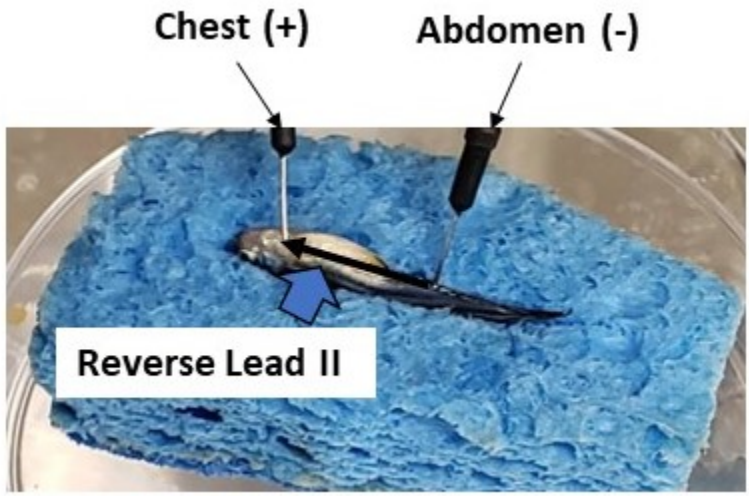

Figure 3.4: Positioning of the electrodes in zebrafish ECG recording. The positive electrode is placed on the chest above the heart, while the negative electrode is placed on the abdomen. The pair of electrodes generates reverse lead II, as depicted by the black arrow along the length of the fish. The orientation of this lead is opposite in direction to lead II found in human ECG. This orientation was implemented to generate upright waveforms similar to human ECG.

3.5 Summary

In this chapter, the acquisition and applications of ECG were discussed. Additionally, the incorporation of ECG in zebrafish studies has been explored. While ECG is widely used in clinical diagnostic settings today, it is not as commonly used in cardiovascular research, due to the difficulty of instituting the methodology. There has also been a general disconnect between organ-level cardiac electrophysiology and molecular-level mechanisms, which are more commonly studied in cardiovascular pathology. Thus, more effort should be placed on understanding how individual mechanisms may influence the systemic-level physiology via ECG.

Chapter 4

Development of Zebrafish ECG System for Extended Measurement of Drug Screening and Genetic Functional Analysis

4.1 Introduction

Due to the similarities between zebrafish and human ECG, several research groups have developed systems to assess zebrafish ECG for biomedical applications. Regarding sensor design, conventional needle electrodes are commonly used. Lin *et al.*, designed and tested the needle electrode with different materials, including tungsten filament, stainless steel, and silver wire to investigate the recorded data quality [61]. Stainless steel proved to be the optimal material for recording due to its high conductivity and durability, as tungsten and silver would easily deform upon application. These ECG systems were produced to

serve as a standard and portable design for research and teaching laboratories. The needle system was also deployed in other studies to conduct biological and/or drug-induced research [61, 62, 63, 64]. Although the system demonstrated promising results, the needles had to be gently inserted through the dermis of zebrafish in order to collect favorable signals. During implantation of the electrodes, the sharpness of the needles could cause injury to the fish's heart, thus possibly changing signal morphology [63]. Moreover, it requires an intensive effort to precisely position the electrode on the relatively small heart (approximately 1 mm in diameter) in order to achieve clear ECG acquisition.

Several alternative probe systems have been developed, including the micro-electrode array (MEA) and the 3D-printed sensors. Our lab and other research groups have demonstrated the use of MEAs for acquisition and provided data with a favorable signal-to-noise ratio (SNR) and high spatial and temporal resolution [65, 66, 67]. For instance, we presented a MEA array covering the fish's heart, which enabled site-specific ECG signals [65, 66]. Cho *et al.*,, developed a MEA printed on a flexible printed circuit board (FPCB) based on a polyimide film for multiple electroencephalogram (EEG) acquisition for epilepsy studies [68]. Although the MEA allowed multiple signal recordings, only one fish can be assessed at a time due to the limited number of electrode channels. To address this shortcoming, our group recently demonstrated a prolonged system for acquiring ECG from multiple fish simultaneously [69]. The MEA was replaced with two sputtered-Au electrodes embedded on a flexible polyimide film. However, noise generated from a pump used for water circulation reduced the SNR for ECG signals. The MEA was difficult to conform to zebrafish of varying sizes and curvatures. Furthermore, bulky and expensive acquisition tools were used to collect and transfer data through a cable to a computer. In the market, commercially available systems, such as the iWORX system, can provide improved system mobility with a compact amplifier. However, several challenges have not been resolved, such as i) the commercial systems only record for a short period of time (3–5 min), which may be inadequate for experiments that need longer recording such as dose-response experiments; ii) the ECG acquisition requires anesthetized

animals, which may be a confounding factor for electrophysiological signals; and iii) manual one-by-one measurement limits the capability of conducting studies necessitating a large number of fish. Additionally, no high throughput systems integrated with microelectronic systems have been utilized for characterizing mutant phenotypes. Therefore, developing high throughput systems capable of prolonged ECG acquisition may be vital for finding associations between arrhythmic phenotypes and mutant genotypes, identifying multiple arrhythmic phenotypes that are linked to a single mutant genotype, as well as elucidating cardiac drug efficacy using the zebrafish model.

In this chapter, the novel Zebra II system is introduced, which is capable of prolonged ECG acquisition from multiple fish simultaneously. The system was validated through numerous experiments, displaying its potential with 1) simultaneous ECG acquisition from 4 fish; 2) continuous ECG acquisition for up to 1 hr compared to several minutes (min) of currently available systems; 3) reduction in confounding effects from anesthesia with the use of up to 50% lower Tricaine concentration. Overall, the developed ECG system holds promise and solves current drawbacks in order to greatly accelerate arrhythmic phenotype analysis and drug screening applications in zebrafish.

4.2 Sick Sinus Syndrome and the *Tg(SCN5A-D1275N)* Mutant

Cardiovascular diseases (CVDs) come in various facets based on the specific origin of their pathology. One such CVD is the sick sinus syndrome (SSS), which is a form of an arrhythmic disease [70]. The sick sinus syndrome is characterized by age-associated dysfunction of the sinoatrial node (SAN), with varying symptoms such as syncope, heart palpitations, and insomnia [71]. The SSS has multiple manifestations on electrocardiogram (ECG) data,

including sinus bradycardia, sinus arrest (SA), and sinoatrial block. If left untreated, SSS could lead to more serious conditions such as atrial fibrilation and heart disease. The most optimal treatment for SSS is pacemaker implantation, but the procedure carries drawbacks such as internal bleeding, collapsed lung, and necessitation of future replacements [72]. The pathophysiology of SSS is not fully understood, but scientists have determined that it can be caused by numerous factors ranging from pharmacological medications and sleep disturbances to fibrosis and ion channel dysfunction [73]. Recent breakthroughs have emphasized SSS-associated genetic pathways as potential avenues to a more permanent treatment for SSS [74, 75]. Previous work has isolated $Na_v1.5$ as a potential factor in the manifestation of SSS, as the overexpression of the mutation *SCN5A-D1275N* in zebrafish has induced bradycardia and conduction abnormalities, symptoms of SSS. $Na_v1.5$ is a crucial ion channel in cardiac conduction as it is primarily responsible for the initiation and propagation of cardiac conduction. Defects of this ion channel has been linked to various arrhythmic diseases such as long QT syndrome, Brugada syndrome, and atrial fibrillation [76]. As many mutations of this ion channel have been characterized, it is vital to understand the resulting functional changes that is caused by each mutation. The work presented in this chapter will expand on the current knowledge of the mutation *Tg(SCN5A-D1275N)*, including the electrophysiological responses to differences in sodium ion concentrations.

4.3 Methodology

4.3.1 Zebrafish Husbandry

Both adult wild/mutant *Tg(SCN5A-D1275N)* zebrafish with the age of 13–20 months (body lengths approximately 3–3.5 cm) were used in this study. Zebrafish were kept in a circulating system that was continuously filtered and aerated to maintain the water quality required for

a healthy aquatic environment. The fish room was generally maintained between 26 and 28.5°C, pH 7.0 and the lighting conditions were regulated within a 14:10 h light:dark cycle. These parameters were checked at least once daily.

All animal protocols in this study were reviewed and approved by the Institutional Animal Care and Use Committee (IACUC) (protocol AUP-18-115 at University of California, Irvine). Prior to ECG measurement, fish were first anesthetized with tricaine via immersion for approximately 5 minutes or until no opercular movement has been observed. Under a stereo microscope, scales (above the coelomic cavity and the posterior site above the tail) were removed with forceps, exposing flesh, to allow more direct electrode contact. A small incision, approximately 2-3 mm, was made on the ventral surface of the fish above the heart. The incision cut through the chest wall, and the heart was visible afterward. The fish were recovered in fresh fish water for a few minutes. The incision was not closed via suture, staple, clips, or glue as the chest wall and scales have been observed to regrow within 4 weeks. All drug administration experiments, chemicals, reagents, and materials were performed in accordance with relevant guidelines and regulations.

4.3.2 Design and Validation of the Zebra II system

The Zebra II system was composed of a perfusion system, an in-house electronic system, apparatuses, and sensors (Figure 4.1). The perfusion system consisted of four sets of syringes, valves, and tubing. The four syringes contained Tricaine solution with low concentration, which were continuously fed to the fish through the tubing system. Tricaine (MS-222) was used as an anesthetic to reduce the fish's aggressiveness and activity while maintaining their consciousness. The four valves were used to adjust the solution's flow rate within a range of 5.5–6 ml/min, while housing apparatuses and sensors were improved from the previous work [69]. Specifically, multiple side-fitted housings were made of polydimethylsiloxane (PDMS),

a biocompatible polymer which provided comfort to the fish and minimized unwanted movements. The zebrafish ECG system was placed within a home-made incubator (Figure 4.1). Temperature within the chamber ranged from 20 °C to 32 °C, as measured by a thermometer and controlled by a thermostat with an accuracy range of ±1 °C. With the temperature-controlled incubator, a specific temperature was set by the thermostat control, and the light bulb was turned on so that the incubator's temperature can be maintained at the setup temperature and vice versa. Experiments were conducted to validate the performance of

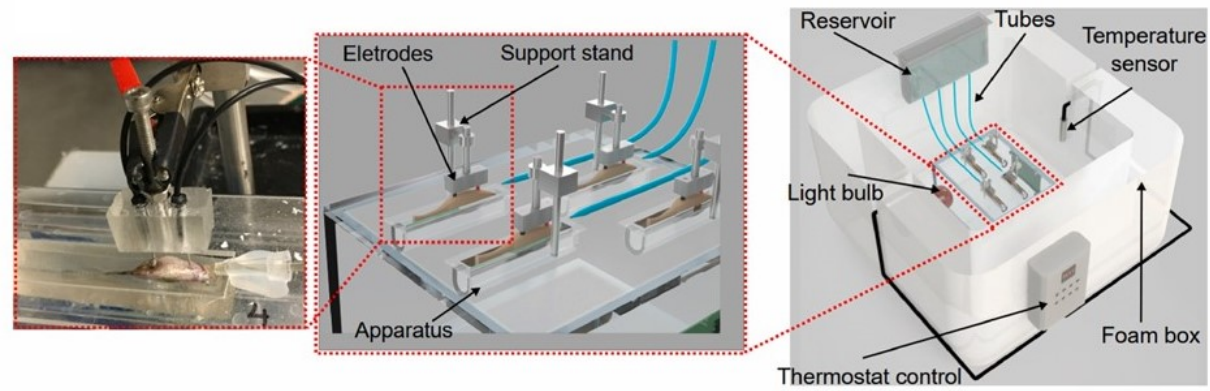

Figure 4.1: Design of the Zebra II system. Right: Setup of the whole system, including the perfusion system (reservoir, tubes) and temperature control system. Middle: View of the zebrafish beds made with PDMS and electrodes. Each bed provides attachment to tubes from the reservoir and a drain for the fluid from the tubes. Left: Image of sedated zebrafish placed on the bed with electrodes attached.

the developed system. The general workflow is displayed in figure 4.2. First, zebrafish ECG signals were acquired simultaneously using the Zebra II and the commercial system developed by iWORX to assess the data quality from fish under Amiodarone treatment. Then, the optimal Tricaine concentration and temperature were determined for ECG acquisition (n = 64). To demonstrate the benefit of prolonged ECG measurement, zebrafish (n=8) were subjected to increasing doses of Amiodarone (70-200 μM). Each dose lasted for 5 minutes, and the representative regimen is displayed in 4.12. To characterize the effect of high sodium intake and ion concentration on developing arrhythmic phenotypes in *Tg(SCN5A-D1275N)*, zebrafish were treated with varying concentrations of NaCl from 0.0‰ to 1.8 ‰ for 30 min.

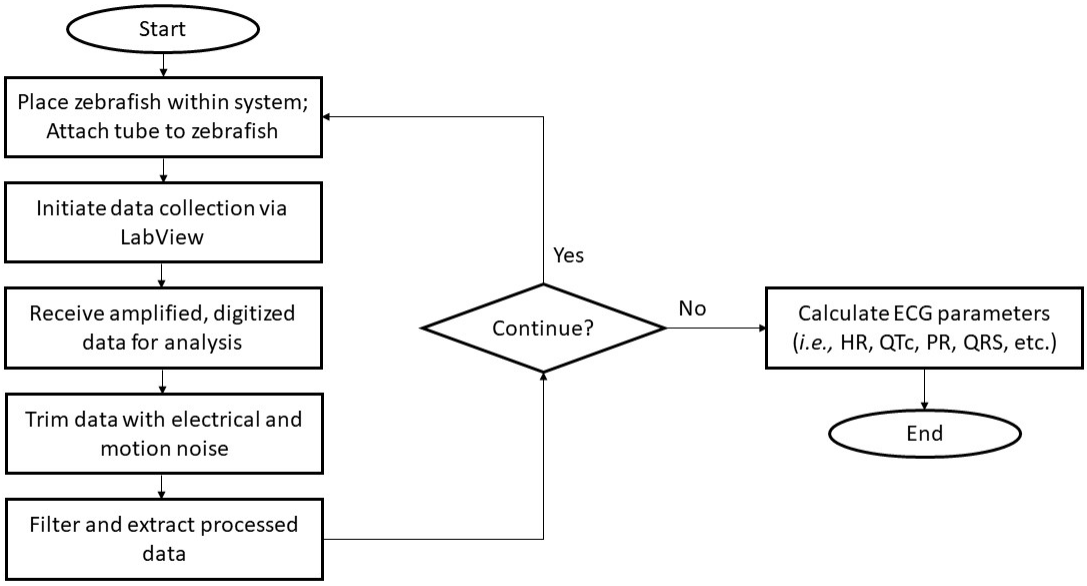

Figure 4.2: Flowchart of the acquisition and processing of ECG data.

The ECG was then measured to determine the presence of sinus arrest episodes.

To further characterize this mutant line for cardiac studies, we assessed the relationship between *SCN5A* and Meth [77]. Several groups have studied its connection of using addictive drugs with sudden death. For instance, Nagasawa *et al.* screened several variations in the long QT syndrome-associated genes *KCNQ1* and *KCNH2*, showing the increased risk of severe cardiac arrhythmia for addictive drug abusers [78]. However, previous literature lacked the functional characterization of *SCN5A*. Additionally, rescuing arrhythmic phenotypes induced by high sodium intake could provide insights into the nature of those arrhythmic phenotypes, as Meth has been previously demonstrated to increase HR after administration [79]. Specifically, we treated two groups of zebrafish (labelled as "control" – WT fish and "mutant" – *Tg(SCN5A-D1275N)*) in 0.9‰ NaCl for 30 min before immersing the fish in 50 μM Meth for 30 min. As shown in figure 4.12, the HR, SDNN, and QTc interval were compared between the two groups in the following three treatments: without drug treat-

ment, with NaCl treatment, and with NaCl + Meth treatment (n = 12 WT fish and n = 8 *Tg(SCN5A-D1275N fish)*).

4.3.3 Signal Processing and Statistics

The recorded ECG data were analyzed, and several parameters were extracted, including heart rate (HR), QT, and QTc intervals, based on previous work in our lab [80]. To assess the signal quality, the SNR was calculated as follows [80]:

$$\mathrm{SNR} = \frac{\sqrt{\frac{1}{\mathrm{b_{s2}}-\mathrm{b_{s2}}+1}\sum_{\mathrm{k=b_{s1}}}^{\mathrm{b_{s2}}}\frac{1}{\mathrm{t_{s2}}-\mathrm{t_{s1}}+1}\sum_{\mathrm{i=t_{s2}}}^{\mathrm{t_{s2}}}\mathrm{X_k^2(i)}}}{\sqrt{\frac{1}{\mathrm{b_{n2}}\text{-}\mathrm{b_{n2}}+1}\sum_{\mathrm{k=b_{n1}}}^{\mathrm{b_{n2}}}\frac{1}{\mathrm{t_{n2}}-\mathrm{t_{n1}}+1}\sum_{\mathrm{i=t_{n1}}}^{\mathrm{t_{n2}}}\mathrm{X_k^2(i)}}} \tag{2}$$

where b_{s2}, b_{s1}, t_{s2}, and t_{s1} are the final beat number, start beat number, final time, and initial time for the signal segment, respectively. b_{n2}, b_{n1}, t_{n2}, and t_{n1} are the final beat number, start beat number, final time, and initial time for the noise segment, respectively. X_k(i) represents the amplitude. The QRS complex represents the signal segment, and the T-P segment between ECG cycles represents the noise segment.

A highpass and lowpass filter with 15 Hz and 70 Hz cut-off frequencies were applied to the ECG signal to remove respiratory, motion, and electrical artifacts. To accentuate the R wave morphology, a db06 (Daubechies) wavelet was convolved with the filtered signal, chosen due to minimizing error while preserving the ECG waveform. To better detect the R waves, the difference between adjacent samples was derived, squared, and smoothed using a 15-point moving average filter. A peak-finding algorithm was applied to the residual signal to determine the locations of the R waves in the ECG, and corrections were applied for mapping inaccuracies. The P, Q, and S waves were detected by identifying the highest maxima and lowest minima preceding and following the R wave. Given the energy of the T wave was usually weak compared to the noise, the PQRST waveforms of the entire segment were averaged

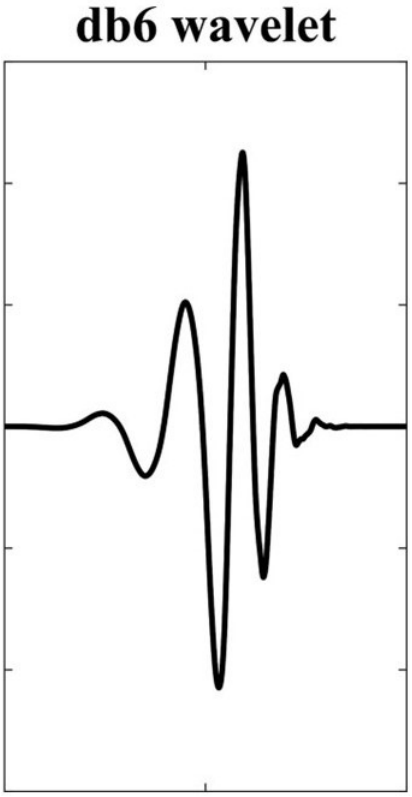

Figure 4.3: Depiction of the Daubechies 6 wavelet mother function. This function was used as a basis for detecting the ECG waveform due to their similar forms. Reproduced from [5] under the CC BY license.

in order to extrapolate the general morphology of the PQRST, which produces an identifiable T wave. These annotations were manually inspected and corrected after automatic detection. After annotating all of the waveforms in the signals, parameters including the heart rate (HR), heart rate variation, QRS interval, PR interval, and QTc interval were derived. The heart rate (in beats per minute) was calculated from the determined RR interval based on the following formula:

$$HR = 60/(1000(RR))$$

where RR is in ms.

The corrected QT interval (QTc), in ms, was determined as shown in previous literature

[81]:

$$QTc = QT/\sqrt{RR}$$

The standard deviation of normal sinus beats (SDNN), utilized as a form of heart rate variation, was calculated based on the short-term, beat-to-beat variance of HR in each 5 min segment of the data, and was determined by:

$$SDNN = \sqrt{(1/N-1)\Sigma_{i=1}^{N}(RR_i - \bar{RR})^2}$$

where N represents the number of beats. $\bar{RR}$ represents the average RR interval was determined for each 5 min segment.

The standard deviation of the average normal-to-normal (SDANN) intervals was calculated based on the variance of average HR from each 5 min segment. The equation for SDANN is the same as for SDNN, as noted above. However, N would represent the number of 5 min segments, RR is the average RR interval for each 5 min segment, and $\bar{RR}$ is the average RR interval for the whole 40 min segment. SDNN was used for short-term data analysis based on each 5 min segment, and SDANN was used for long-term data analysis for the whole 40 min segment [82].

Statistical analysis was performed as follows. Multiple comparisons were tested with one-way ANOVA, and significant results ($P<0.05$) were analyzed with pairwise comparisons using Student's t-test. Significant P-values are indicated with asterisks (*) with *$P<0.05$, **$P<0.01$ and ***$P<0.001$. Correlation analysis was performed using Pearson's correlation.

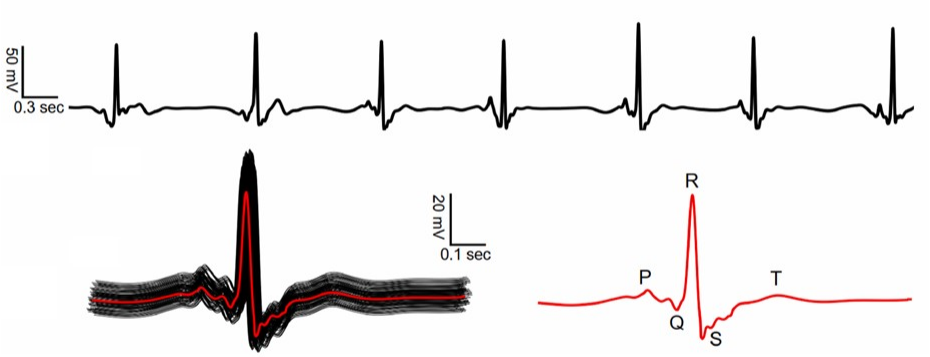

Figure 4.4: Representative ECG figures obtained from the system. The bottom figures show the superimposition of the ECG cycle obtained in a single recording. The averaged ECG cycle, labelled in red, display the PQRST waveforms. Superimposition is done to detect the T wave, which was the most difficult to detect.

4.4 Results and Discussion

4.4.1 ECG Acquisition with Zebra II

Representative ECG data collected from Zebra II are shown in 4.4. The data were pre-processed using the Wavelet technique to reduce various types of noise [80]. The bottom ECG signals in figure 4.4 depict the ECG segments superimposed during the measurement, with each line representing one cardiac cycle. The full set of ECG waves symbolized with the P-wave, QRS-complex, and T-wave was present in the mean of ECG segments as highlighted in red, showing waveform reproducibility and stability during the recording period. The Zebra II's performance was comparable to that of the commercial iWORX system, as shown in 4.5. An experiment comparing the iWORX and Zebra II was performed on 36 wildtype

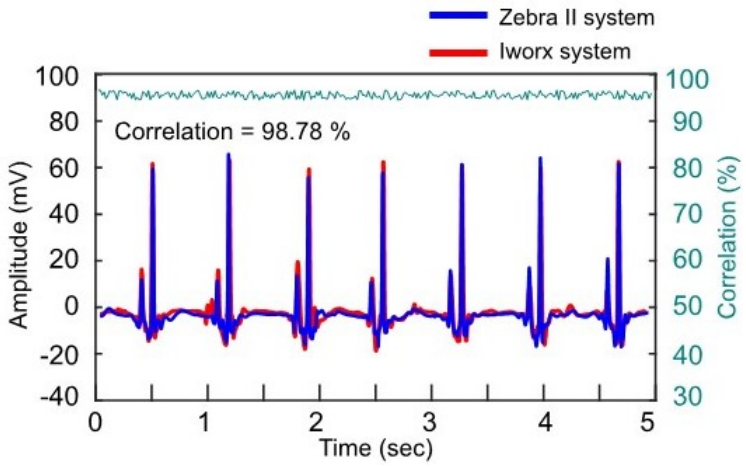

Figure 4.5: Comparison of ECG acquisition between the iWORX (red) and Zebra II (blue) systems. The ECG signals display a correlation of 98.78%, demonstrating similar performances between both systems.

(WT) zebrafish divided into the following 2 groups: 1) control (n = 20) and 2) Amiodarone treated (n = 16) fish. HR, QRS duration and QTc interval were analyzed. With the control group, no significant difference (P>0.05) between two systems in terms of QRS and QTc interval was observed. Similarly, the HR value and QTc value showed no significant difference in the treated group.

4.4.2 Effects of Tricaine and Temperature on Cardiac Electrophysiology

As shown in figure 4.7a, the ECG data from 8 fish per concentration group (75, 100, and 150 ppm) of Tricaine were obtained. At the low concentration of 75 ppm, the ECG data displayed prominent gill motion noise, manifested as low frequency, cyclic perturbations in the data. The noise interfered with the identification of ECG waves such as P waves, T waves and QRS complexes from fish treated with 75 ppm Tricaine, while the noise appeared to be more subdued in data obtained from fish treated with 100 ppm and 150 ppm. As a result, ECG data acquired from fish treated with 100 ppm and 150 ppm displayed clear ECG waves.

After the 40 min measurement, the recovery time and the survival rate after treatment were collected (Figure 4.7b). It was found that fish treated with higher Tricaine concentrations necessitated longer recovery times. Specifically, fish treated with 150 ppm Tricaine took an average of 7 min to recover compared to the 3 min and 4.2 min for fish treated with 75 and 100 ppm, respectively. Furthermore, the survival rate of fish treated with 150 ppm Tricaine was about 75%, while other concentrations yielded survival rates above 90%. It reflected the effect of extremely high Tricaine concentration similar to that used for euthanasia (*i.e.,* 168 ppm) [83]. Given the recovery time, the survival rate, and the acquired ECG data, the Tricaine concentration of 100 ppm was most optimal for ECG acquisition. Additionally, the HR variation was also assessed in each 5-min segment during the 40-min measurement, as shown in figure 4.6. No significant changes were observed between the 5–min to 10–min, 10-min to 15–min, 15-min to 20–min, and 20-min to 25–min segments for ECG data from fish treated with either 75 ppm or 100 ppm Tricaine. The only difference occurred in the last 10 min of the 40-min measurement when the HR displayed more variability with 75 ppm Tricaine (115.67 $\pm$ 25.29 BPM) than that with 100 ppm (115.93 $\pm$ 11.28 BPM). This suggests that a concentration of at least 100 ppm is most optimal for the stable measurements. After

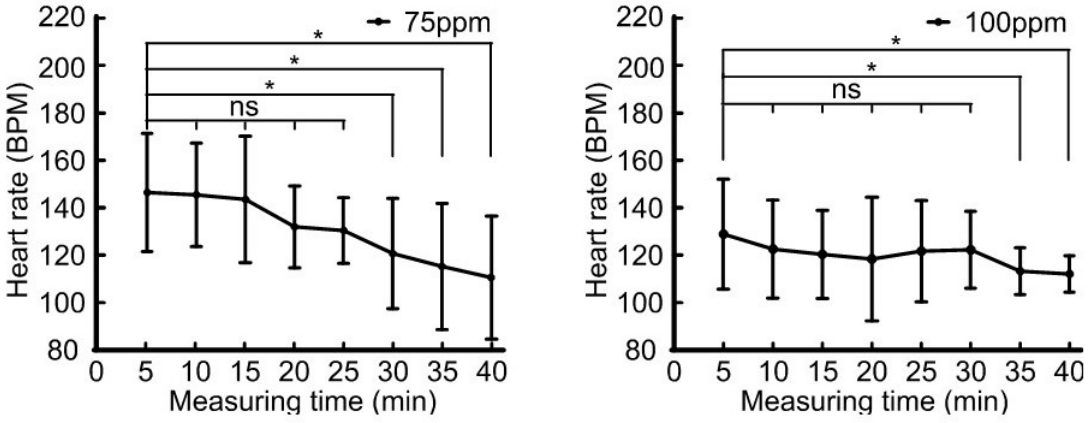

Figure 4.6: Determining heart rate variation over the course of prolonged measurement. The heart rate variation was assessed for each 5-min segment as shown in the figures. During the course of the experiment, the heart rate decreases for both Tricaine concentrations of 75 and 100 ppm, but the variation during the late stages (30-40-min measurement) remains higher for zebrafish treated at 75 ppm. *P<0.05.

determining the optimal Tricaine concentration, the effect of temperature on acquired ECG was investigated. As shown in figure4.8a, SDANN at 26 °C had the lowest value with the range of 36 ms (msec) to 75 msec, while the SDANN at 24 °C is highest with the range of 50 msec–139 msec. Moreover, the data distribution from HR collected every 5 min at 26 °C was the most condensed (Figure 4.8b). Thus, the HR obtained at 26 °C was the most stable compared to the values obtained at other temperatures. Tricaine (MS-222) and temperature have been shown to affect cardiac physiology of adult zebrafish and the HR of the treated subjects [61, 84]. Tricaine, a known sodium channel inhibitor and a euthanasia reagent, could affect the viability rate and recovery of zebrafish during prolonged sessions [85]. However, tricaine must be utilized for anesthetic purposes to improve SNR and reduce unexpected injury. In this study, we determined the optimal concentration of Tricaine to optimize signal quality while reducing mortality rates. Additionally, the temperature was also optimized to reduce confounding factors, as temperature has been shown to be a vital factor in cardiac physiology [86]. At low temperatures (18 - 20 °C), myocyte activity would be reduced as a natural adaptive mechanism to aid survival during colder climates or seasons, which leads to a reduction in HR. At higher temperatures, increased HR facilitates greater cardiac output to support a higher metabolic activity/demand for oxygen consistent with normal physiological function [87]. While zebrafish can adapt to a wide range of temperatures (6-38 °C), the effect of temperature on the stability of cardiac electrophysiology was poorly understood [86]. In this work, we determined the optimal temperature by analyzing the heart rate variability. Notably, 26 °C was within to the optimal temperature range for zebrafish (28 ± 2 °C) [88].

4.4.3 Response Analysis to Drug Treatment with the Zebra II System

One of the key novelties of the Zebra II system is the capacity to test drugs with different concentrations on an individual fish with a continuously prolonged assay. First, the effect

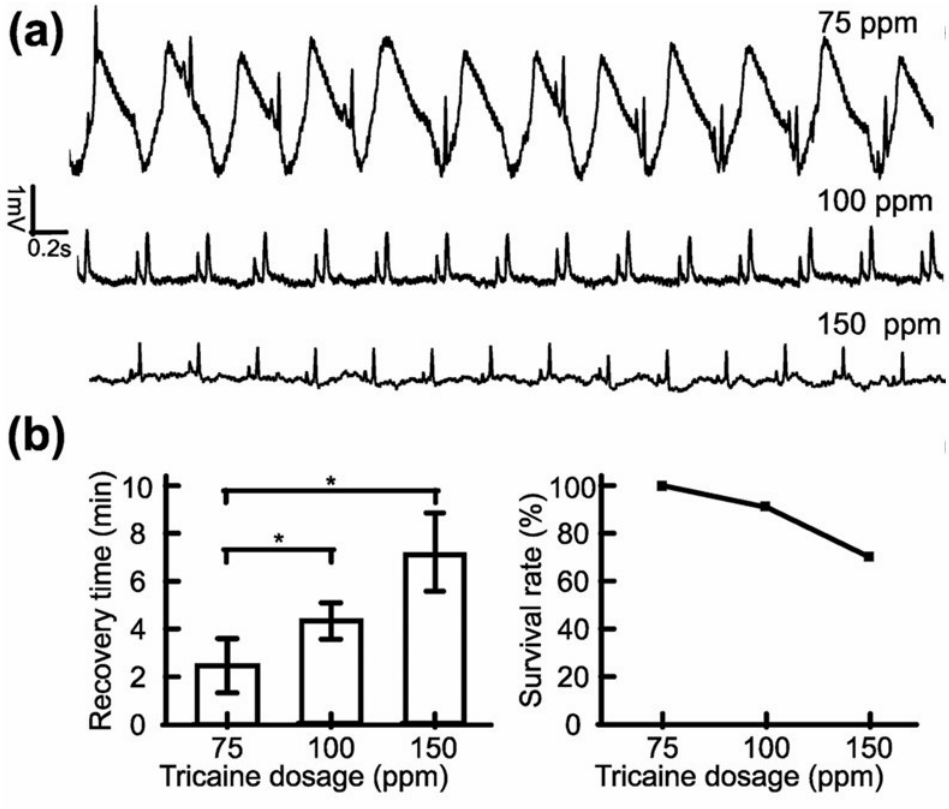

Figure 4.7: Optimization of Tricaine concentration. (a) depicts the representative ECG figures of zebrafish treated with varying concentrations of Tricaine. As shown, there is noticeable gill motion noise for zebrafish treated with 75 ppm Tricaine, depicted as the low-frequency, sinusoidal waveform overlaying the ECG signal. This is not found in zebrafish treated in 100 and 150 ppm Tricaine. (b) depicts the recovery time and survival rate of zebrafish treated at the same set of Tricaine concentrations. As expected, larger doses of Tricaine yielded longer recovery times and lower survival rates. Based on these results, a Tricaine concentration of 100 ppm was the most optimal concentration.

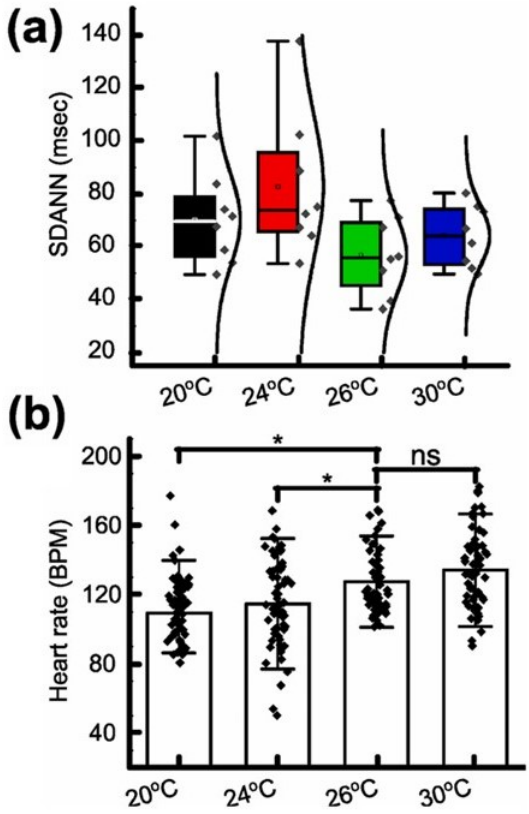

Figure 4.8: Optimization of temperature in zebrafish ECG recording. (a) depicts the SDANN, a measure of heart rate variability, for zebrafish treated at various temperatures. As indicated in the figure, measurement at 26 °C yielded the lowest variability. (b) depicts the heart rate of zebrafish measured at various temperatures. The heart rate progressively increased as the temperature increased. The results at 26 °C and 30 °C did not show significance, corroborating with the idea that those temperatures reside within the optimal temperature range. Significant differences were seen at 20 °C and 24 °C. *P<0.05

of Amiodarone with different concentrations on zebrafish ECG was analyzed. Three doses of Amiodarone were consecutively filled in the reservoir to feed to the fish during ECG acquisition, and each dose lasted around 5 min. As shown in Fig. 3a, the changes in response to different dosages in all four fish were apparent. Each dosage of Amiodarone was added to the system at timepoints specified from 1-4 on figure 4.9a. QTc interval displayed considerable changes during the course of the experiment. The baseline QTc interval was determined to be 310 msec. Noticeable increases in QTc interval were observed after Amiodarone treatment. Specifically, the interval was 330 msec at 70 μM of Amiodarone, 476

msec at 100 μM, and 536 msec at 200 μM. Figure 4.9b depicts the overall changes in terms of HR, QTc interval, and QRS interval in response to different Amiodarone concentrations. As Amiodarone concentration increased over the duration of the experiment, QTc interval and QRS interval increased, while the average HR decreased. This was the expected result from the treatment with Amiodarone. In drug response studies, conducting real time or pseudo-real time measurements with the same fish is most ideal due to biological variability among subjects. The perfusion system is equipped with multiple chambers for multiple drug doses in order to provide seamless transitions of multiple drug treatments, decreasing potential noise and perturbations. The developed system was able to demonstrate that a longer acquisition time enables the treatment of multiple drugs, as indicated by the successful demonstration of dose-response Amiodarone-associated ECG changes described earlier, as well as sodium-associated ECG changes described later in chapter 4.4.4. The utility of the perfusion system can also be expanded to include the testing of multiple drugs simultaneously to assess ECG changes due to drug-drug interactions, a developing field of study [89]. The chambers in the perfusion system can also contain multiple drugs for the precise modulation of zebrafish drug intake in order to accurately determine the effects of each tested drug as well as the onset of potential drug-drug interactions. While the subsequent ECG analysis of *Tg(SCN5A-D1275N)* indicates that Methamphetamine (Meth) did not improve SA frequency and HR, it demonstrated the assessment of effects of multiple drugs, as seen from the prolongation of the QTc interval after treatment of 50 μM of Meth in the mutant model (Figure 4.11). In both groups, the QTc interval was longer (by 350 msec for WT and 385 msec for *Tg(SCN5A-D1275N)*) after Meth treatment. This result was consistent with the effects of Meth [90]. Thus, the robust performance of the system allowed incorporation of multiple drugs with different effects (*i.e.,* antagonistic effects) in a single continuously prolonged assay to study the effect of drug-drug interactions on ECG changes, which was previously heavily performed on the short time course of other existing systems. Various ECG changes due to drug treatment were detected in prolonged ECG acquisition) to pro-

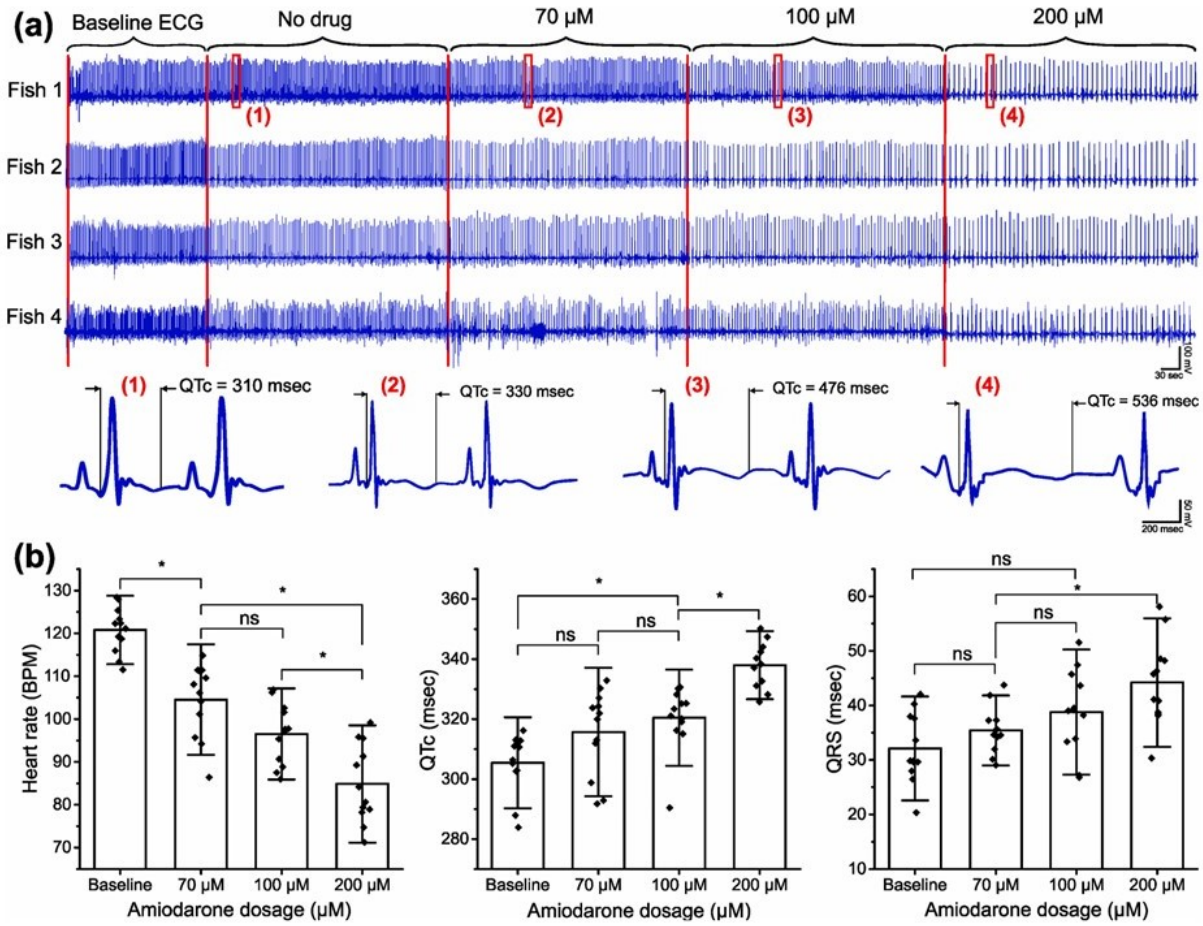

Figure 4.9: Effect of increasing Amiodarone dosage on ECG over time. (a) depicts the representative ECG signals obtained from 4 fish over the Amiodarone treatment regimen. Each section of the ECG signal has been labelled with the corresponding treatment for the specific period in time. Each treatment was applied at the start of each section shown by the red lines. Specific snapshots of the ECG signals are taken, and the QTc intervals were determined at the specified timepoints 1-4, displaying that QTc interval increased as Amiodarone concentration increased. (b) depicts the change in heart rate, QTc interval, and QRS due to Amiodarone treatment. As Amiodarone concentration increased, the heart rate decreased, and the QTc and QRS intervals decreased.

vide intuitive insights into drug-drug interaction effects, demonstrating the potential of the developed system to evaluate drug efficacy.

4.4.4 Effect of High Sodium Intake on the Development of Arrhythmic Symptoms in *Tg(SCN5A-D1275N)*

No previous research studies investigated the role of high sodium intake on the development of arrhythmic symptoms for zebrafish with increased susceptibility to arrhythmia due to genetic causes. Here, the developed system demonstrated the role of excess sodium ions in inducing ECG changes in the *Tg(SCN5A-D1275N)* mutant, successfully characterizing the onset of arrhythmic phenotypes such as sinus arrest (SA). Figure 4.10a represents the ECG data obtained from *Tg(SCN5A-D1275N)* fish with different NaCl concentrations. Mutant zebrafish displayed a reduction in HR when treated with a low NaCl concentration of 0.1‰. More significant reductions were detected when the fish were treated with higher concentrations. According to the SA criteria (*i.e.,* RR interval is greater than 1.5 s) determined in our previous work, SA appeared more frequently after treatment with 0.6‰ NaCl and above (Figure 4.11) [91]. The result confirmed a strong association between high sodium intake and arrhythmic phenotypes, previously reported in hypertensive populations [92]. As shown in figure 4.10b, mutant fish exhibited a significant decrease in HR after treatment of 0.6‰ NaCl. In contrast, NaCl treatment did not show a profound effect to the WT fish, as evidenced by the smaller decrease in HR after NaCl treatment. It was worth noting that these WT fish were at 1.5 years old, which could attribute to an increase of SA, and the slight reduction of HR in the experiment [91]. In terms of HRV, *Tg(SCN5A-D1275N)* fish showed a remarkable increase at high NaCl concentrations (0.9‰ and 1.8‰) compared with other concentrations. These results provided evidence that the *Tg(SCN5A-D1275N)* triggered more SA under NaCl treatment (Figure 4.11). Moreover, the SDNN and QTc interval in response to NaCl treatment were also measured, exhibiting similar trends for both WT

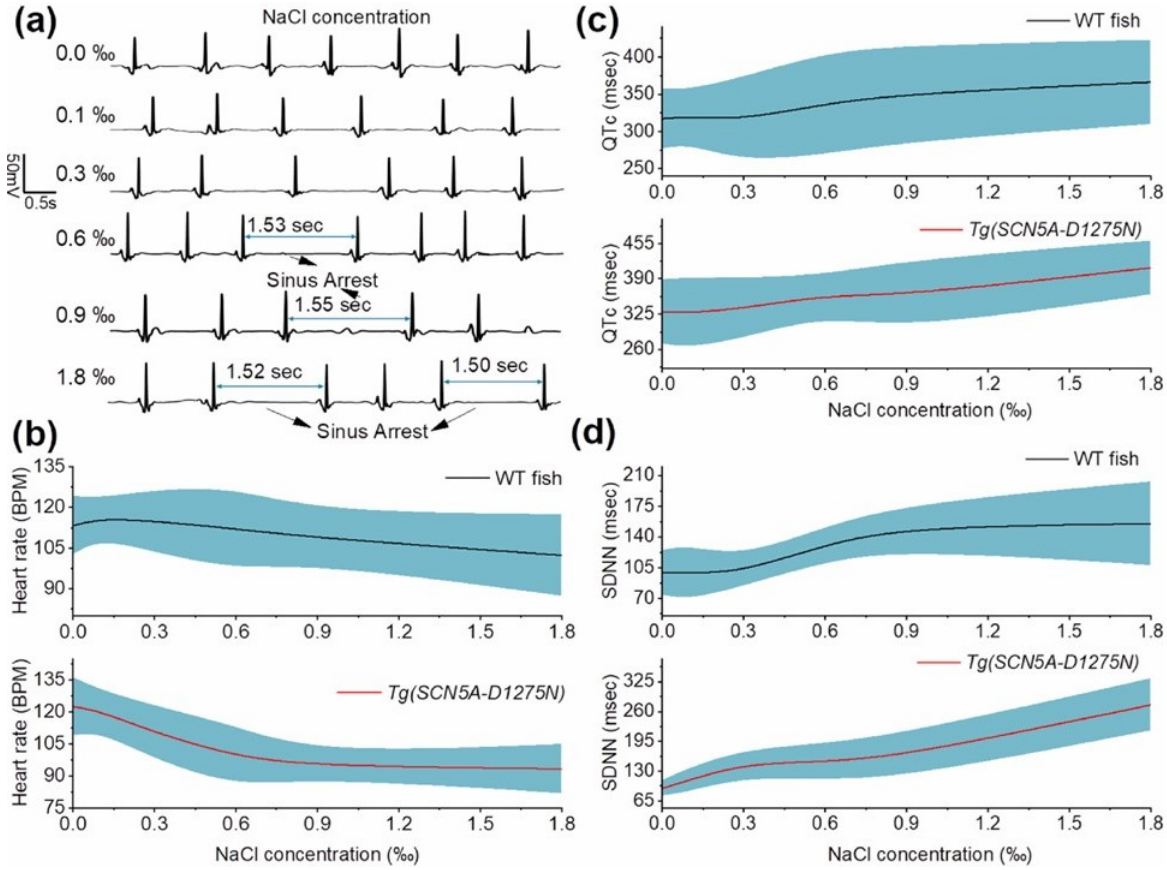

Figure 4.10: Effect of high sodium intake on *Tg(SCN5A-D1275N)* fish. (a) depicts the representative ECG figures for *Tg(SCN5A-D1275N)* fish treated at various concentrations of NaCl. Sinus arrest, defined as instances where the RR interval is greater than or equal to 1.5 sec., is present at higher NaCl concentrations, starting from 0.6‰. (b) depicts the comparisons of heart rate between wild-type and mutant fish as NaCl concentration increases, displaying a greater decrease in heart rate for mutant fish. (c) QTc displayed a substantially greater increase for mutant fish. (d) SDNN also displayed a higher increase in mutant fish, most likely indicating the presence of sinus arrests.

Fish	WT				Tg(*SCN5A-D1275N*)			
Drug	Average HR (BPM)	Percentage of fish with SA (No. of cycles)	SA frequency (epm)	QTc (msec)	Average HR (BPM)	Percentage of fish with SA (No. of cycles)	SA frequency (epm)	QTc (msec)
0 ‰ NaCl	113.3 ± 10.8	8.3(1)	0.08	317.2 ± 40.7	122.6 ± 13.7	12.5 (1)	0.125	329.8 ±59.1
0.1‰ NaCl	115.9 ± 7.5	8.3(1)	0.08	319.7 ± 36.3	120.4 ± 9.9	12.5(1)	0.125	327.2 ±64.8
0.3‰ NaCl	114.9 ± 11.5	8.3(1)	0.08	316.1 ± 56.6	110.3 ± 12.6	37.5(7)	0.875	335.7 ±55.8
0.6‰ NaCl	112.1 ± 15.2	16.6(2)	0.16	337.2 ± 68.2	98.9 ± 14.4	75(8)	1	359.9 ±37.1
0.9‰ NaCl	108.7 ± 9.5	25(3)	0.25	350.7 ± 64.7	94.6 ± 5.7	75(15)	1.875	360.1 ± 64.0
1.8‰ NaCl	102.4 ± 15.0	50(7)	0.42	366.1 ± 56.4	93.3 ± 11.5	87.5(17)	2.125	410.5 ±49.5
0.9‰ NaCl + 50 µM Meth	109.4 ± 12.3	25(3)	0.25	360.2 ± 70.3	96.95 ± 21.2	75(15)	1.875	391.3 ± 76.1*

Figure 4.11: Table of HR and SA frequency of wild-type and mutant fish in high sodium intake and Meth experiment

and mutant fish. (Figure 4.10c). As shown in figure 4.10d, the average SDNN was 125 msec for WT fish but was 255 msec for *Tg(SCN5A-D1275N)*, consistent with reduced conduction velocities due to sodium ion channel dysfunction [93].

High sodium intake is associated with alterations in various proteins responsible for transmembrane ion homeostasis and myocardial contractility. Recent studies provided important evidence that high sodium intake promotes structural and functional impairment of the heart, especially in populations bearing mutant phenotypes of the major cardiac sodium channels such as $Na_v1.5$ and its corresponding gene *SCN5A*. However, there was a current lack of a functional prolonged ECG acquisition system to characterize arrhythmic phenotypes from $Na_v1.5$ sodium channel mutants, including the functional response of $Na_v1.5$ to initiate action potentials based on high sodium intake. SA induced by high sodium intake was observed in this study and may be associated with a rise in intracellular sodium concentration within cardiomyocytes due to the gain-of-function of *Tg(SCN5A-D1275N)* for sodium ions traveling into the cardiomyocyte. Detection of SA by the developed system im-

plied that the *Tg(SCN5A-D1275N)* fish is susceptible to arrhythmic phenotypes after high sodium intake due to hastening epicardial repolarization and causing idiopathic ventricular conduction. These pathological changes were manifested as ECG changes and ventricular arrhythmias. ECG data acquired by the developed system were consistent with clinical reports, indicating that Brugada syndrome in human and animals resulted in ventricular conduction abnormalities due to high sodium intake [94, 95]. High sodium intake can cause destabilized closed-state inactivation gating of $Na_v1.5$ that may attenuate the ventricular conduction delay as shown in the ECG data (Figure 4.11).

Notably, the results indicated that high sodium intake induced more drastic ECG changes in *Tg(SCN5A-D1275N)* fish. NaCl treatments at 0.6‰, 0.9‰, and 1.8‰ resulted in SA with durations of 1.53 s, 1.55 s and 1.52 s, respectively. Additionally, slower HR and prolonged QTc intervals were observed only in mutant fish. These results provided a significant association between the increased frequency of SA, slower HR, and prolonged QTc with increased sodium intake in mutants. According to previous reports, $Na_v1.5$ can disrupt the heart's electrical activity and lead to a dramatic decrease of HR [96, 97]. The slow-conducting *Tg(SCN5A-D1275N)* mutant has been demonstrated previously by voltage-clamp measurement, which corroborated with the results in this study [98, 99]. The average QTc intervals were as high as 385 msec, indicating that the QTc intervals in mutant fish were generally more prolonged than wild type animals. Overall, high sodium intake led to various arrhythmic phenotypes, including slow HR, prolonged QTc, and increased SA frequency in *Tg(SCN5A-D1275N)* fish (Figure 4.10).

4.4.5 Use of Meth to Rescue Arrhythmic Phenotypes in *Tg(SCN5A-D1275N)* Fish

The average HR of mutant fish after the NaCl + Meth treatment was slightly higher than that of mutant fish solely treated with NaCl (Figure 4.12); however, the difference was not significant ($P>0.05$). Similarly, the SDNN value did not show any significant difference between mutant fish treated with NaCl + Meth and those solely treated with NaCl (Figure 4.12). Meth was administered to the fish to determine if their cardiac systems could respond to the drug's mechanism of inducing ECG changes (*i.e.,* increased HR, QTc prolongation). However, the obtained data indicated that Meth treatment did not affect the HR and SDNN in both groups (Figure 4.11), implying that NaCl administration resulted in some irreversible arrhythmic phenotypes (*i.e.,* slow HR) that could not be easily rescued with other agents that increase HR. In contrast, a significant increase in QTc interval was detected in the mutant fish after Meth treatment (391.3 ± 76.1 msec vs. 360.1 ± 64.0 msec), indicating the additive effect of Meth to QTc interval prolongation (Figure 4.11). Considering that no significant increase in QTc interval was seen in WT fish, the data indicated the mutant fish were more susceptible to agents causing QTc prolongation. Therefore, these results suggested different susceptibilities for arrhythmic phenotypes in the mutant *Tg(SCN5A-D1275N)*. The ECG data obtained from this study provided new evidence that high sodium intake increased the susceptibility of *Tg(SCN5A-D1275N)* fish to arrhythmic phenotypes. Results from mutant fish indicated the pathological slowing of HR, prolonged QTc interval, and higher frequency of SA. Although the developed system cannot provide other cardiac indices, such as ejection fraction and cardiac output, the system's ability to detect arrhythmic phenotypes in real time is valuable for many applications such as drug screening and phenotype assessment.

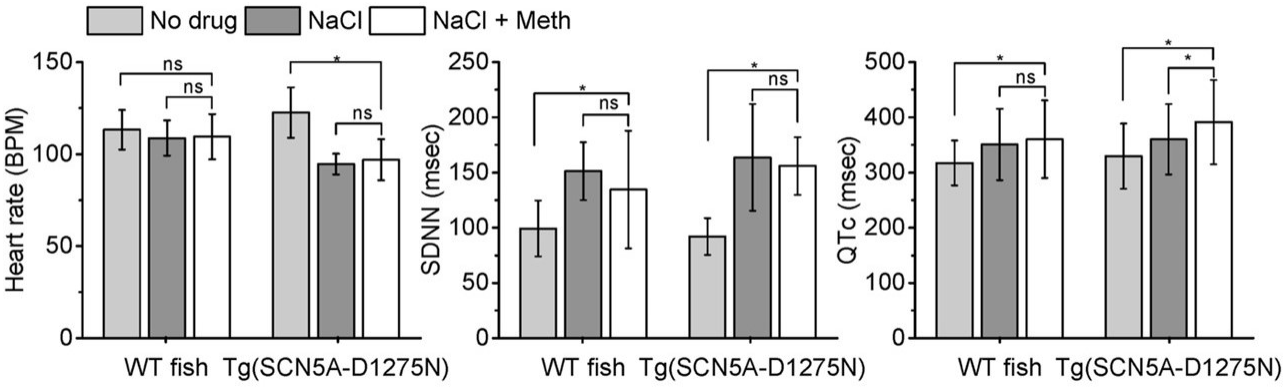

Figure 4.12: Additional treatment of Methamphetamine in wild-type and mutant fish after high sodium intake. In an attempt to rescue the symptoms present in the high sodium intake experiment, 50 μM of Meth was added after 0.9‰ NaCl. Results show that the Meth treatment did not induce a significant difference in heart rate and SDNN in fish treated with high amounts of sodium. Interestingly, QTc was significantly changed in mutant fish but not wild-type fish after Meth treatment, suggesting that mutant fish were more susceptible to the arrhythmic effects of agents.

4.5 Conclusion

The novelties of the developed Zebra II lie in the extended measurement for multi-step experiments (up to 1 hr), high throughput screening with multiple zebrafish, controlled setting, and reduced confounding effects. The system was successfully demonstrated to investigate the arrhythmic mutant line *Tg(SCN5A-D1275N)*, revealing the effect of high sodium intake on the development of sinus arrest (SA), slow HR, and prolonged QTc. In the future, the Zebra II can be used for a host of cardiac disease studies, including phenotypic screening for genetic engineering studies and new drug screening applications.

Chapter 5

Consecutive Treatments of Methamphetamine Promote the Development of Cardiac Pathological Symptoms in Zebrafish

5.1 Introduction

5.1.1 Methamphetamine and the Cardiovascular System

Methamphetamines are sympathomimetic amines with a range of adverse effects upon multiple organ systems. Based around a phenylethylamine core, methamphetamine (Meth) and its analog, d-amphetamine, have high affinity with transporters associated with catecholamine signaling, significantly increasing the number of neurotransmitters such as dopamine and norepinephrine [100]. Unlike Meth, d-amphetamine has been prescribed as medication to

treat neurological disorders such as attention deficit hyperactivity disorder (ADHD) and narcolepsy [101]. A possible reason for limited legal Meth use is the addition of the N-methyl group compared to amphetamine, which has been shown to confer better penetration through the blood-brain barrier for Meth, leading to stronger and more addictive responses [102]. Meth has been shown to induce heightened catecholamine response by promoting catecholamine release, preventing their reuptake, and destabilizing their levels [103, 104]. Thus, Meth is responsible for numerous neurotoxic symptoms, including potential neuronal apoptosis, decreased immune response, and associated memory deterioration [104, 105, 106, 107]. Given that the elucidation of the direct mechanism of Meth was on neurological response, the major focus in researching treatments for Meth-related abuse has been associated with neurological modulation. Therefore, less attention was given to researching the direct mechanism of Meth in other physiological systems, such as the cardiovascular system.

Cardiotoxicity is one of the most adverse consequences of Meth abuse, leading to a notable increase of morbidity and mortality [100]. Cardiovascular complications are the second leading cause of death in Meth abusers. Cardiotoxicity can appear early in the course of the drug use and cause numerous significant effects, such as pulmonary hypertension, atherosclerosis, cardiac arrhythmias, acute coronary syndrome, and other associated cardiomyopathies [108]. Furthermore, a Meth 'binge' study in rats to determine long-term effects discovered that Meth decreased the sensitivity of nervous and cardiovascular physiology through successive treatments, implying the potential remodeling of electrophysiological responses through chronic Meth abuse [109]. Previous human case studies have determined that Meth abusers experienced increased ventricular tachycardia and QTc prolongation [110, 111]. However, case studies are generally retrospective, and there is a scarcity in animal studies regarding the effect of Meth on the actual initiation of arrhythmic symptoms [100]. Moreover, data on the underlying mechanism of cardiac dysfunction during drug abuse and the susceptibility of long-term cardiotoxic development are limited.

Despite the prevailing issue of Meth abuse, studies have shown that cardiac pathology induced by Meth can be attenuated and even reversed through the discontinuation of Meth use and the initiation of subsequent treatment [112]. A study in rats regarding the administration of Meth and eventual withdrawal revealed that the rats were able to recover from myocardial pathologic symptoms such as atrophy, fibrosis, and edema starting from 3 weeks after discontinued Meth administration [113]. A human case study indicated that attenuation of Meth use and subsequent therapy led to recovery from ventricular hypertrophy and ECG ST deviations [114]. While evidence of recovery from Meth abuse is promising for the development of future treatments, it is essential to conduct research to understand the specific mechanisms underlying Meth-induced cardiovascular pathologies. Therefore, a better understanding of the cardiac dynamics of Meth abuse in zebrafish, a relevant model for human cardiac studies, may be vital for the future Meth-associated research.

5.1.2 Methamphetamine and G-Protein Coupled Receptors

In neurological studies associated with Meth, the drug-induced effect of G protein-coupled receptors (GPCRs) on subsequent neuropathology has been frequently investigated due to the receptors' association with neurotransmitters, hormones, and other neuromodulatory responses [115]. cAMP, a prominent secondary messenger within the GPCR signaling pathway, tends to be upregulated due to drug exposure, and it has been shown to influence sensitization and addiction to psychostimulant drugs [116]. However, given the ubiquity of GPCRs in numerous physiological systems, the effects of GPCRs on other symptoms of drug toxicity have also been explored. GPCRs have been demonstrated to be influential in the development of cardiovascular diseases. Studies have found that GPCRs induced increased Ca^{2+} release and myocardial contractility, leading to a higher susceptibility to hypertrophy and cardiomyopathy [117]. GPCRs have also demonstrated the ability to modulate remodeling processes within the biological system, including epithelial-mesenchymal transition (EMT)

and collagen deposition [118]. For example, TAAR1, a prominent GPCR targeted by Meth, was determined to be an integral player in the psychostimulant activity and addictive response of Meth [119]. However, TAAR1 has also been found outside of the neurological system, including the heart [120]. Therefore, cAMP and GPCRs may play a crucial role in the further elucidation of the effects of Meth on cardiac electrophysiology.

5.1.3 Rationale

In this chapter, we first demonstrate the potential of zebrafish ECG in the diagnosis of Meth-induced cardiotoxicity. We then sought to explain the results by conducting molecular analysis of the GPCR pathway within heart tissue, including the effect on fibrotic and Ca^{2+} dysregulation, which attribute to cardiac toxicity. With the implementation of our ECG system in Meth studies, we hope to provide a new insight into the mechanisms of Meth-induced cardiotoxicity, further uncovering the multifactorial nature of Meth and assisting in the development of novel treatment methods.

5.2 Methodology

5.2.1 Zebrafish Husbandry

Wild-type zebrafish were housed in a custom built circulating fish rack system as described in the previous chapter. Zebrafish (AB-wild type strain) were approximately 6-12 months old at the onset of the experiment. Prior to Meth treatment, zebrafish underwent open chest surgery to improve subsequent ECG signal acquisition as described in the previous chapter. The zebrafish groups were then housed in separate tanks throughout the duration of the study. All zebrafish were checked every day for the first week and then at least 3

days/week in the second week until the experiment was concluded. Observations were made to see whether the fish displayed some abnormal activities (*i.e.,* erratic swimming, strained breathing, bloating). The fish would be removed from the study if any abnormal activity was detected. In rare cases where extreme behavior/distress was seen, the fish would be euthanized. Euthanasia was conducted by immersing the fish in Tricaine (250 mg/L) for at least 30 min after the last observed opercular movement. All fish carcasses will be frozen post-euthanasia. All zebrafish procedures were conducted in accordance to IACUC guidelines (AUP-21-066 at University of California, Irvine).

5.2.2 Methamphetamine Preparation, Treatment, and ECG Recording

The Meth solution for treatment (200 μM) was prepared by mixing the specified amount of Meth stock into regular fish water obtained from the fish rack system. Solutions were prepared fresh for each day of treatment. The Meth stock (1 mg/mL) was obtained from Sigma-Aldrich (MDL MFCD00056130). The solution (10 mL) was then placed in a small custom polydimethylsiloxane (PDMS) chamber suitable for housing one zebrafish. PDMS is a flexible and biocompatible polymer most commonly used in biosensors and implants [121]. Untreated fish were placed in the same custom chamber with regular fish water. Each zebrafish was treated in the designated treatment for 20 minutes before ECG recording, as determined in a previous study [122]. This treatment was conducted 3 times a week over a period of two weeks, following similar studies. ECG recording was conducted as described in the previous chapter.

5.2.3 ECG Data Collection and Analysis

Before applying signal processing, the ECG signal was manually inspected and trimmed to remove segments with significant noise such as gill breathing and power line noise. The analysis of ECG signals was performed in a similar fashion as the procedure described in the previous chapter. The relevant parameters of heart rate (HR), QRS, PR, and QTc intervals were calculated accordingly. The HRV, in ms, was determined by the root mean square of successive differences between normal heartbeats (RMSSD), given by the formula:

$$HRV = \sqrt{\Sigma_{i=1}^{N-1}(RR_{i+1} - RR_i)^2/(N-1)}$$

where N represents the number of ECG cycles within each recording. RMSSD was utilized for this study because of the short duration in recording.

5.2.4 Isolation of Zebrafish Cardiomyocytes

Zebrafish cardiomyocytes were isolated according to the protocol presented by Sander *et al.* [123]. Briefly, zebrafish hearts (n=6) were first excised from anesthetized fish via incision with a pair of forceps. After incubating in heparin buffer immediately after excision, the hearts were placed in a digestion buffer (1x PBS, 10 mM HEPES, 30 mM taurine, 5.5 mM glucose, 10 mM BDM (butanedione monoxime, a contraction inhibitor), 12.5 μM $CaCl_2$, 5 mg/mL collagenases II and IV) for 2 hours in a thermomixer set at 32°C and 800 rpm. The digested tissue was then washed with a sequential series of stopping buffers (1x PBS, 10 mM HEPES, 30 mM taurine, 5.5 mM glucose, 10 mM BDM, 5-10% FBS, 12.5-1000 μM $CaCl_2$). After washing, the isolated cardiomyocytes were plated on 2 wells in a 96-well plate. The plating medium consisted of DMEM with 2 mM glutamine, 5 mM BDM, 5% FBS, 100 U/mL penicillin-streptomycin, and 1:500 Normocin (InvivoGen).

5.2.5 Cloning, Cell Culture and Transfection

Rat *TAAR1* gene was amplified from total cDNA using the set of primers:
(BamHI)ACCATGGCATCTTTGCCACAATAGCGC and,
(NotI)ACAAAAATAACTTAGACCTAGATGAATCT.
After amplification, the *TAAR1* gene was cloned into pcDNA3.1 Zeo (+) (Invitrogen) and transformed in *E. coli DH5α*. The cloned plasmid product was sequenced (Sanger method) using the Sanger Sequencing Kit (Applied Biosystems). For transient expression, the plasmid (10 μg) was transfected to human embryonic kidney cells (HEK293) transiently expressing the recombinant TAAR1 protein. The HEK293 cells were maintained in DMEM containing 10% FBS and 1% penicillin/streptomycin at 37 °C in a 5% CO2 incubator. After 24 h, the cells were maintained in the media containing zeocin (100 μg/mL) for stable expression of *TAAR1* in HEK293 cells. The transfected HEK293 cells were used in the subsequent cAMP assay and calcium assay.

5.2.6 GloSensor cAMP Assay

The HEK293 and isolated zebrafish cardiomyocytes were cultured in DMEM (10% FBS and 1% PS) in a poly-D-lysine pre-coated 96 well microplate and incubated in the CO_2 incubator at 37°C. 0.2 mL of cardiomyocyte selective growth supplement (Sciencell) was added to the cardiomyocyte culture. The pGloSensor-22F-cAMP plasmid (10 μg was transfected into HEK293 cells and isolated zebrafish cardiomyocytes (1.5×10^4 cells) using the Lipofectamine 3000 reagent as the manufacturer described. 48 hours after transfection, cells expressing the plasmid (15,000 cells/well) were collected. The desiderated cell number was incubated in equilibration medium containing a 2% (v/v) GloSensor cAMP reagent (Luciferin) stock solution, 10% FBS and 88% CO2-independent medium in 2 hours at 37°C according to the manufacturer's instructions. The cells were dispensed in wells of 96-well plate and a basal

signal was obtained before treating with Meth with doses from $10^{-}10$ to $10^{-}2$ M was added before luminescence detection. The original cell population isolated from the zebrafish heart was separated into the respective groups for treatment with different doses. EPPTB was also utilized as a selective TAAR1 and GPCR antagonist in this assay [124]. Therefore, according to the proposed pathway seen in figure 5.4, EPPTB would inhibit cAMP expression.

5.2.7 FLIPR Calcium Assay

Two days after transfection, cells were washed with FLIPR buffer (1x HBSS, 20 mM HEPES, 2.5 mM probenecid, pH 7.4), loaded with the calcium-sensitive fluorophore Fluo-3 (ThermoFisher) for 1.5 h at 37 °C, 5% CO2. During the incubation, two separate 96-well polypropylene compound plates were prepared. Meth was prepared at concentrations of $10^{-}10$ to $10^{-}2$ M, dissolved in the FLIPR buffer. EPPTB was prepared in 1% DMSO in FLIPR buffer. After the incubation with Fluo-3 dyes on the assay plate, different Meth doses were added to the assay plate and incubated for 15 min at 37 °C. Subsequently, the assay plate was read with a Fluorescent Imaging Plate Reader (FLIPR) Tetra (Molecular Devices). Data of calcium-responsive changes in fluorescence were collected every second over a 60-second time period. Regarding the antagonist assay, the assay plate with EPPTB were incubated for 15 min before monitoring fluorescence.

5.2.8 Collagen Assay

The level of collagen in tissues was measured by the collagen assay kit (Sigma Aldrich) following standard protocol. Briefly, collagen in samples was first enzymatically digested into collagen peptides in master reaction mix including 35 μL buffer and 0.5 μL Collagen I. The reaction mix was incubated at 37 °C for 60 min. Subsequently, 40 μL of Dye Reagent to wells and incubated at 37 °C for 10 min. The collagen levels are determined by reading

fluorescence at 465 nm.

5.2.9 Histochemical Staining and Immunofluorescent Staining for Collagen

After treatment of Meth, zebrafish hearts were isolated as described in previous literature [123]. Briefly, the fish were anesthetized by Tricaine before undergoing chest incisions. The heart was then located and excised, which were then placed in a solution of perfusion buffer (10 mM HEPES, 30 mM taurine, 5.5 mM glucose and 10 mM BDM in 1x PBS solution). After excision of all hearts, they were subsequently fixed by 4% formaldehyde and cryo-sectioned with a cryostat. The tissue slices were placed onto frosted microscope slides (Thermofisher Scientific) and underwent Masson's Trichrome staining (following the provided protocol from American Master Tech, TKMTR2). Myocardial tissue is stained red, and collagenous tissue is stained blue. For immunofluorescence, mouse anti-collagen I antibody (Novus Biologicals) and rabbit anti-collagen III antibody were incubated overnight on cryosections of cardiac tissues, followed by staining for 2 hours with goat anti-mouse IgG conjugated Alexa 568 (Abcam) and donkey anti-rabbit IgG conjugated FITC (Thermo Fisher). Sections were mounted in Antifade Mounting Medium with 4,6-diamidino-2-phenylindole (DAPI) (Thermo Fisher) and mounted in Antifade Mounting Medium. Fluorescent imaging was taken with the Keyence Digital Microscope (BZ-X800) system.

5.2.10 Statistical Analysis

Statistical analysis was conducted via the JMP Suite, a statistical data analysis tool derived from SAS. All parameters derived from data analysis (*i.e.,* HR, HRV, QRS, PR, QTc) were averaged within each experimental group. Statistical significance was determined by the

one-way ANOVA test between experimental groups with significance level $p<0.05$. Data in figures were plotted as mean ± standard error (SE). Outputs of the cAMP and calcium assays were expressed as relative luminescence units (RLU) and relative fluorescent units (RFU), respectively. A non-linear regression was used to quantify methamphetamine potency for EC50 value calculations. EC50 is the concentration of agonists required to produce 50% of the maximum effect. The maximum effect obtained in the cAMP and calcium assays were approximately 1400000 RLU and 12000 RFU, respectively. Each concentration was tested three times in triplicate, and the values were given as mean ± SE. Significance was determined via the Student's T-test.

5.3 Results

5.3.1 Methamphetamine Induced Significant ECG Changes over the Course of Two Weeks

Using the ECG setup designed in our lab, we acquired ECG signals over a two-week period. The control (n=6) and Meth-treated (n=8) groups were immersed in the designated solutions for 20 minutes for 3 instances per week, and their ECG were subsequently acquired after treatment. The raw signals were then processed to eliminate external noise, and the PQRST waveforms were labelled on the processed ECG signals. Relevant ECG parameters including HR, HRV, QRS, QTc, and PR intervals were then quantified. The day number was defined as follows: day 1 corresponded to the first day of Meth treatment, and subsequent days were numbered accordingly. Figures 5.1 and 5.3 comprise ECG diagrams obtained during baseline, week 1, and week 2 of the treatment regimen. Figure 5.1 represents individual ECG signals after filtering and smoothing. Figure 5.3 represents the averaged outcome of all ECG signals for the specific experimental group and time period, developed for the detection of

the T wave. The representative ECG figures indicate a progressive decrease in heart rate for the Meth-treated group with instances of sinus arrhythmia, highlighted by blue brackets (Figure 5.1). The QTc interval also displayed a decrease in the treated group (Figure 5.3). Calculated ECG parameters are displayed in figure 5.2. All ECG parameters were verified to display no significant differences during baseline measurement between the experimental groups. Additionally, the results also indicate that there were no significant differences in QRS duration between the Meth-treated fish and the untreated (control) fish throughout the duration of the study (Figure 5.2). The heart rate (HR) for treated fish decreased

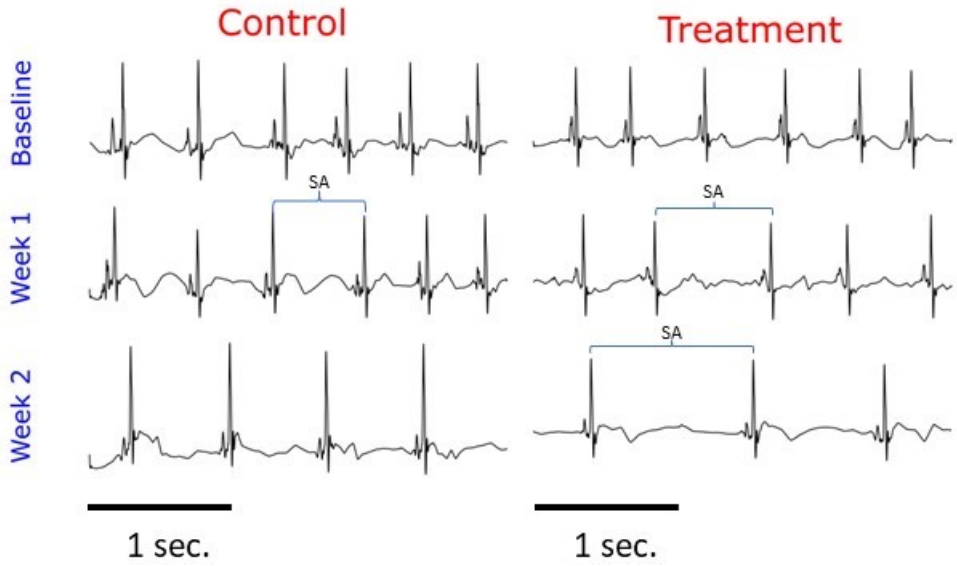

Figure 5.1: Meth induces decreased heart rate and higher presence of sinus arrhythmia. These ECG signal figures were processed from both untreated (control, n=6) and Meth-treated (treatment, n=8) fish, taken during baseline, week 1, and week 2 of the study. The ECG waveforms (PQRST) were labelled on the first cycle of each figure. These figures depict that Meth treatment has significantly decreased heart rate over the duration of the study compared to no treatment. Additionally, Meth-treated zebrafish exhibited more pronounced bradyarrhythmia, as indicated by the blue brackets spanning across the occurrence of the bradyarrhythmia. Note that while control fish also exhibit bradyarrhythmia, the occurrences in Meth-treated fish were more pronounced. Figures shown represent 3 seconds of recording. Scale bar depicts 1 second.

throughout the course of the treatment, exhibiting signs of bradyarrhythmia (Figure 5.1). The HR presented significant differences at the end of the first week of the treatment (Figure

5.2A). The HRs on day 5 were 79.77 BPM and 111.9 BPM for treated and untreated fish, respectively. The HR stabilized in the second week (days 10 and 12), displaying a consistent decrease through the remainder of the study. The HRs for treated fish were 71.17 BPM for day 10 and 68.99 BPM for day 12. These were in contrast with the HRs seen in untreated fish, which displayed 107.9 BPM and 95.89 BPM for days 10-12, respectively.

Throughout the course of the study, the heart rate variation (HRV) displayed a biphasic trend for the treated fish (Figure 5.2B). The HRV between Meth-treated fish and control fish exhibited no differences on days 1 and 3, but Meth seemed to have induced an increase in HRV during the first week of treatment. Treated fish exhibited a significant increase in HRV during day 5, reaching up to 338.6 ms vs 121.7 ms seen in untreated fish. This also corresponds to the maximum HRV attained by the treated fish during the study. The increase in HRV may be attributed to the presence of sinus arrest as indicated by the blue brackets in Figure 5.1. The HRV decreased during the second week of treatment, although it still remained above the HRV for untreated fish. On day 12, the heart rate variation for Meth-treated fish was 181.2 ms compared to 164.1 ms seen in untreated fish. Meth induced significant changes in the PR interval during the first week of treatment (Figure 5.2C). On day 1, the Meth-treated fish exhibited a PR interval of 56.00 ms, compared to the PR interval of untreated fish, which was 66.37 ms. For day 5, the PR intervals for Meth-treated fish and untreated fish were 57.55 ms and 68.91 ms, respectively. There were no significant differences found during the second week of treatment.

The QTc interval displayed a significant decrease during the first week for Meth-treated fish (Figure 5.2D). The most significant decrease occurred on day 5, with QTc interval being 226.8 ms and 281.5 ms for treated and untreated fish, respectively. The QTc interval stabilized during the second week, generally maintaining the significant decrease for Meth-treated fish. On day 12, the QTc interval was 222.2 ms and 262.7 ms for treated and untreated fish, respectively.

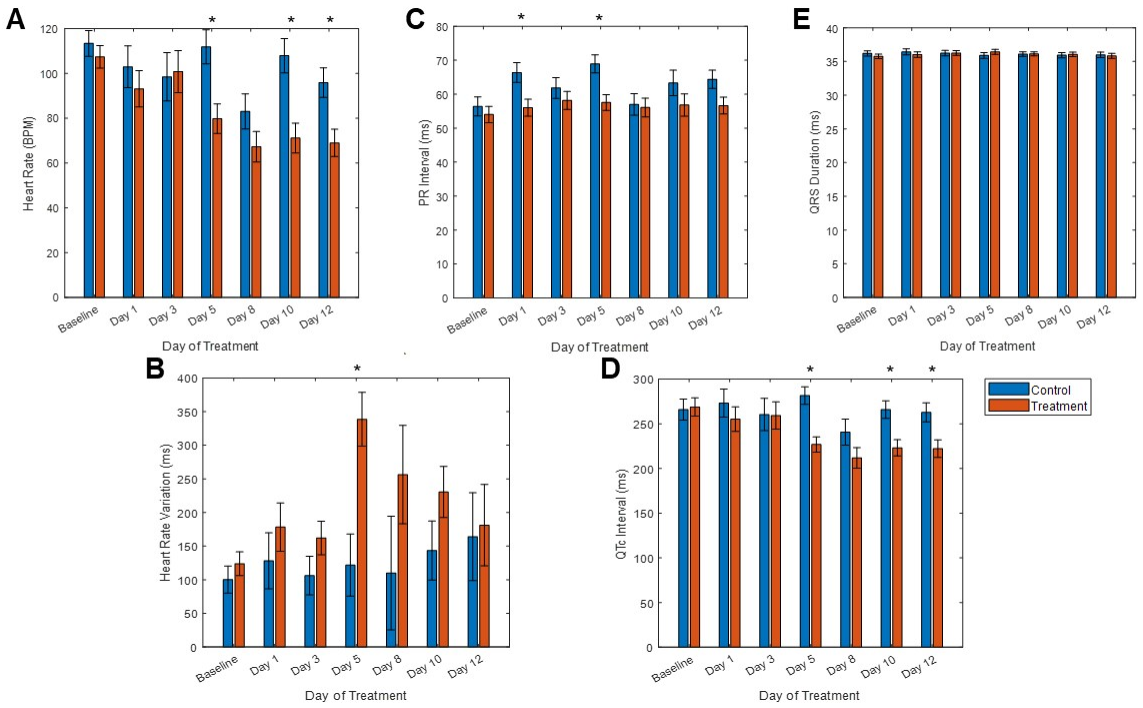

Figure 5.2: Tabulated averages from all ECG data acquired from both untreated (control, n=6) and Meth-treated (treatment, n=8) groups across the 2-week study. (A) Meth-treated fish displayed decreased heart rate compared to the untreated fish starting from the end of the week 1. (B) Meth-treated fish exhibited a biphasic trend in heart rate variation (HRV) throughout the duration of treatment, reaching a peak at the end of week 1 before decreasing during week 2. (C) Meth treatment induced a significant decrease in PR interval during week 1 but not week 2 of treatment. (D) Meth treatment induced a significant decrease in QTc during the end of week 1 before maintaining the depressed QTc throughout week 2. (E) Meth treatment did not exhibit a change in QRS duration. * denotes $p<0.05$.

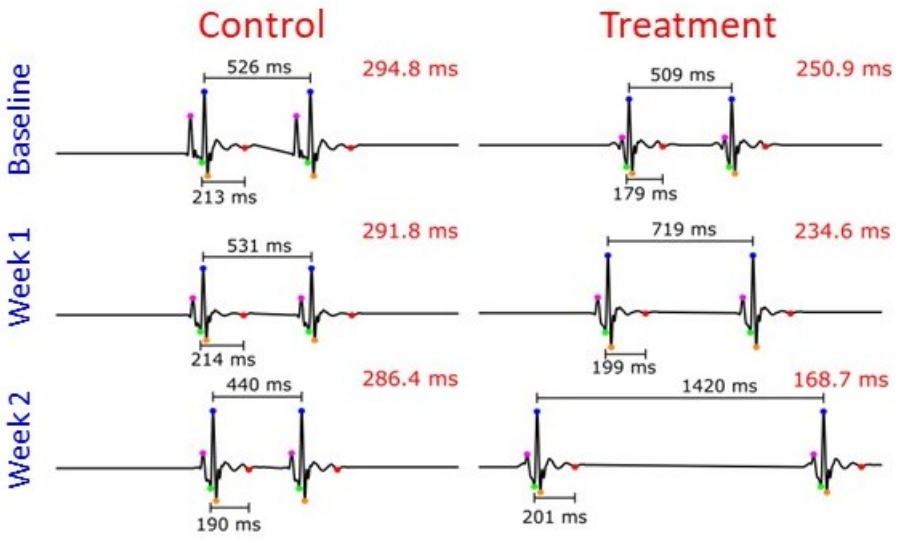

Figure 5.3: Meth induces a decrease in QTc over the course of the study. These figures were produced by averaging all ECG segments from each recording, extrapolating the ECG waveforms in order to determine the T wave. The waveforms are depicted as follows: Magenta=P; Green=Q; Blue=R; Orange=S; and Red=end of T wave. The RR and QT intervals are labelled for all waveforms, and the calculated QTc interval is shown on the top right of each figure. In comparison between untreated (control, n=6) and Meth-treated (treatment, n=8) fish, treated fish exhibited progressively lower QTc throughout the duration of the experiment, likely due to decreasing heart rate (depicted as increasing RR interval).

5.3.2 Methamphetamine Treatment leads to Increased Expression of cAMP and Ca^{2+} in a TAAR1-mediated, Dose-dependent Manner

To help uncover the direct molecular mechanism in the induction of Meth-induced cardiotoxicity, zebrafish cardiomyocytes (n=6 zebrafish) were isolated and treated with Meth to determine Meth induced cAMP expression via the GloSensor cAMP assay, which is involved in regulating GPCR pathways. TAAR1-overexpressed HEK293 cells have also been produced to complement the assay as the positive control, and original HEK293 cells served as the negative control. Figure 5.4 depicts the proposed GPCR/cAMP pathway that enables Meth-induced cardiotoxicity.

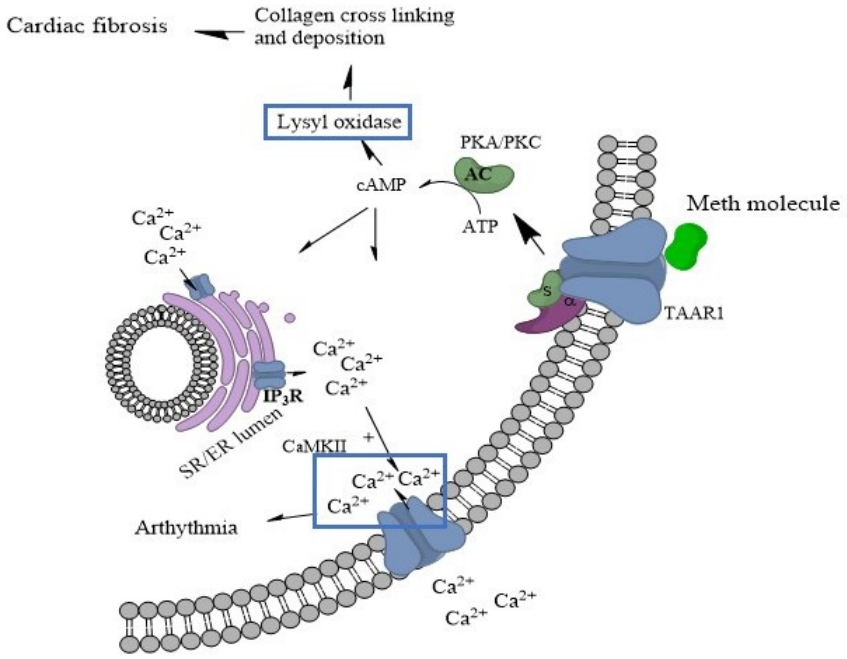

Figure 5.4: Meth induces downstream dysregulation in the GPCR pathway. This figure depicts the proposed mechanism of the pathologic effects of Meth on cardiomyocytes, including the upregulation of cardiac fibrosis via lysyl oxidase and the increased frequency of arrhythmia via the calmodulin CaMKII leading to the dysregulation of Ca^{2+}. cAMP, the upstream factor for both processes, and Ca^{2+}, the ion modulated by CaMKII, are both highlighted to indicate that they were investigated in this study.

In previous studies, Meth has been discovered to bind to GPCRs such as TAAR1 to trigger the upregulation of cAMP in cardiomyocytes [125]. cAMP downstream signaling may be linked with the onset of cardiac pathology, such as fibrotic dysregulation via lysyl oxidase and arrhythmia via CaMKII. The results from the cAMP assay indicate that Meth led to a dose-dependent upregulation in cAMP expression within zebrafish cardiomyocytes (Figure 5.5). Additionally, TAAR1-overexpressed HEK293 cells displayed a greater increase in cAMP expression than original HEK293 cells, indicating that TAAR1 mediated cAMP expression due to Meth exposure. In a similar fashion, Ca^{2+} was also upregulated due to Meth exposure within zebrafish cardiomyocytes (Figure 5.5). TAAR1-overexpressed HEK293 cells displayed a greater increase in Ca^{2+} concentration than original HEK293 cells, indicating that TAAR1

also mediated Ca^{2+} dysregulation due to Meth exposure.

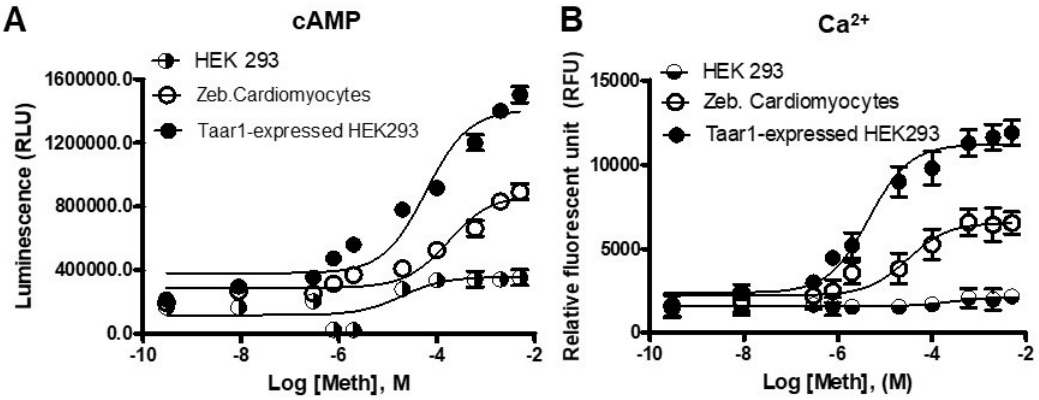

Figure 5.5: Downstream expression of TAAR1 and GPCR pathway due to Meth treatment. (A) Detection of cAMP expression after Meth treatment from zebrafish cardiomyocytes, HEK293, and TAAR1-overexpressed HEK293 cells via the GloSensor cAMP assay. TAAR1-overexpressed HEK293 cells served as the positive control for this assay. HEK293 cells served as the negative control. Results display that Meth induced dose-dependent cAMP expression in zebrafish cardiomyocytes. cAMP expression from TAAR1-overexpressed HEK293 cells exhibited a greater dose-dependent increase, demonstrating TAAR1-mediated cAMP expression due to Meth treatment. (B) Detection of Ca^{2+} after Meth treatment from zebrafish cardiomyocytes, HEK293, and TAAR1-overexpressed HEK293 cells. Results display that Meth increased Ca^{2+} concentration within zebrafish cardiomyocytes in a dose-dependent manner. Ca^{2+} expression from TAAR1-overexpressed HEK293 cells exhibited a greater dose-dependent increase, demonstrating that TAAR1 mediates Ca^{2+} concentration due to Meth treatment.

These results are further corroborated by experiments involving EPPTB, a TAAR1 antagonist. As indicated in figure 5.6, EPPTB attenuated Meth-induced cAMP and Ca^{2+} upregulation in a dose-dependent manner. This also suggests that Meth-induced cardiotoxicity involving cAMP and Ca^{2+} dysregulation may be attenuated by targeting TAAR1 and the GPCR pathway.

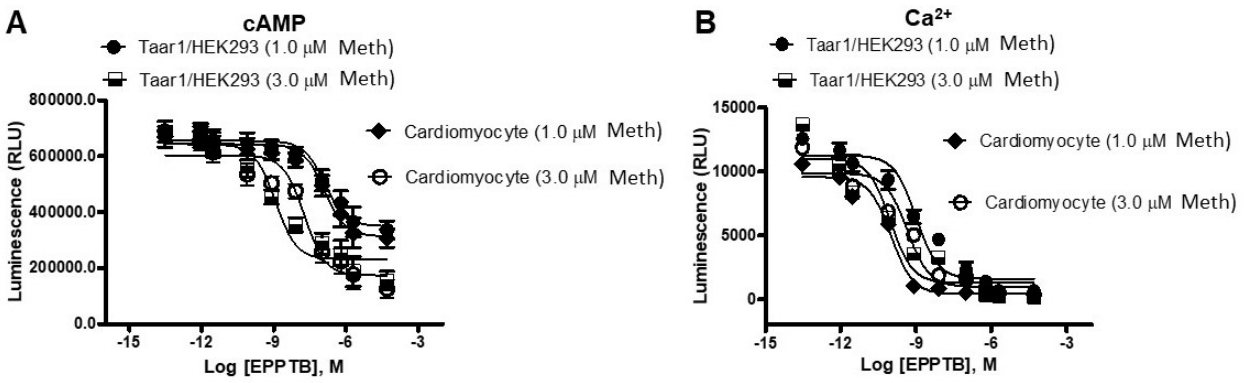

Figure 5.6: Inhibition of the GPCR pathway by EPPTB decreases downstream expression due to Meth treatment. Zebrafish cardiomyocytes and TAAR1-overexpressed HEK293 cells were treated with 1-3 μM Meth and subsequently treated with EPPTB at various concentrations for a dose-response curve. Results from the experiment with EPPTB, an inhibitor of TAAR1, in the presence of Meth, corroborated with previous results of TAAR1-mediated increases of cAMP expression (A) and Ca^{2+} concentration (B). This indicates that downstream expression was mediated by TAAR1 and the GPCR pathway.

5.3.3 Methamphetamine Treatment Produce Excessive Fibrosis in Zebrafish Cardiac Tissue

To determine if Meth induces fibrotic dysregulation, which was delineated above as one of the potential cardiotoxic factors contributing to arrhythmias, Masson's Trichrome staining for collagen and collagen type I immunological staining were conducted on cardiac tissue obtained from both untreated and Meth-treated fish (n=6 per group). Images obtained from Masson's Trichrome staining (Figure 5.7A-B) revealed a higher presence of collagen deposits in Meth-treated cardiac tissue, as highlighted in the dotted boxes. Immunological staining (Figure 5.7C-D) further revealed a higher presence of collagen type I with Meth-treated tissue. Collagen fluorescent assay of purified protein samples revealed that the collagen content increases from Meth treatment in a dose-dependent manner, displaying the highest difference at the highest concentration of Meth (Figure 5.8A). An expression profile of genes associated with fibrosis was also conducted, and the results determined that Meth-treated tissue displayed significantly higher expression ($p<0.005$) in lysyl oxidase (LOX) and lysyl

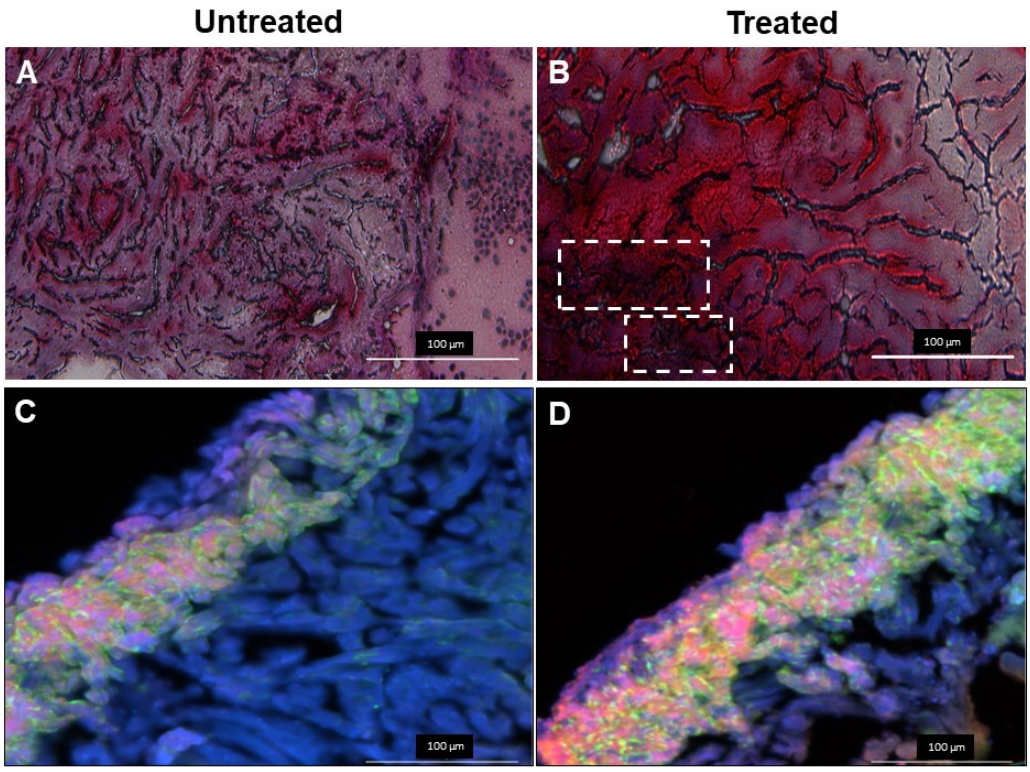

Figure 5.7: Histochemical and immunological staining on collagenous tissue due to Meth treatment (A) Masson's Trichrome Staining of cardiac tissue obtained from untreated zebrafish (n=6) and Meth-treated zebrafish (n=6). Myocardial tissue is stained in red, and collagen is stained in blue. Areas of collagen deposits are labeled by white dashed boxes in Meth-treated cardiac tissue. (C-D) Collagen type I immunological staining of untreated and treated cardiac tissue. Presence of lighter colors (*i.e.,* pink, yellow, green) indicates the presence of collagen. DAPI was used as control and is displayed as a blue stain. Meth-treated tissue displays higher amounts of collagen I.

hydroxylase (*PLOD*) (Figure 5.8B). This result signifies that the lysyl oxidase family of proteins was upregulated in response to Meth treatment. While the other genes involved in the profibrotic response (*COL1A1*, *COL3A1*, *MMP1*, and *TMP1*) did not display significance, their expressions have also shown marginal increases in Meth-treated cardiac tissue over its untreated counterpart. Overall, these results display an uptick in the fibrotic response due to Meth treatment, further outlining Meth-associated cardiotoxicity in relation to the GPCR/cAMP pathway.

5.4 Discussion

The methamphetamine epidemic continues to fester worldwide, and cardiovascular diseases remain leading causes of death for methamphetamine abusers. Utilizing animal models to study cardiovascular associated mechanisms could be critical in devising treatments for Meth associated diseases. The zebrafish is an excellent model for drug screening studies due to high fecundity, low maintenance, and similar genetic homology to that in humans. As the zebrafish model is constantly evolving, studies have continued to delineate the applicability of the zebrafish in human medical research. During the initial conception of this study, we sought to 1. Establish the zebrafish model as an adequate model of drug screening for cardiotoxic effects, and 2. Characterize the electrophysiological abnormalities due to meth administration in a controlled environment. Utilizing our custom-designed zebrafish ECG acquisition system in our lab, we were able to acquire ECG from zebrafish during the two-week treatment period with Meth. Based on our results, we determined several significant ECG changes occurring between the Meth-treated and untreated fish. The progressive decrease in heart rate for treated zebrafish, while contradictory to the results seen in human clinical studies, was actually consistent with the results seen in previous animal model studies, including those performed on rats, monkeys, and zebrafish embryos [109, 126]. Those previous studies suggested that the decrease in heart rate due to Meth administration may be attributed to the baroreceptor reflex, a homeostatic response to the increase in blood pressure [127]. Schindler *et al.* documented a consistent blood pressure increase with the dosage of Meth administered in squirrel monkeys [126]. However, they noted that heart rate modulation from Meth administration may be biphasic, as lower Meth concentrations induces tachycardia, while higher Meth concentrations induces bradycardia. This suggests that there is a critical Meth concentration where it achieves a maximum catecholaminergic effect without triggering a significant baroreceptor reflex. The small decrease in PR interval due to Meth treatment may suggest quicker atrial conduction, which is consistent with

the mechanism of Meth to induce ventricular tachycardia [128]. The heart rate variability exhibited a peak at the end of the first week before decreasing during the second week.

HRV is used in cardiac physiology as a measure of healthy function and as a potential parameter for determining cardiovascular diseases such as sudden cardiac death [129]. More importantly, HRV may also provide insight into the brain-heart axis and how the autonomic nervous system impacts cardiac function, critical to the analysis of stimulant drugs such as Meth [130]. The initial increase in HRV may likely be due to the presence of sinus arrest in Meth-treated fish. As shown in figure 5.1, ECG acquired from Meth-treated fish displayed episodes of sinus arrest, where an instance of cardiac conduction normally present in regular sinus rhythm is absent. The HRV increase may also be attributed to the baroreceptor reflex, as the reflex would naturally adjust the heart rate in order to maintain stability in blood pressure and cardiac output. Most notably, the decrease in HRV during the second week of treatment is most likely associated with cardiac tissue damage and inflammation, consistent with the symptoms seen in Meth-induced cardiomyopathy [131, 132]. This is corroborated with research indicating that persistent hypertension induced a decrease in HRV, presenting the long-term pathophysiological effects of Meth [133]. Additionally, previous case studies involving Meth and amphetamine abusers indicated that the presence of elevated cardiac biomarkers such as troponin I and creatine kinase-MB, further suggesting that common symptoms of Meth use may be associated with cardiac damage [134, 135, 136]. Overall, the HRV results from this study suggest the biphasic nature behind the mechanism of Meth, where the cardiovascular system may initially respond to the effects of the drug before sustaining damage after a period of persistent exposure.

Additionally, the QTc interval, associated with ventricular contraction and proper heart function, decreased for Meth-treated fish, displaying the most pronounced differences in the second week of treatment. Initial observation suggested that the decrease in QTc interval seemed to be associated with the decrease in heart rate (or increase in RR interval, as depicted

in figure 5.3. The QT/HR relation has been widely documented, leading to the creation of the corrected QT interval to account for the effect of heart rate changes on the QT interval [137]. Nevertheless, the results obtained from this study remained contrary to the results seen in previous case studies, where Meth abusers tended to exhibit prolonged QTc intervals in response to Meth intake [138]. However, these case studies utilized data from humans who were already predisposed to Meth for varying periods of time, usually to the point of drug dependence. Therefore, QTc prolongation could potentially be a symptom seen in the later stages of Meth-induced cardiotoxicity. Previous clinical trial research has associated the development of QTc prolongation with ventricular tachycardia and cardiomyopathy, which are common symptoms of Meth abuse [131, 139, 140]. QTc shortening seen in this study may also suggest that calcium channels are downregulated by Meth, as decreased calcium influx also reduces action potential duration. This is corroborated by ion channel expression analysis from rats suggesting that Meth reduces calcium channel expression [141]. Potassium channel expression may also play a role in analyzing the effect of Meth on modulating the QT intervals. Numerous anticonvulsants and antiarrhythmics have been known to shorten QTc by upregulating potassium channel function [142]. Moreover, Meth has been shown to induce upregulation of potassium channels in the brain in relation to its neuropathic effects, suggesting that Meth has the potential to modulate potassium channels in other pathologies [143]. However, more research will be needed to elucidate the direct effects of Meth on ion channels in vivo, as patch clamp results from rat cardiomyocytes regarding the effect of Meth on calcium channels remain controversial [144, 145]. In general, ion channel analysis in cardiovascular pathology remains scarce.

We surmise that Meth might pose an antagonizing interaction with Tricaine, the anesthetic agent used to acquire ECG. Tricaine usage was also mandatory for this study due to regulatory purpose. However, both Meth and Tricaine have opposing mechanisms, as Meth is a stimulant while Tricaine is an established anesthetic, known for preventing action potential firing by blocking voltage-gated sodium channels [146]. The data revealed that Meth-treated

zebrafish exhibited significant decreases in PR interval on certain days in the early stage of treatment due to the excitatory properties of Meth. However, a closer inspection of the data indicated that the increase in PR interval for untreated fish was responsible for the significant change instead. Indeed, Tricaine may induce a decrease in myocardial contractility, which results in a decrease in heart rate and increase in PR interval during zebrafish sedation [147, 148]. Additionally, zebrafish subjected to repeated Tricaine treatment exhibited increased susceptibility to anesthetic effects [149]. Meth may also induce arrhythmic instances, which could confound HRV measurements [150]. Insignificant but noticeable increases in HRV were evident in days 10 and 12 for untreated fish. Meth studies involving other animal models have also suggested the confounding effect of anesthetics. Research concerning the hemodynamic response to Meth reported differing results, as a study conducted on anesthetized cats documented a decrease in blood pressure due to Meth administration, while a study conducted on conscious monkeys indicated an increase in blood pressure [126, 151]. It is unclear if the difference in results was due to the presence of anesthesia or an underlying combinatorial effect of Meth and the anesthetic agent. Research has also suggested that Meth confers a depressor effect in addition to the commonly known pressor effect, and the depressor effect may dominate for animals under anesthesia. Vaupel *et al.* reported a significant decrease in blood pressure after the onset of Meth administration in anesthetized rhesus monkeys, suggesting the presence of the depressor effect [152]. In addition, Tricaine has been shown to induce augmented effects with other agents. Muntean *et al.* treated zebrafish larva with dopamine and verapamil under both Tricaine-anesthetized and methylcellulose-embedded conditions, and their results indicate that the effects of the agents on myocardial calcium signaling and heart rate were greater in anesthetized fish than embedded fish [153]. This suggests that Tricaine has the potential to induce drug-drug interactions with other agents to influence underlying electrophysiology. Therefore, future improvements should be implemented to reduce the effect of Tricaine for zebrafish cardiotoxic studies, as Tricaine could introduce confounding circumstances, especially when testing psychostimu-

lants on zebrafish. Future studies should also seek to explain the effect of these chemical entities on ion channel function through analysis of sodium and calcium transients for zebrafish. These future experiments would determine the mechanism of methamphetamine in inducing cardiotoxicity as well as bolster the use of zebrafish as a suitable model for cardiotoxic studies.

GPCRs and one of their prominent secondary messengers, cAMP, have been attributed to modulate numerous neurological dysregulations due to Meth exposure [116, 154]. Due to ubiquitous nature of TAAR and GPCRs, this signaling pathway is also located in other physiological systems. Fehler *et al.* determined the presence of TAAR receptors within the aorta and their role in drug-associated vasoconstriction, which leads to cardiovascular conditions such as high blood pressure [155]. Interestingly, this process does not appear to be mediated by the neuronal system [156]. Recent research has indicated that GPCRs may also play a role in producing detrimental cardiac effects of Meth, including arrhythmia, fibrosis, cardiomyopathy, and tissue remodeling [157, 158]. As depicted in figure 5.4, cAMP interfaces with numerous factors within the GPCR pathway that may induce such cardiovascular effects [159]. cAMP upregulation is known to lead to fibrosis via increased lysyl oxidase production, as lysyl oxidase plays a major role in collagen and ECM crosslinking [160]. cAMP is also involved in the modulation of CaMKII, principal in the maintenance of myocardial calcium ion homeostasis [161]. CaMKII dysregulation has been attributed to the development of cardiac pathologies, such as the regulation of cardiac extraction-contraction coupling and the activation of inflammatory and hypertrophic pathways [162]. Using the GloSensor cAMP assay, we demonstrated that the upregulation of cAMP occurred in a dose-dependent manner within zebrafish cardiomyocytes. This upregulation was inhibited by, EPPTB, an antagonist of TAAR1 and cAMP. We also demonstrated that Ca^{2+} was upregulated by Meth in a TAAR1-dependent fashion. Collagenic assays on untreated and Meth-treated zebrafish further indicated that Meth induced an increased fibrotic response in cardiac tissue, consistent with the concept that Meth-associated fibrosis led to the dysregulation in cardiac

electrophysiology. The significant upregulation in the family of lysyl oxidase proteins further suggests that TAAR1 and GPCRs modulate this response. Overall, the results from this study indicate that Meth upregulated cAMP in zebrafish cardiomyocytes, causing dysregulation in Ca^{2+} homeostasis and fibrotic response, suggesting that cAMP and GPCRs play a role in Meth-induced cardiotoxicity.

Additional research should be conducted to further understand the role of heart-brain axis due to Meth exposure, such as the link between neurotransmitter response and cAMP/GPCR expression to cardiovascular abnormalities, as well as an investigation on ion channel function in the heart after Meth administration. The zebrafish model has already been utilized in numerous Meth studies, mostly related to behavioral studies due to the ability of Meth to disrupt dopamine release and reuptake, thus increasing dopamine expression [163]. Therefore, it would be intriguing to understand the role of dopamine in Meth-induced cardiotoxicity, as it would explain whether Meth-induced cardiotoxicity is caused by dopamine or through a direct effect from Meth. One consequence of dopamine response is the change in ion channel expression. For example, studies have shown the modulation of L-type calcium channels by Meth, but it is not fully understood whether Meth alters calcium channel function directly or via dopamine [144, 164, 165]. As mentioned earlier, ion channel modulation may also be integral in understanding the cardiac electrical remodeling induced by Meth. Meth has been determined to alter the expression and functionality of potassium and calcium within cardiomyocytes, which were correlated to Meth-associated arrhythmic events [144, 145]. These effects were not attributed to neuronal functions, indicating that separate mechanisms may also be in play for Meth-associated alterations in the neuronal and cardiovascular system.

5.5 Conclusion

The goal of this study is to provide elucidation into the effect of Meth on cardiac physiology and electrophysiology in a standardized, controlled setting. Utilizing the developed technology presented in chapter 4, the generated results suggests that Meth induces a predominant depressor effect on cardiac electrophysiology most likely due to the baroreceptor reflex and cardiac damage. This was manifested as a progressive decrease in heart rate and eventual decrease in HRV. This effect persisted through the end of the two-week treatment, which may be a sign of cardiac damage as seen in Meth-induced cardiotoxicity. Molecular analysis suggested that the Meth exposure via cAMP upregulation and Ca^{2+} dysregulation leads to the development of fibrosis and arrhythmia, respectively.

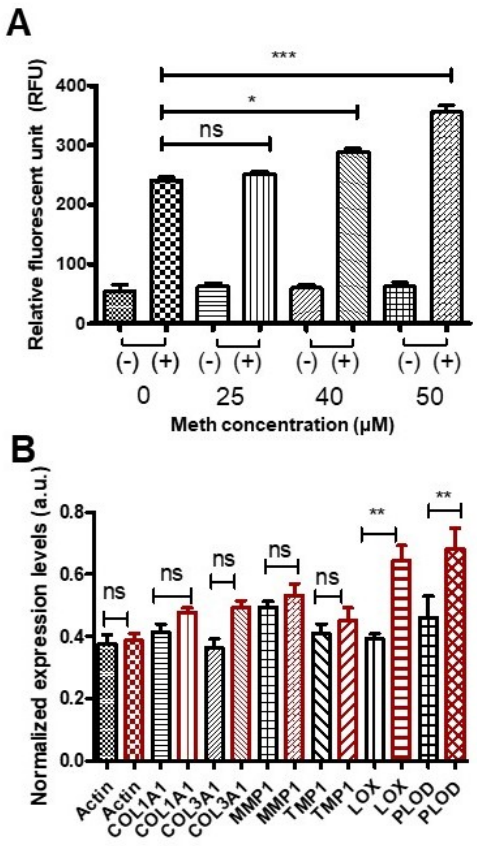

Figure 5.8: Collagenic expression analysis of zebrafish heart tissue (n=6 per group) with and without Meth treatment. (A) Collagen fluorescent assay conducted on protein samples treated at various concentrations of Meth. Positive symbol (+) signifies collagenase I treatment and negative symbol signifies no treatment. Results indicate that collagen content increases due to Meth treatment in a dose-dependent manner. (B) Expression analysis of genes associated with fibrosis, including the family of lysyl oxidases. (*COL1A1* = collagen I; *COL3A1* = collagen III; *MMP1* = matrix metalloproteinase I; *TMP1* = thymidylate kinase; *LOX* = lysyl oxidase; *PLOD* = lysyl hydroxylase) Meth-treated tissue exhibited significantly higher expression of lysyl oxidase and lysyl hydroxylase, associated with the GPCR pathway. Expression of other genes displayed marginal increases in treated tissue, indicating higher instance of fibrosis. * denotes $p<0.05$. ** denotes $p<0.005$. *** denotes $p<0.0005$.

Chapter 6

Development of a Hypoxia-Inducible System for Zebrafish Cardiovascular Studies

6.1 Introduction

In chapters 4 and 5, various zebrafish ECG phenotypes induced by drug treatments were explored, further establishing the zebrafish model as a viable candidate for drug screening in cardiovascular studies. In this chapter, the zebrafish model will be utilized for its other applications: genetic analysis and tissue regeneration. Specifically, the hypoxia pathway will be discussed, and a system to induce physical hypoxia in zebrafish will be delineated below.

6.1.1 Hypoxia Inducible Factor (HIF) and the Hypoxia Pathway

Hypoxia is a natural physiological condition that develops from the onset of myocardial infarction due to the occlusion of blood flow. The role of hypoxia in regeneration is perhaps best exemplified by comparing aquatic species and mammals. It is believed that aquatic and amphibian species, such as zebrafish, starfish, and salamanders, are capable of regeneration due to adapting to their aquatic environments, known to have widely fluctuating oxygen concentrations [166]. In contrast, mammals, known to be mostly nonregenerative, tend to live in land environments with stable oxygen levels. Thus, hypoxia and its associated signaling pathway could be a key to understanding the regenerative capabilities of those aquatic species. Over the past three decades, researchers have been trying to understand the roles that hypoxia play in various cellular and physiological processes. The discovery of the main element, hypoxia inducible factor-1 (HIF-1), was credited to Semenza in 1992 [167]. Along with his fellow researchers Ratcliffe and Kaelin, both credited for uncovering the regulation process of HIF-1 in cells, Semenza was awarded the 2019 Nobel Prize in Physiology or Medicine for their work on the hypoxic pathway [168, 169, 170]. Under normoxic conditions, HIF-1α is hydroxylated and then ubiquitinated by the von-Hippel Lindau tumor suppressor (pVHL) [171]. However, hydroxylation is suppressed in hypoxic conditions, allowing HIF-1α to avoid ubiquitination and to dimerize with HIF-1β for downstream gene regulation. While it is mainly viewed as a detriment to the myocardium downstream of the blocked coronary artery, hypoxia could play a role in cardioprotection and regeneration [172]. A previous study by Jopling *et al.* demonstrated that chemically induced hypoxia promotes zebrafish cardiomyocyte proliferation compared with normoxia both *in vitro* and *in vivo* [173]. Interestingly, this study also revealed that hyperoxic conditions reduce the cardiomyocyte proliferation rate compared to normoxic conditions, indicating that a dynamic continuum could exist in how oxygen concentration modulates cardiomyocyte proliferation. This continuum could be exhibited due to the dynamic hypoxic signaling response via varying HIF-1α

concentrations, indicating the necessity of careful HIF modulation in regeneration studies. Inducing cardiac regeneration by hypoxia have also been demonstrated in mice, demonstrating the potential for translating results regarding the HIF pathway into mammalian models and human therapies [174] Through recent research, the HIF pathway has continued to demonstrate its significance in the role of underlying cardiac regenerative processes.

While the complete mechanism of the HIF pathway remains to be elucidated, research has indicated its possible interactions with other signaling pathways in promoting regeneration. For example, HIF has been demonstrated to be an upstream factor of the Notch pathway [175, 176, 177]. The Notch pathway is a ubiquitous and vital pathway for the development and maintenance of various tissues. The Notch pathway induces such development through factors such as bone morphogenic proteins (BMPs) and cross-talks with other ubiquitous developmental and regenerative pathways such as the Wnt pathway [178]. Similar to the HIF pathway, the Notch pathway requires careful modulation, as zebrafish cardiac regeneration can be hindered by both inhibition and overexpression [179, 180]. Elucidating the mechanism of the HIF pathway in regeneration could also help uncover more information regarding other regenerative pathways, which will ultimately provide a clearer picture to intrinsic regenerative capabilities.

One of the major downstream processes stemming from the HIF pathway is angiogenesis. Previous studies have demonstrated that angiogenesis is critical to the wound healing process in both mammalian and zebrafish hearts [181, 182]. While numerous studies have indicated its importance in the regenerative process, angiogenesis also bears significance in potentially modulating the hypoxic environment within the infarct tissue. At the onset of myocardial injury, the infarct area is relatively devoid of adequate blood circulation due to damaged vessels, resulting in the development of local hypoxia [183]. However, as angiogenesis develops, the local oxygen concentration begins to increase, potentially affecting the dynamics of the HIF pathway and subsequent crosstalking. Research by Guo *et al.* demonstrated that

prolonging the upregulation of angiogenic factors for up to a month promoted cell survival within the heart and reduced scar size, suggesting that sustained angiogenic upregulation may enhance regeneration [184]. While a model has yet to be developed to fully explain this phenomenon, it serves to further emphasize that hypoxia and the HIF pathway is critical to the regeneration process.

6.1.2 Rationale

While hypoxia and the HIF pathway is well established as a critical factor in zebrafish regeneration studies, current methods in the induction of hypoxia for zebrafish remains inadequate for both long-term regeneration studies and potential translation into clinical practice. These methods tend to include the administration of drugs and agents known to upregulate HIF [173, 185] While they were effective in demonstrating the role of the pathway in regeneration, these agents could also introduce confounding effects not inherent to the original hypoxic response. For example, cobalt chloride, a well-known stabilizer for the HIF pathway, has been documented to induce oxidative stress not seen in hypoxic conditions, which could introduce regulation of genes independent of the HIF pathway [186]. Additionally, the methodology for the zebrafish studies tend to restrict treatment for these agents to short periods of time (approximately 1 hour), which may not be conducive for further optimization for future applications. Some zebrafish hypoxia studies do utilize gas sparging to induce direct hypoxia, but they were generally developed for embryonic and larval studies [187, 188]. These methods lack both the long-term monitoring for stable hypoxia induction and the adult zebrafish husbandry practices mandated for research. This chapter outlines a feedback-controlled hypoxia system designed for zebrafish and tailored for regenerative studies.

6.2 Methods

6.2.1 Zebrafish Husbandry

Wild-type adult zebrafish were obtained and raised in the lab as indicated in the previous chapters. These fish were separated randomly into their respective experimental groups. All procedures were performed under anesthesia with Tricaine (MS-222). All procedures were reviewed and approved to be in compliance with the guidelines provided by the Institutional Animal Care and Use Committee at University of California-Irvine (AUP-21-066).

6.2.2 Development of Hypoxia System

The developed hypoxia system is shown in figure 6.1. The fish tank consisted of a 8-liter container capable of holding up to 42 fish. 5 holes were punched along the walls and lid of the container for water inlet, nitrogen gas inlet, water/gas outlet, dissolved oxygen (DO) sensor, and for general maintenance. 10 mm-diameter valve tubes were attached to the tank for the transport of water and nitrogen gas. Water was circulated through the tubes connected to a pre-built reservoir for sanitation. Nitrogen was used to purge oxygen and reduce the dissolved oxygen concentration in the water. Nitrogen was purged at a rate of approximately 1 psi. A bubble diffuser was installed to disperse the nitrogen gas for a much larger surface area.

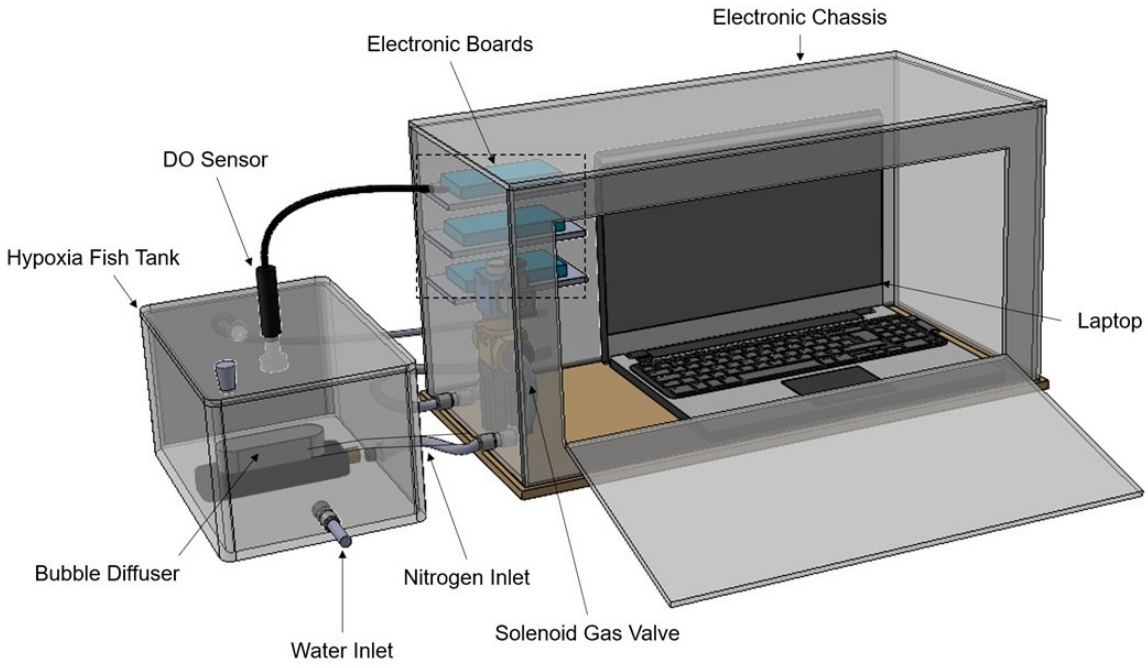

Figure 6.1: Schematic of the feedback-controlled hypoxia system. The hypoxia fish tank on the left was outfitted with water circulation, nitrogen inflow, and constant DO monitoring. The electronic system on the right, encased in the acrylic chassis, was designed to continuously monitor and maintain stable dissolved oxygen (DO) concentration with a feedback control algorithm.

To control DO concentration, a feedback control system was developed. The DO sensor attached to the tank relayed the signal to an Arduino microcontroller, which was the main component facilitating the feedback control. An Arduino code was implemented to record the DO concentration once per second and modulate the switch of the gas valve for nitrogen sparging when necessary. When the Arduino detected that the DO concentration has risen above the desired hypoxic concentration of 2 mg/L, it sent a signal to a relay module, which was responsible for switching the solenoid gas valve open, allowing nitrogen influx into the tank. The Arduino was connected to a laptop for displaying and recording the DO concentration. This electronic feedback control system was encased in an acrylic chassis with a laminated wood base to protect the electronic components from water damage.

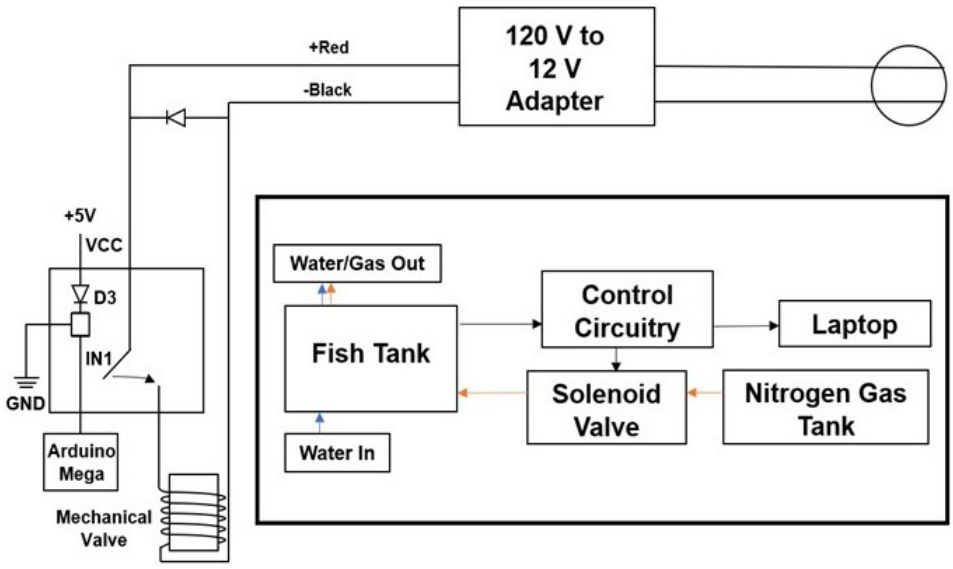

Figure 6.2: Hypoxia system circuit diagram and flowchart. The feedback control circuitry consists of an Arduino microcontroller connected to both the DO sensor for sensing and the mechanical valve for actuating nitrogen gas flow into the fish tank. A custom algorithm is developed to maintain DO concentration at 2 mg/L. The inset provides a general flowchart of the various components of the system. Blue arrows indicate water flow; orange indicates nitrogen gas flow; black indicates DO recording signal flow.

6.2.3 Zebrafish Cryosurgery and Subsequent Treatment

The zebrafish undergo cryosurgery based on the method outlined in Gonzalez-Rosa *et al.* [189] Briefly, the zebrafish were anesthetized in 200 mg/L tricaine (MS-222) for approximately 5 minutes. After anesthesia, the zebrafish was placed on a moist sponge ventral side up. Under the microscope, an incision was made on the body wall to expose the chest cavity and open the pericardial sac, exposing the heart. A custom made cryoprobe equipped with a stainless steel tip approximately 0.5 mm. in diameter, was chilled in liquid nitrogen prior to cryosurgery. After the heart was exposed, the cryoprobe tip was placed on the surface of the heart for 10 seconds. The site displayed paleness with some bleeding, indicating successful infarction. The fish was allowed to recover in fish tank water treated with 50 mg/L acetyl-

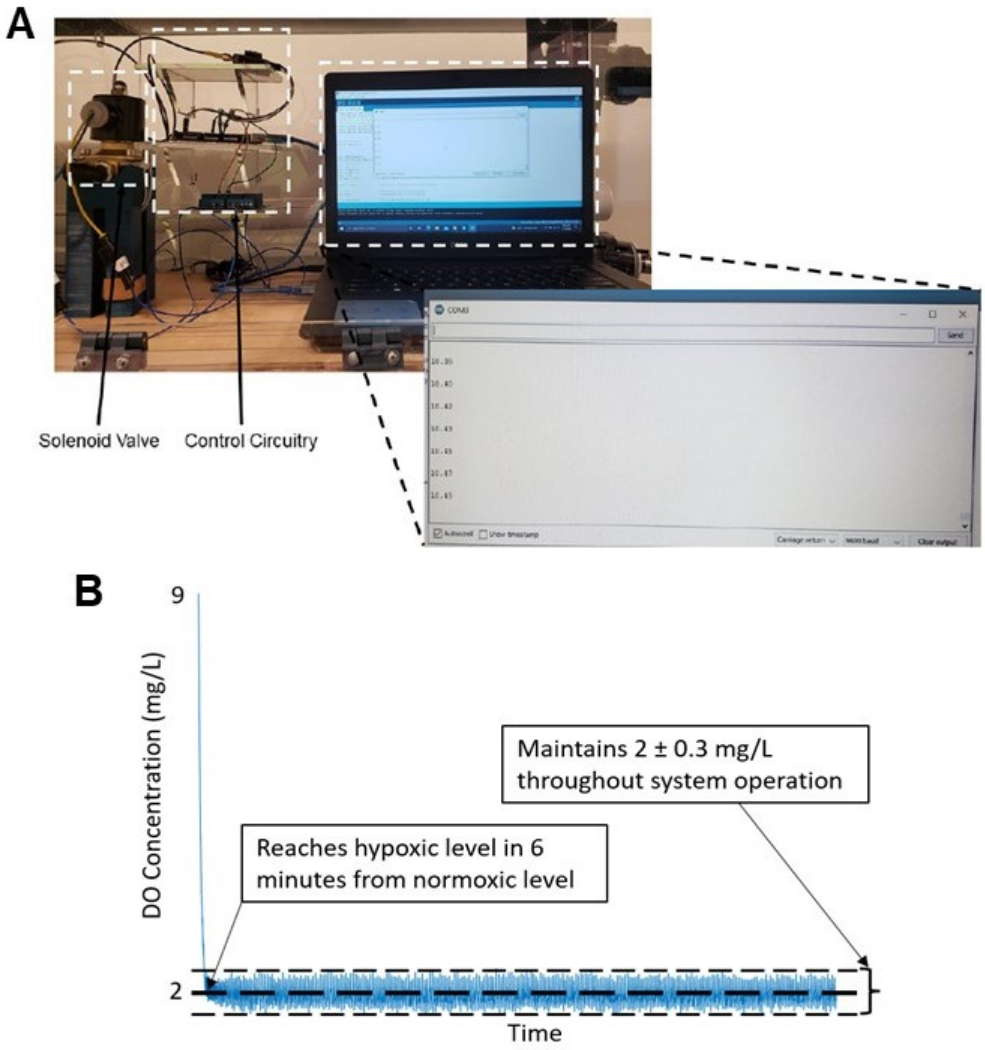

Figure 6.3: Hypoxia system circuit diagram and flowchart. The feedback control circuitry consists of an Arduino microcontroller connected to both the DO sensor for sensing and the mechanical valve for actuating nitrogen gas flow into the fish tank. A custom algorithm is developed to maintain DO concentration at 2 mg/L. The inset provides a general flowchart of the various components of the system. Blue arrows indicate water flow; orange indicates nitrogen gas flow; black indicates DO recording signal flow.

salicylic acid. After 15 minutes of monitoring for any abnormal symptoms, the recovered fish were placed for their respective treatments. For the hypoxia system, the fish (n=24) were placed in the fish tank prior to initiating nitrogen gas purging. The fish will remain in the hypoxia system for the duration of the study. For treatment with cobalt chloride, the fish (n=24) were placed in fish tank water containing 10 mM and 20 mM cobalt chloride for 1 hour before returning them to regular fish tank water for the remainder of the study.

6.2.4 qPCR Expression Analysis

After subsequent treatments, fish hearts were excised for genetic and protein expression analysis. For heart excision, the chest cavity and pericardial sac was exposed similar to the aforementioned cryosurgery protocol. The heart was then removed from the cavity with a set of forceps. The fish hearts were excised at 0, 1, 4, and 7 days post injury (dpi). Zebrafish cardiac RNA was isolated with the Trizol reagent, following the provided protocol. First-strand cDNA synthesis was conducted after RNA isolation. qPCR was conducted to determine the expression levels of *HIF-1α* and *VEGF*. Relative expression levels were calculated with the double-delta Ct method. The double-delta Ct method is calculated by the following:

$$RelativeExpression = 2^{-\Delta\Delta Ct}$$

$$\Delta\Delta Ct = (Ct_{EGene,ESample} - Ct_{CGene,ESample}) - (Ct_{EGene,RSample} - Ct_{CGene,RSample})$$

where EGene represents the experimental gene (*HIF* or *VEGF*), CGene is the control gene (*β-actin*), ESample represents the experimental sample (days 1, 4, and 7), and0 RSample is the reference sample (day 0).

6.3 Results and Discussion

6.3.1 Hypoxia System Performance

The developed hypoxia system has been developed as shown in figure 6.1. The electronic schematic, including the Arduino microcontroller and solenoid mechanical valve are shown in figure 6.2. The actual setup, including the computer interface displaying the dissolved oxygen concentration, is shown in figure 6.3. With an outflow nitrogen pressure of approximately 1 psi, the system was able to decrease the DO concentration from the atmospheric level of 9 mg/L to the desired level of 2 mg/L in approximately 6 minutes. The system was able to maintain a DO concentration of 2 $\pm$ 0.3 mg/L. Comparing the survival rates of the hypoxia system and cobalt chloride treatment, the zebrafish (n=24) in the hypoxia system was able to achieve a larger survival rate of 91.7%, whereas zebrafish (n=24 each concentration) undergoing cobalt chloride treatment only achieved survival rates of 66.7% and 37.5% for 10 mM and 20 mM, respectively (Figure 6.4).

6.3.2 Expression Analysis

In order to understand how hypoxia induced by the hypoxia system may modulate normal physiological response and cryoinjured response, zebrafish (n=24 per experimental group) was placed in the hypoxia system after their respective treatments. At days 0, 1, 4, and 7, zebrafish hearts were extracted for expression analysis of *HIF* and *VEGF*. As shown in figure 5, both *HIF* and *VEGF* expression peaked at 4 days of treatment for uninjured fish, whereas the same expression peaked at 7 days for injured fish. This data indicates that under hypoxic conditions, injured tissue results in a delayed response of heightened *HIF* and *VEGF* expression, suggesting that the physiological response after injury necessitates a delayed response. Previous literature determined that the *VEGF* expression after injury

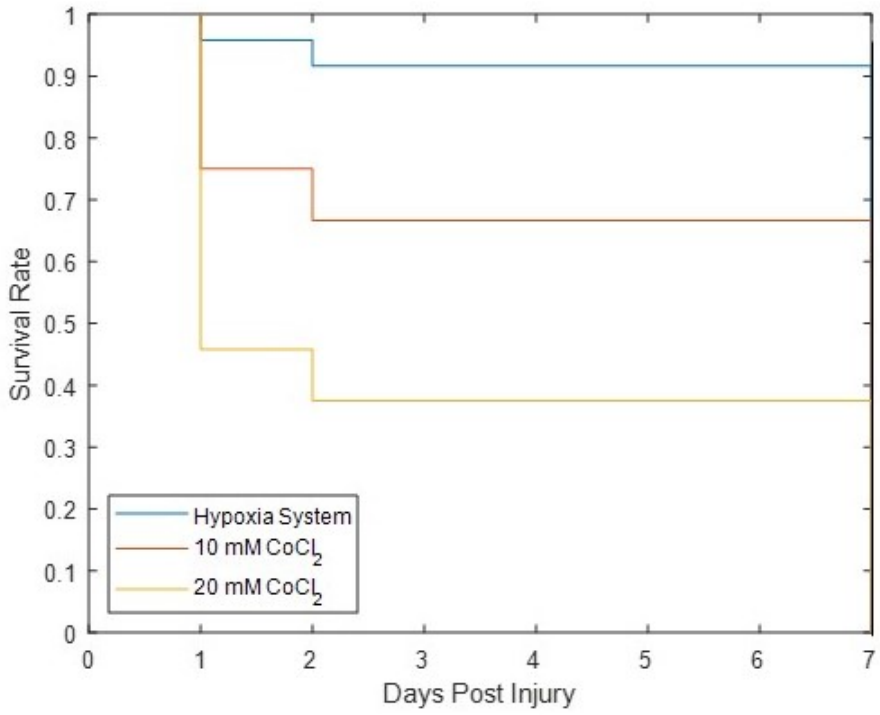

Figure 6.4: Comparison of survival rate between zebrafish in hypoxia system and in $CoCl_2$ treatment. Data yielded that over 7 days post cryoinjury, the zebrafish in the hypoxia system exhibited the highest survival at 92%, followed by 10 mM $CoCl_2$ at 67% and 20 mM $CoCl_2$ at 38%. This demonstrated that the hypoxia system was the most viable method for inducing hypoxia.

would typically peak at 1 day post injury before decreasing in subsequent days [182, 190]. This further suggests that the physical hypoxia condition delays the normal physiological response seen after injury. Interesting to note is the decrease in *HIF* expression during days 1 and 4 for zebrafish after cryoinjury. This may be attributed to the non-canonical HIF pathway, which is independent of oxygen concentration. Studies showed that damage to the mitochondrial respiration process in oxidative phosphorylation destabilizes HIF-1α expression [191]. Whether that translates to expression in injured tissue remains unknown.

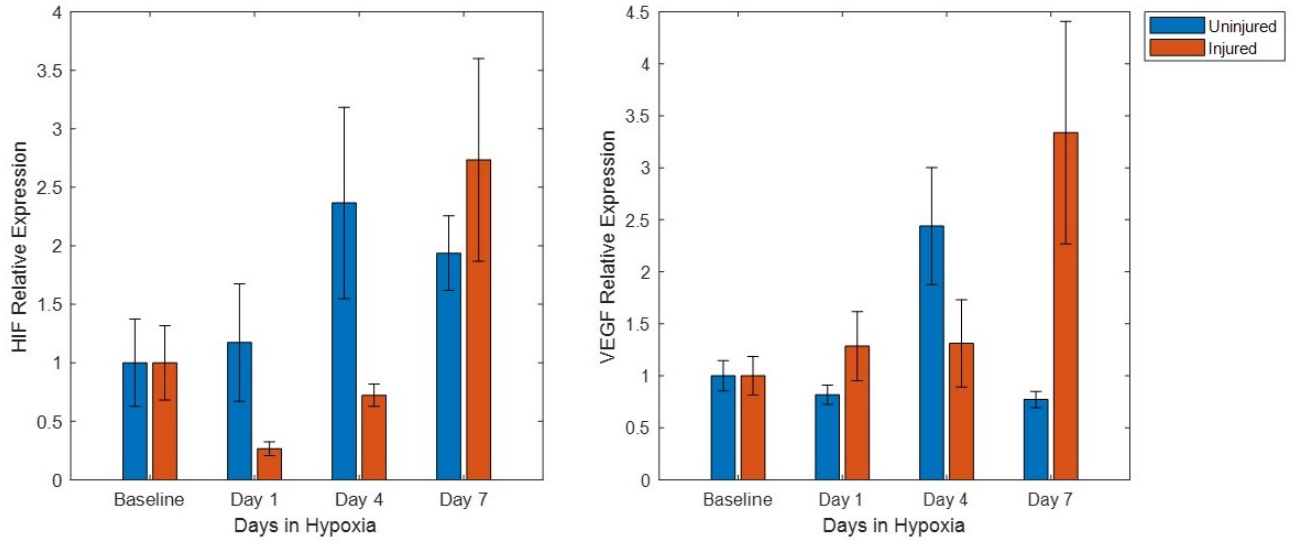

Figure 6.5: Expression Analysis of *HIF* and *VEGF* for Both Uninjured and Cryoinjured Fish in Physical Hypoxia. *HIF* and *VEGF* expression peaked at day 4 of hypoxia treatment for uninjured fish and day 7 for injured fish.

Numerous studies have demonstrated the the benefit of expressing *VEGF* in wound closure after injury, as angiogenesis is a fundamental factor in wound healing [192, 193, 194, 195]. However, *VEGF* overexpression has also led to unintended consequences, such as perpetuation of the inflammatory response and development of chronic scars [196, 197]. This suggests that persistent *VEGF* may be detrimental to the wound healing process. Interestingly, delaying *VEGF* expression post injury may improve prognosis [198]. Thus, understanding when *VEGF* and *HIF* should be expressed to promote healing after injury is crucial in treating cardiovascular diseases.

6.4 Conclusion

In this chapter, the development of a hypoxia system for zebrafish studies was introduced, and validation studies were performed to determine the effects of induced hypoxia on the

HIF and *VEGF* genes. The hypoxia system was able to maintain a steady DO concentration of 2 $\pm$ 0.3 mg/L, and the survival rate of zebrafish was 92%, compared to 38% - 67% in the alternative $CoCl_2$ treatment. The *HIF* and *VEGF* expressions peaked at different days of hypoxic treatment for uninjured and injured fish, suggesting that the wound healing process may alter the physiological response to hypoxia. This may be vital to understanding how the difference in the timing of expression may influence the regeneration process.

Chapter 7

Conclusion and Prospective

7.1 Summary of contributions

This dissertation provides a number of contributions in the use of the zebrafish model in various cardiovascular studies, including (1) development of an ECG system suitable for long-term drug/agent assessment and genetic characterization for arrhythmic phenotypes; (2) elucidation of the effect of methamphetamine on arrhythmic phenotypes with an in-depth analysis into how G-couple protein receptors may induce such phenotypes; and (3) fabrication of a hypoxia system suitable for zebrafish cardiac regeneration studies in relation to the HIF pathway and the wound healing process.

This dissertation provides a demonstration into how the zebrafish may be used for a multitude of investigation for cardiovascular pathologies. The zebrafish model possesses many advantages, such as similar homology to humans, a solid foundation of zebrafish genome characterization with the understanding that over 70% of human genes have orthologues in zebrafish, the ability to regenerate cardiac tissue, and the relative ease of maintenance compared to mammalian models [28]. These qualities make the zebrafish model ideal for

drug screening analysis, genetic phenotyping, and exploration of cardiovascular regenerative strategies. Previous chapters discuss how zebrafish studies may elucidate and corroborate current knowledge on arrhythmic phenotypes in association to drug treatments and genetic mutations, as well as enable the investigation of how modulation of the wound healing process may promote regeneration after cardiac injury.

7.2 Conclusion

7.2.1 Development of a Zebrafish ECG System

To enable the analysis of multiple drug dosing and functionalization of genetic mutations, a zebrafish ECG system was designed and fabricated. A comparison with the commercial system was conducted, and both system yielded similar performances. Various validation studies were also completed, such as the optimization of temperature and Tricaine (anesthetic) concentration, to determine the most stable ECG recording with high signal-to-noise ratio. Of particular attention is the Tricaine concentration, as Tricaine is known to affect electrophysiology. Finding a suitable concentration for minimizing confounding effects while maintaining an adequate signal-to-noise ratio was most vital in acquiring ECG data. To demonstrate the application of dose-response experiments with the developed system, Amiodarone treatment of varying doses were completed, and results demonstrate that the heart rate decreased and QTc interval increased with each increasing dose, which were the expected results. Finally, a high sodium intake analysis was conducted to investigate the effect of the mutation *Tg(SCN5A-D1275N)* on arrhythmic phenotypes. The mutation *Tg(SCN5A-D1275N)* is significant in arrhythmic diseases such as the sick sinus syndrome, an arrhythmic disease characterized by pathologies in the sinoatrial node, where cardiac conduction initiates [70]. Results suggest that the mutation led to an increased susceptibility to arrhythmic

phenotypes from conditions that may affect the ion channel function, where the mutation lies. Overall, this piece of work outlined the capability of the developed ECG system for zebrafish studies.

7.2.2 Effect of Methamphetamine on Inducing Arrhythmic Phenotypes

The methamphetamine (Meth) epidemic is an ongoing public issue due to the addictive nature of the psychostimulant. The epidemic is responsible for the rising number of deaths each year [199]. While the neurological effects of Meth are well documented, the cardiovascular effects are not well understood. Clinical reports only provide meager detail on the possible mechanism due to the varied nature of these accounts. Utilizing the ECG technology outlined earlier, zebrafish were subjected to Meth treatments over 2 weeks to simulate consecutive intakes due to addiction. Results indicate a progressive decrease in heart rate, decrease in QTc interval, and a biphasic trend in heart rate variation, indicating the increase in sinus arrhythmia, followed by the progressive decrease in heart rate due to cardiac damage. Subsequent experiments delineated the possible mechanism of Meth in inducing such arrhythmic phenotypes, including the analysis of how G-couple protein receptors (GPCRs) may induce excessive fibrosis and calcium ion dysregulation. Both of these conditions may result in the presence of arrhythmic phenotypes due to Meth intake.

7.2.3 A Novel System for Inducing Hypoxia in Zebrafish

One of the most notable features of the zebrafish is the ability to regenerate cardiac tissue after injury [35]. Thus, research focused on uncovering the mechanism behind the regenerative capability. Hypoxia and the HIF pathway have been linked as possible factors, as zebrafish

tend to live in aquatic environments with variable oxygen levels [166]. Regenerative studies regarding hypoxia also yielded positive benefits in hypoxic conditions [173]. However, those studies utilized drugs, agents, and genetic engineering to investigate, which are not conducive for translation for human clinical practice. A physical hypoxia system was developed to induce a stable dissolved oxygen concentration of 2 ± 0.3 mg/L. Resulting expression analysis of *HIF* and the angiogenic factor *VEGF*, relevant in the wound healing process after injury, displayed that the physical hypoxia system delayed expression upregulation. Previous literature demonstrated that a delayed response to an angiogenesis in wound healing may promote regeneration. In future work, understanding how modulation of hypoxic expression along the wound healing process would be vital in elucidating cardiac regeneration.

7.3 Future works

A number of general items identified for future works are summarised below.

- Optimize the placement of the ECG electrodes for more accurate recordings, with the possibility of adding additional leads for multidimensional electrophysiological analysis.
- Reduce the Tricaine concentration through various methods, such as the development of a 'wireless ECG jacket' for zebrafish, and the 'pseudo-ECG' video system.
- Analyze the immediate/acute effects of Meth on ECG to analyze how arrhythmic effects develop from the onset of treatment.
- Assess the effect of hypoxia on the cardiac regeneration process, including characterization with ECG.

Bibliography

[1] Giorgia Beffagna. Zebrafish as a smart model to understand regeneration after heart injury: How fish could help humans. *Frontiers in Cardiovascular Medicine*, 6, 2019.

[2] Aarti Asnani and Randall T. Peterson. The zebrafish as a tool to identify novel therapies for human cardiovascular disease. *Disease Models Mechanisms*, 7(7):763–767, 2014.

[3] K. L. Poon and T. Brand. The zebrafish model system in cardiovascular research: A tiny fish with mighty prospects. *Glob Cardiol Sci Pract*, 2013(1):9–28, 2013.

[4] Jianwei Zheng, Jianming Zhang, Sidy Danioko, Hai Yao, Hangyuan Guo, and Cyril Rakovski. A 12-lead electrocardiogram database for arrhythmia research covering more than 10,000 patients. *Scientific Data*, 7(1):48, 2020.

[5] Ennio Idrobo-Ávila, Humberto Loaiza-Correa, Rubiel Vargas, Flavio Muñoz-Bolaños, and Leon Van Noorden. Can the application of certain music information retrieval methods contribute to the machine learning classification of electrocardiographic signals? *Heliyon*, 7:e06257, 2021.

[6] Tai Le, Jimmy Zhang, Anh H. Nguyen, Ramses Seferino Trigo Torres, Khuong Vo, Nikil Dutt, Juhyun Lee, Yonghe Ding, Xiaolei Xu, Michael P. H. Lau, and Hung Cao. A novel wireless ecg system for prolonged monitoring of multiple zebrafish for heart disease and drug screening studies. *Biosensors and Bioelectronics*, 197:113808, 2022.

[7] S. S. Virani, A. Alonso, E. J. Benjamin, M. S. Bittencourt, C. W. Callaway, A. P. Carson, A. M. Chamberlain, A. R. Chang, S. Cheng, F. N. Delling, L. Djousse, M. S. V. Elkind, J. F. Ferguson, M. Fornage, S. S. Khan, B. M. Kissela, K. L. Knutson, T. W. Kwan, D. T. Lackland, T. T. Lewis, J. H. Lichtman, C. T. Longenecker, M. S. Loop, P. L. Lutsey, S. S. Martin, K. Matsushita, A. E. Moran, M. E. Mussolino, A. M. Perak, W. D. Rosamond, G. A. Roth, U. K. A. Sampson, G. M. Satou, E. B. Schroeder, S. H. Shah, C. M. Shay, N. L. Spartano, A. Stokes, D. L. Tirschwell, L. B. VanWagner, and C. W. Tsao. Heart disease and stroke statistics-2020 update: A report from the american heart association. *Circulation*, 141(9):e139–e596, 2020.

[8] N. Townsend, M. Nichols, P. Scarborough, and M. Rayner. Cardiovascular disease in europe–epidemiological update 2015. *Eur Heart J*, 36(40):2696–705, 2015.

[9] J. Perk, G. De Backer, H. Gohlke, I. Graham, Z. Reiner, M. Verschuren, C. Albus, P. Benlian, G. Boysen, R. Cifkova, C. Deaton, S. Ebrahim, M. Fisher, G. Germano, R. Hobbs, A. Hoes, S. Karadeniz, A. Mezzani, E. Prescott, L. Ryden, M. Scherer, M. Syvänne, W. J. Scholte op Reimer, C. Vrints, D. Wood, J. L. Zamorano, and F. Zannad. European guidelines on cardiovascular disease prevention in clinical practice (version 2012). the fifth joint task force of the european society of cardiology and other societies on cardiovascular disease prevention in clinical practice (constituted by representatives of nine societies and by invited experts). *Eur Heart J*, 33(13):1635–701, 2012.

[10] Michael J. Pencina, Ann Marie Navar, Daniel Wojdyla, Robert J. Sanchez, Irfan Khan, Joseph Elassal, Ralph B. D'Agostino, Eric D. Peterson, and Allan D. Sniderman. Quantifying importance of major risk factors for coronary heart disease. *Circulation*, 139(13):1603–1611, 2019.

[11] J. Stewart, G. Manmathan, and P. Wilkinson. Primary prevention of cardiovascular disease: A review of contemporary guidance and literature. *JRSM Cardiovasc Dis*, 6:2048004016687211, 2017.

[12] Mark McClellan, Nancy Brown, Robert M. Califf, and John J. Warner. Call to action: Urgent challenges in cardiovascular disease: A presidential advisory from the american heart association. *Circulation*, 139(9):e44–e54, 2019.

[13] F. J. Lin, W. K. Tseng, W. H. Yin, H. I. Yeh, J. W. Chen, and C. C. Wu. Residual risk factors to predict major adverse cardiovascular events in atherosclerotic cardiovascular disease patients with and without diabetes mellitus. *Sci Rep*, 7(1):9179, 2017.

[14] J. Rockberg, L. Jørgensen, B. Taylor, P. Sobocki, and G. Johansson. Risk of mortality and recurrent cardiovascular events in patients with acute coronary syndromes on high intensity statin treatment. *Prev Med Rep*, 6:203–209, 2017.

[15] Y. Hammer, Z. Iakobishvili, D. Hasdai, I. Goldenberg, N. Shlomo, M. Einhorn, T. Bental, G. Witberg, R. Kornowski, and A. Eisen. Guideline-recommended therapies and clinical outcomes according to the risk for recurrent cardiovascular events after an acute coronary syndrome. *J Am Heart Assoc*, 7(18):e009885, 2018.

[16] Kristin M. Engebretsen, Kathleen M. Kaczmarek, Jenifer Morgan, and Joel S. Holger. High-dose insulin therapy in beta-blocker and calcium channel-blocker poisoning. *Clinical Toxicology*, 49(4):277–283, 2011.

[17] Kristian Thygesen, Joseph S. Alpert, Allan S. Jaffe, Bernard R. Chaitman, Jeroen J. Bax, David A. Morrow, Harvey D. White, and null null. Fourth universal definition of myocardial infarction (2018). *Circulation*, 138(20):e618–e651, 2018.

[18] Anita Krishnan, Rajeev Samtani, Preeta Dhanantwari, Elaine Lee, Shigehito Yamada, Kohei Shiota, Mary T. Donofrio, Linda Leatherbury, and Cecilia W. Lo. A detailed comparison of mouse and human cardiac development. *Pediatric Research*, 76(6):500–507, 2014.

[19] Asif T. Chinwalla, Lisa L. Cook, Kimberly D. Delehaunty, Ginger A. Fewell, Lucinda A. Fulton, Robert S. Fulton, Tina A. Graves, LaDeana W. Hillier, Elaine R. Mardis, John D. McPherson, Tracie L. Miner, William E. Nash, Joanne O. Nelson, Michael N. Nhan, Kymberlie H. Pepin, Craig S. Pohl, Tracy C. Ponce, Brian Schultz, Johanna Thompson, Evanne Trevaskis, Robert H. Waterston, Michael C. Wendl, Richard K. Wilson, Shiaw-Pyng Yang, Peter An, Eric Berry, Bruce Birren, Toby Bloom, Daniel G. Brown, Jonathan Butler, Mark Daly, Robert David, Justin Deri, Sheila Dodge, Karen Foley, Diane Gage, Sante Gnerre, Timothy Holzer, David B. Jaffe, Michael Kamal, Elinor K. Karlsson, Cristyn Kells, Andrew Kirby, Edward J. Kulbokas, Eric S. Lander, Tom Landers, J. P. Leger, Rosie Levine, Kerstin Lindblad-Toh, Evan Mauceli, John H. Mayer, Megan McCarthy, Jim Meldrim, Jim Meldrim, Jill P. Mesirov, Robert Nicol, Chad Nusbaum, Steven Seaman, Ted Sharpe, Andrew Sheridan, Jonathan B. Singer, Ralph Santos, Brian Spencer, Nicole Stange-Thomann, Jade P. Vinson, Claire M. Wade, Jamey Wierzbowski, Dudley Wyman, Michael C. Zody, Ewan Birney, Nick Goldman, Arkadiusz Kasprzyk, Emmanuel Mongin, Alistair G. Rust, Guy Slater, Arne Stabenau, Abel Ureta-Vidal, Simon Whelan, Rachel Ainscough, John Attwood, Jonathon Bailey, Karen Barlow, Stephan Beck, John Burton, Michele Clamp, Christopher Clee, Alan Coulson, James Cuff, Val Curwen, Tim Cutts, Joy Davies, Eduardo Eyras, Darren Grafham, Simon Gregory, Tim Hubbard, Adrienne Hunt, Matthew Jones, Ann Joy, Steven Leonard, Christine Lloyd, et al. Initial sequencing and comparative analysis of the mouse genome. *Nature*, 420(6915):520–562, 2002.

[20] Xiaoyu Kan, Yina Wu, Youcai Ma, Congcong Zhang, Ping Li, Lifei Wu, Shuai Zhang, Yulin Li, and Jie Du. Deficiency of il-12p35 improves cardiac repair after myocardial infarction by promoting angiogenesis. *Cardiovascular Research*, 109(2):249–259, 2016.

[21] Vijay K. Singh and Thomas M. Seed. How necessary are animal models for modern drug discovery? *Expert Opinion on Drug Discovery*, 16(12):1391–1397, 2021.

[22] Florian Simon, Alexander Oberhuber, and Hubert Schelzig. Advantages and disadvantages of different animal models for studying ischemia/reperfusion injury of the spinal cord. *European Journal of Vascular and Endovascular Surgery*, 49, 2015.

[23] P. D. Anderson and H. I. Battle. Effects of chloramphenicol on the development of the zebrafish, brachydanio rerio. *Can J Zool*, 45(2):191–204, 1967.

[24] R. Rehwoldt and D. Karimian-Teherani. Uptake and effect of cadmium on zebrafish. *Bull Environ Contam Toxicol*, 15(4):442–6, 1976.

[25] J. F. Skidmore. Resistance to zinc sulphate of the zebrafish (brachydanio rerio hamilton-buchanan) at different phases of its life history. *Ann Appl Biol*, 56(1):47–53, 1965.

[26] George Streisinger, Charline Walker, Nancy Dower, Donna Knauber, and Fred Singer. Production of clones of homozygous diploid zebra fish (brachydanio rerio). *Nature*, 291(5813):293–296, 1981.

[27] Judith S. Eisen. *Chapter 1 - History of Zebrafish Research*, pages 3–14. Academic Press, 2020.

[28] Kerstin Howe, Matthew D. Clark, Carlos F. Torroja, James Torrance, Camille Berthelot, Matthieu Muffato, John E. Collins, Sean Humphray, Karen McLaren, Lucy Matthews, Stuart McLaren, Ian Sealy, Mario Caccamo, Carol Churcher, Carol Scott, Jeffrey C. Barrett, Romke Koch, Gerd-Jörg Rauch, Simon White, William Chow, Britt Kilian, Leonor T. Quintais, José A. Guerra-Assunção, Yi Zhou, Yong Gu, Jennifer Yen, Jan-Hinnerk Vogel, Tina Eyre, Seth Redmond, Ruby Banerjee, Jianxiang Chi, Beiyuan Fu, Elizabeth Langley, Sean F. Maguire, Gavin K. Laird, David Lloyd, Emma Kenyon, Sarah Donaldson, Harminder Sehra, Jeff Almeida-King, Jane Loveland, Stephen Trevanion, Matt Jones, Mike Quail, Dave Willey, Adrienne Hunt, John Burton, Sarah Sims, Kirsten McLay, Bob Plumb, Joy Davis, Chris Clee, Karen Oliver, Richard Clark, Clare Riddle, David Elliott, Glen Threadgold, Glenn Harden, Darren Ware, Sharmin Begum, Beverley Mortimore, Giselle Kerry, Paul Heath, Benjamin Phillimore, Alan Tracey, Nicole Corby, Matthew Dunn, Christopher Johnson, Jonathan Wood, Susan Clark, Sarah Pelan, Guy Griffiths, Michelle Smith, Rebecca Glithero, Philip Howden, Nicholas Barker, Christine Lloyd, Christopher Stevens, Joanna Harley, Karen Holt, Georgios Panagiotidis, Jamieson Lovell, Helen Beasley, Carl Henderson, Daria Gordon, Katherine Auger, Deborah Wright, Joanna Collins, Claire Raisen, Lauren Dyer, Kenric Leung, Lauren Robertson, Kirsty Ambridge, Daniel Leongamornlert, Sarah McGuire, Ruth Gilderthorp, Coline Griffiths, Deepa Manthravadi, Sarah Nichol, Gary Barker, et al. The zebrafish reference genome sequence and its relationship to the human genome. *Nature*, 496(7446):498–503, 2013.

[29] P. Giardoglou and D. Beis. On zebrafish disease models and matters of the heart. *Biomedicines*, 7(1), 2019.

[30] M. S. Dickover, R. Zhang, P. Han, and N. C. Chi. Zebrafish cardiac injury and regeneration models: a noninvasive and invasive in vivo model of cardiac regeneration. *Methods Mol Biol*, 1037:463–73, 2013.

[31] R. Ryan, B. R. Moyse, and R. J. Richardson. Zebrafish cardiac regeneration-looking beyond cardiomyocytes to a complex microenvironment. *Histochem Cell Biol*, 154(5):533–548, 2020.

[32] Tae-Young Choi, Tae-Ik Choi, Yu-Ri Lee, Seong-Kyu Choe, and Cheol-Hee Kim. Zebrafish as an animal model for biomedical research. *Experimental Molecular Medicine*, 53(3):310–317, 2021.

[33] D. Bournele and D. Beis. Zebrafish models of cardiovascular disease. *Heart Fail Rev*, 21(6):803–813, 2016.

[34] B. J. Haubner, M. Adamowicz-Brice, S. Khadayate, V. Tiefenthaler, B. Metzler, T. Aitman, and J. M. Penninger. Complete cardiac regeneration in a mouse model of myocardial infarction. *Aging (Albany NY)*, 4(12):966–77, 2012.

[35] M. Gemberling, T. J. Bailey, D. R. Hyde, and K. D. Poss. The zebrafish as a model for complex tissue regeneration. *Trends Genet*, 29(11):611–20, 2013.

[36] A. W. Seifert and K. Muneoka. The blastema and epimorphic regeneration in mammals. *Dev Biol*, 433(2):190–199, 2018.

[37] S. A. Brittijn, S. J. Duivesteijn, M. Belmamoune, L. F. Bertens, W. Bitter, J. D. de Bruijn, D. L. Champagne, E. Cuppen, G. Flik, C. M. Vandenbroucke-Grauls, R. A. Janssen, I. M. de Jong, E. R. de Kloet, A. Kros, A. H. Meijer, J. R. Metz, A. M. van der Sar, M. J. Schaaf, S. Schulte-Merker, H. P. Spaink, P. P. Tak, F. J. Verbeek, M. J. Vervoordeldonk, F. J. Vonk, F. Witte, H. Yuan, and M. K. Richardson. Zebrafish development and regeneration: new tools for biomedical research. *Int J Dev Biol*, 53(5-6):835–50, 2009.

[38] S. P. Singh, J. E. Holdway, and K. D. Poss. Regeneration of amputated zebrafish fin rays from de novo osteoblasts. *Dev Cell*, 22(4):879–86, 2012.

[39] K. Kikuchi, J. E. Holdway, A. A. Werdich, R. M. Anderson, Y. Fang, G. F. Egnaczyk, T. Evans, C. A. Macrae, D. Y. Stainier, and K. D. Poss. Primary contribution to zebrafish heart regeneration by gata4(+) cardiomyocytes. *Nature*, 464(7288):601–5, 2010.

[40] Chris Jopling, Eduard Sleep, Marina Raya, Mercè Martí, Angel Raya, and Juan Carlos Izpisúa Belmonte. Zebrafish heart regeneration occurs by cardiomyocyte dedifferentiation and proliferation. *Nature*, 464(7288):606–609, 2010.

[41] E. Elizabeth Patton, Leonard I. Zon, and David M. Langenau. Zebrafish disease models in drug discovery: from preclinical modelling to clinical trials. *Nature Reviews Drug Discovery*, 20(8):611–628, 2021.

[42] Calum A. MacRae and Randall T. Peterson. Zebrafish as tools for drug discovery. *Nature Reviews Drug Discovery*, 14(10):721–731, 2015.

[43] David J. Milan, Travis A. Peterson, Jeremy N. Ruskin, Randall T. Peterson, and Calum A. MacRae. Drugs that induce repolarization abnormalities cause bradycardia in zebrafish. *Circulation*, 107(10):1355–1358, 2003.

[44] E. de Pater, L. Clijsters, S. R. Marques, Y. F. Lin, Z. V. Garavito-Aguilar, D. Yelon, and J. Bakkers. Distinct phases of cardiomyocyte differentiation regulate growth of the zebrafish heart. *Development*, 136(10):1633–41, 2009.

[45] S. Lazic and I. C. Scott. Mef2cb regulates late myocardial cell addition from a second heart field-like population of progenitors in zebrafish. *Dev Biol*, 354(1):123–33, 2011.

[46] S. Burkhard, V. van Eif, L. Garric, V. M. Christoffels, and J. Bakkers. On the evolution of the cardiac pacemaker. *J Cardiovasc Dev Dis*, 4(2), 2017.

[47] I. P. Temple, S. Inada, H. Dobrzynski, and M. R. Boyett. Connexins and the atrioventricular node. *Heart Rhythm*, 10(2):297–304, 2013.

[48] Giuseppe Moruzzi. The electrophysiological work of carlo matteucci. *Brain Research Bulletin*, 40(2):69–91, 1996.

[49] M. AlGhatrif and J. Lindsay. A brief review: history to understand fundamentals of electrocardiography. *J Community Hosp Intern Med Perspect*, 2(1), 2012.

[50] J. R. Henson. Descartes and the ecg lettering series. *J Hist Med Allied Sci*, 26(2):181–6, 1971.

[51] W. Einthoven, G. Fahr, and A. De Waart. On the direction and manifest size of the variations of potential in the human heart and on the influence of the position of the heart on the form of the electrocardiogram. *Am Heart J*, 40(2):163–211, 1950.

[52] G. D. Gargiulo, P. Bifulco, M. Cesarelli, A. L. McEwan, H. Moeinzadeh, A. O'Loughlin, I. M. Shugman, J. C. Tapson, and A. Thiagalingam. On the einthoven triangle: A critical analysis of the single rotating dipole hypothesis. *Sensors (Basel)*, 18(7), 2018.

[53] D. E. Becker. Fundamentals of electrocardiography interpretation. *Anesth Prog*, 53(2):53–63; quiz 64, 2006.

[54] Tibor Stracina, Marina Ronzhina, Richard Redina, and Marie Novakova. Golden standard or obsolete method? review of ecg applications in clinical and experimental context. *Frontiers in Physiology*, 13, 2022.

[55] Lionte Catalina, Bologa Cristina, and Sorodoc Laurentiu. *Toxic and Drug-Induced Changes of the Electrocardiogram*, page Ch. 15. IntechOpen, Rijeka, 2012.

[56] Mina Behzadi, Siyavash Joukar, and Ahmad Beik. Opioids and cardiac arrhythmia: A literature review. *Medical Principles and Practice*, 27(5):401–414, 2018.

[57] Y. Zhao, M. Yun, S. A. Nguyen, M. Tran, and T. P. Nguyen. In vivo surface electrocardiography for adult zebrafish. *J Vis Exp*, (150), 2019.

[58] Bonifasius Putera Sampurna, Gilbert Audira, Stevhen Juniardi, Yu-Heng Lai, and Chung-Der Hsiao. A simple imagej-based method to measure cardiac rhythm in zebrafish embryos. *Inventions*, 3(2):21, 2018.

[59] D. S. Peal, R. W. Mills, S. N. Lynch, J. M. Mosley, E. Lim, P. T. Ellinor, C. T. January, R. T. Peterson, and D. J. Milan. Novel chemical suppressors of long qt syndrome identified by an in vivo functional screen. *Circulation*, 123(1):23–30, 2011.

[60] Yali Zhao, Nicholas A. James, Ashraf R. Beshay, Eileen E. Chang, Andrew Lin, Faiza Bashar, Abram Wassily, Binh Nguyen, and Thao P. Nguyen. Adult zebrafish ventricular electrical gradients as tissue mechanisms of ecg patterns under baseline vs. oxidative stress. *Cardiovascular Research*, 117(8):1891–1907, 2021.

[61] M. H. Lin, H. C. Chou, Y. F. Chen, W. Liu, C. C. Lee, L. Y. M. Liu, and Y. J. Chuang. Development of a rapid and economic in vivo electrocardiogram platform for cardiovascular drug assay and electrophysiology research in adult zebrafish. *Scientific Reports*, 8(1), 2018.

[62] G. H. Chaudhari, K. S. Chennubhotla, K. Chatti, and P. Kulkarni. Optimization of the adult zebrafish ecg method for assessment of drug-induced qtc prolongation. *Journal of Pharmacological and Toxicological Methods*, 67(2):115–120, 2013.

[63] C. C. Liu, L. Li, Y. W. Lam, C. W. Siu, and S. H. Cheng. Improvement of surface ecg recording in adult zebrafish reveals that the value of this model exceeds our expectation. *Scientific Reports*, 6, 2016.

[64] M. R. Stoyek, E. A. Rog-Zielinska, and T. A. Quinn. Age-associated changes in electrical function of the zebrafish heart. *Progress in Biophysics and Molecular Biology*, 138:91–104, 2018.

[65] H. Cao, F. Yu, Y. Zhao, X. Zhang, J. Tai, J. Lee, A. Darehzereshki, M. Bersohn, C. L. Lien, N. C. Chi, Y. C. Tai, and T. K. Hsiai. Wearable multi-channel microelectrode membranes for elucidating electrophysiological phenotypes of injured myocardium. *Integrative Biology (United Kingdom)*, 6(8):789–795, 2014.

[66] M. Lenning, J. Fortunato, T. Le, I. Clark, A. Sherpa, S. Yi, P. Hofsteen, G. Thamilarasu, J. Yang, X. Xu, H. D. Han, T. K. Hsiai, and H. Cao. Real-time monitoring and analysis of zebrafish electrocardiogram with anomaly detection. *Sensors (Basel)*, 18(1), 2017.

[67] F. Yu, Y. Zhao, J. Gu, K. L. Quigley, N. C. Chi, Y. C. Tai, and T. K. Hsiai. Flexible microelectrode arrays to interface epicardial electrical signals with intracardial calcium transients in zebrafish hearts. *Biomedical Microdevices*, 14(2):357–366, 2012.

[68] S. J. Cho, D. Byun, T. S. Nam, S. Y. Choi, B. G. Lee, M. K. Kim, and S. Kim. Zebrafish as an animal model in epilepsy studies with multichannel eeg recordings. *Scientific Reports*, 7(1), 2017.

[69] T. Le, J. Zhang, X. Xia, X. Xu, I. Clark, L. Schmiess-Heine, A. H. Nguyen, M. P. H. Lau, and H. Cao. Continuous electrocardiogram monitoring in zebrafish with prolonged mild anesthesia. In *Proceedings of the Annual International Conference of the IEEE Engineering in Medicine and Biology Society, EMBS*, volume 2020-July, pages 2610–2613.

[70] O. Monfredi and M. R. Boyett. Sick sinus syndrome and atrial fibrillation in older persons — a view from the sinoatrial nodal myocyte. *Journal of Molecular and Cellular Cardiology*, 83:88–100, 2015.

[71] V. Adán and L. A. Crown. Diagnosis and treatment of sick sinus syndrome. *American Family Physician*, 67(8):1725–1732+1738, 2003.

[72] M. R. Carrión-Camacho, I. Marín-León, J. M. Molina-Doñoro, and J. R. González-López. Safety of permanent pacemaker implantation: A prospective study. *J Clin Med*, 8(1), 2019.

[73] M. Semelka, J. Gera, and S. Usman. Sick sinus syndrome: A review. *American Family Physician*, 87(10):691–696, 2013.

[74] M. L. Bakker, G. J. J. Boink, B. J. Boukens, A. O. Verkerk, M. Van Den Boogaard, A. D. Den Haan, W. M. H. Hoogaars, H. P. Buermans, J. M. T. De Bakker, J. Seppen, H. L. Tan, A. F. M. Moorman, P. A. C. T Hoen, and V. M. Christoffels. T-box transcription factor tbx3 reprogrammes mature cardiac myocytes into pacemaker-like cells. *Cardiovascular Research*, 94(3):439–449, 2012.

[75] M. Choudhury, N. Black, A. Alghamdi, A. D'souza, R. Wang, J. Yanni, H. Dobrzynski, P. A. Kingston, H. Zhang, M. R. Boyett, and G. M. Morris. Tbx18 overexpression enhances pacemaker function in a rat subsidiary atrial pacemaker model of sick sinus syndrome. *Journal of Physiology*, 596(24):6141–6155, 2018.

[76] A. M. Wilde Arthur and S. Amin Ahmad. Clinical spectrum of scn5a mutations. *JACC: Clinical Electrophysiology*, 4(5):569–579, 2018.

[77] J. E. Tisdale, M. K. Chung, K. B. Campbell, M. Hammadah, J. A. Joglar, J. Leclerc, and B. Rajagopalan. Drug-induced arrhythmias: A scientific statement from the american heart association. *Circulation*, 142(15):e214–e233, 2020.

[78] S. Nagasawa, H. Saitoh, S. Kasahara, F. Chiba, S. Torimitsu, H. Abe, D. Yajima, and H. Iwase. Relationship between kcnq1 (lqt1) and kcnh2 (lqt2) gene mutations and sudden death during illegal drug use. *Sci Rep*, 8(1):8443, 2018.

[79] B. L. Henry, A. Minassian, and W. Perry. Effect of methamphetamine dependence on heart rate variability. *Addict Biol*, 17(3):648–58, 2012.

[80] T. Le, M. Lenning, I. Clark, I. Bhimani, J. Fortunato, P. Marsh, X. Xu, and H. Cao. Acquisition, processing and analysis of electrocardiogram in awake zebrafish. *IEEE Sensors Journal*, 19(11):4283–4289, 2019.

[81] H. C. Bazett. An analysis of the time-relations of electrocardiograms. *Annals of Noninvasive Electrocardiology*, 2(2):177–194, 1997.

[82] Fred Shaffer and J. P. Ginsberg. An overview of heart rate variability metrics and norms. *Frontiers in Public Health*, 5, 2017.

[83] M. Matthews and Z. M. Varga. Anesthesia and euthanasia in zebrafish. *Ilar j*, 53(2):192–204, 2012.

[84] P. Sun, Y. Zhang, F. Yu, E. Parks, A. Lyman, Q. Wu, L. Ai, C. H. Hu, Q. Zhou, K. Shung, C. L. Lien, and T. K. Hsiai. Micro-electrocardiograms to study post-ventricular amputation of zebrafish heart. *Annals of Biomedical Engineering*, 37(5):890–901, 2009.

[85] S. Attili and S. M. Hughes. Anaesthetic tricaine acts preferentially on neural voltage-gated sodium channels and fails to block directly evoked muscle contraction. *PLoS One*, 9(8):e103751, 2014.

[86] L. Lee, C. E. Genge, M. Cua, X. Sheng, K. Rayani, M. F. Beg, M. V. Sarunic, and G. F. Tibbits. Functional assessment of cardiac responses of adult zebrafish (danio rerio) to acute and chronic temperature change using high-resolution echocardiography. *PLoS One*, 11(1):e0145163, 2016.

[87] M. Maricondi-Massari, A. L. Kalinin, M. L. Glass, and F. T. Rantin. The effects of temperature on oxygen uptake, gill ventilation and ecg-waveforms in the nile tilapia, oreochromis niloticus. *Journal of Thermal Biology*, 23(5):283–290, 1998.

[88] Rachael Morgan, Anna H. Andreassen, Eirik R. Åsheim, Mette H. Finnøen, Gunnar Dresler, Tore Brembu, Adrian Loh, Joanna J. Miest, and Fredrik Jutfelt. Reduced physiological plasticity in a fish adapted to stable temperatures. *Proceedings of the National Academy of Sciences*, 119(22):e2201919119, 2022.

[89] R. W. van Leeuwen, D. H. Brundel, C. Neef, T. van Gelder, R. H. Mathijssen, D. M. Burger, and F. G. Jansman. Prevalence of potential drug-drug interactions in cancer patients treated with oral anticancer drugs. *Br J Cancer*, 108(5):1071–8, 2013.

[90] Liang Chih-Sung and Huang Yao-Chin. Methamphetamine-associated qtc prolongation in a dose-dependent and reversible manner. *The Journal of Neuropsychiatry and Clinical Neurosciences*, 25(2):E58–E58, 2013.

[91] J. Yan, H. Li, H. Bu, K. Jiao, A. X. Zhang, T. Le, H. Cao, Y. Li, Y. Ding, and X. Xu. Aging-associated sinus arrest and sick sinus syndrome in adult zebrafish. *PLoS ONE*, 15(5), 2020.

[92] A. Mente, M. O'Donnell, S. Rangarajan, G. Dagenais, S. Lear, M. McQueen, R. Diaz, A. Avezum, P. Lopez-Jaramillo, F. Lanas, W. Li, Y. Lu, S. Yi, L. Rensheng, R. Iqbal, P. Mony, R. Yusuf, K. Yusoff, A. Szuba, A. Oguz, A. Rosengren, A. Bahonar, A. Yusufali, A. E. Schutte, J. Chifamba, J. F. E. Mann, S. S. Anand, K. Teo, and S. Yusuf. Associations of urinary sodium excretion with cardiovascular events in individuals with and without hypertension: a pooled analysis of data from four studies. *The Lancet*, 388(10043):465–475, 2016.

[93] A. L. George Jr. Inherited disorders of voltage-gated sodium channels. *Journal of Clinical Investigation*, 115(8):1990–1999, 2005.

[94] C. Antzelevitch. Brugada syndrome. *PACE - Pacing and Clinical Electrophysiology*, 29(10):1130–1159, 2006.

[95] Y. Mizusawa and A. A. M. Wilde. Brugada syndrome. *Circulation: Arrhythmia and Electrophysiology*, 5(3):606–616, 2012.

[96] D. Darbar, P. J. Kannankeril, B. S. Donahue, G. Kucera, T. Stubblefield, J. L. Haines, A. L. George, and D. M. Roden. Cardiac sodium channel (scn5a) variants associated with atrial fibrillation. *Circulation*, 117(15):1927–1935, 2008.

[97] Man Liu, Kai-Chien Yang, and Samuel C. Dudley. Cardiac sodium channel mutations: why so many phenotypes? *Nature Reviews Cardiology*, 11(10):607–615, 2014.

[98] W. P. McNair, G. Sinagra, M. R. G. Taylor, A. Di Lenarda, D. A. Ferguson, E. E. Salcedo, D. Slavov, X. Zhu, J. H. Caldwell, and L. Mestroni. Scn5a mutations associate with arrhythmic dilated cardiomyopathy and commonly localize to the voltage-sensing mechanism. *Journal of the American College of Cardiology*, 57(21):2160–2168, 2011.

[99] Thao P. Nguyen, Dao W. Wang, Thomas H. Rhodes, and Alfred L. George. Divergent biophysical defects caused by mutant sodium channels in dilated cardiomyopathy with arrhythmia. *Circulation Research*, 102(3):364–371, 2008.

[100] Christopher G. Kevil, Nicholas E. Goeders, Matthew D. Woolard, Md Shenuarin Bhuiyan, Paari Dominic, Gopi K. Kolluru, Connie L. Arnold, James G. Traylor, and A. Wayne Orr. Methamphetamine use and cardiovascular disease. *Arteriosclerosis, Thrombosis, and Vascular Biology*, 39(9):1739–1746, 2019.

[101] D. J. Heal, S. L. Smith, J. Gosden, and D. J. Nutt. Amphetamine, past and present–a pharmacological and clinical perspective. *J Psychopharmacol*, 27(6):479–96, 2013.

[102] M. G. Kirkpatrick, E. W. Gunderson, C. E. Johanson, F. R. Levin, R. W. Foltin, and C. L. Hart. Comparison of intranasal methamphetamine and d-amphetamine self-administration by humans. *Addiction*, 107(4):783–91, 2012.

[103] S. D. Robertson, H. J. Matthies, and A. Galli. A closer look at amphetamine-induced reverse transport and trafficking of the dopamine and norepinephrine transporters. *Mol Neurobiol*, 39(2):73–80, 2009.

[104] A. E. Fleckenstein, T. J. Volz, E. L. Riddle, J. W. Gibb, and G. R. Hanson. New insights into the mechanism of action of amphetamines. *Annu Rev Pharmacol Toxicol*, 47:681–98, 2007.

[105] Matthew W. Warren, Firas H. Kobeissy, Ming Cheng Liu, Ronald L. Hayes, Mark S. Gold, and Kevin K. W. Wang. Concurrent calpain and caspase-3 mediated proteolysis of ii-spectrin and tau in rat brain after methamphetamine exposure: A similar profile to traumatic brain injury. *Life Sciences*, 78(3):301–309, 2005.

[106] S. A. Lloyd, B. Corkill, M. C. Bruster, R. L. Roberts, and R. A. Shanks. Chronic methamphetamine exposure significantly decreases microglia activation in the arcuate nucleus. *J Chem Neuroanat*, 82:5–11, 2017.

[107] P. Melo, A. Magalhães, C. J. Alves, M. A. Tavares, L. de Sousa, T. Summavielle, and P. Moradas-Ferreira. Methamphetamine mimics the neurochemical profile of aging in rats and impairs recognition memory. *Neurotoxicology*, 33(3):491–9, 2012.

[108] S. Won, R. A. Hong, R. V. Shohet, T. B. Seto, and N. I. Parikh. Methamphetamine-associated cardiomyopathy. *Clin Cardiol*, 36(12):737–42, 2013.

[109] K. J. Varner, B. A. Ogden, J. Delcarpio, and S. Meleg-Smith. Cardiovascular responses elicited by the "binge" administration of methamphetamine. *J Pharmacol Exp Ther*, 301(1):152–9, 2002.

[110] J. Li, J. Li, Y. Chen, Y. Xu, W. Li, Y. Chen, and K. Cui. Methamphetamine use associated with monomorphic ventricular tachycardia. *J Addict Med*, 8(6):470–3, 2014.

[111] W. Haning and D. Goebert. Electrocardiographic abnormalities in methamphetamine abusers. *Addiction*, 102 Suppl 1:70–5, 2007.

[112] E. D. Paratz, N. J. Cunningham, and A. I. MacIsaac. The cardiac complications of methamphetamines. *Heart Lung Circ*, 25(4):325–32, 2016.

[113] M. N. Islam, H. Kuroki, B. Hongcheng, Y. Ogura, N. Kawaguchi, S. Onishi, and C. Wakasugi. Cardiac lesions and their reversibility after long term administration of methamphetamine. *Forensic Sci Int*, 75(1):29–43, 1995.

[114] Javier E. Lopez, Khung Yeo, Gary Caputo, Michael Buonocore, and Saul Schaefer. Recovery of methamphetamine associated cardiomyopathy predicted by late gadolinium enhanced cardiovascular magnetic resonance. *Journal of Cardiovascular Magnetic Resonance*, 11(1):46, 2009.

[115] H. Kuribara and Y. Uchihashi. Dopamine antagonists can inhibit methamphetamine sensitization, but not cocaine sensitization, when assessed by ambulatory activity in mice. *J Pharm Pharmacol*, 45(12):1042–5, 1993.

[116] Kari A. Johnson and David M. Lovinger. Presynaptic g protein-coupled receptors: Gatekeepers of addiction? *Frontiers in Cellular Neuroscience*, 10, 2016.

[117] J. Wang, C. Gareri, and H. A. Rockman. G-protein-coupled receptors in heart disease. *Circ Res*, 123(6):716–735, 2018.

[118] N. Kumari, S. Reabroi, and B. J. North. Unraveling the molecular nexus between gpcrs, ers, and emt. *Mediators Inflamm*, 2021:6655417, 2021.

[119] U. Sriram, J. M. Cenna, B. Haldar, N. C. Fernandes, R. Razmpour, S. Fan, S. H. Ramirez, and R. Potula. Methamphetamine induces trace amine-associated receptor 1 (taar1) expression in human t lymphocytes: role in immunomodulation. *J Leukoc Biol*, 99(1):213–23, 2016.

[120] Beth Borowsky, Nika Adham, Kenneth A. Jones, Rita Raddatz, Roman Artymyshyn, Kristine L. Ogozalek, Margaret M. Durkin, Parul P. Lakhlani, James A. Bonini, Sudam Pathirana, Noel Boyle, Xiaosui Pu, Evguenia Kouranova, Harvey Lichtblau, F. Yulina Ochoa, Theresa A. Branchek, and Christophe Gerald. Trace amines: Identification of a family of mammalian g protein-coupled receptors. *Proceedings of the National Academy of Sciences*, 98(16):8966–8971, 2001.

[121] I. Miranda, A. Souza, P. Sousa, J. Ribeiro, E. M. S. Castanheira, R. Lima, and G. Minas. Properties and applications of pdms for biomedical engineering: A review. *J Funct Biomater*, 13(1), 2021.

[122] E. Tackie-Yarboi, A. Wisner, A. Horton, T. Q. T. Chau, J. Reigle, A. J. Funk, R. E. McCullumsmith, F. S. Hall, F. E. Williams, and I. T. Schiefer. Combining neurobehavioral analysis and in vivo photoaffinity labeling to understand protein targets of methamphetamine in casper zebrafish. *ACS Chem Neurosci*, 11(17):2761–2773, 2020.

[123] V. Sander, G. Suñe, C. Jopling, C. Morera, and J. C. Izpisua Belmonte. Isolation and in vitro culture of primary cardiomyocytes from adult zebrafish hearts. *Nat Protoc*, 8(4):800–9, 2013.

[124] Amyaouch Bradaia, Gerhard Trube, Henri Stalder, Roger D. Norcross, Laurence Ozmen, Joseph G. Wettstein, Audrée Pinard, Danièle Buchy, Martin Gassmann, Marius C. Hoener, and Bernhard Bettler. The selective antagonist epptb reveals taar1-mediated regulatory mechanisms in dopaminergic neurons of the mesolimbic system. *Proceedings of the National Academy of Sciences*, 106(47):20081–20086, 2009.

[125] Robert D. Harvey and Colleen E. Clancy. Mechanisms of camp compartmentation in cardiac myocytes: experimental and computational approaches to understanding. *The Journal of Physiology*, 599(20):4527–4544, 2021.

[126] C. W. Schindler, J. W. Zheng, S. R. Tella, and S. R. Goldberg. Pharmacological mechanisms in the cardiovascular effects of methamphetamine in conscious squirrel monkeys. *Pharmacol Biochem Behav*, 42(4):791–6, 1992.

[127] W. Kobinger and L. Pichler. Differentiation of drugs acting centrally upon the cardiovascular system by means of sympathetic and vagal responses. *Clin Exp Hypertens (1978)*, 1(2):229–49, 1978.

[128] M. E. Field, P. Donateo, N. Bottoni, M. Iori, M. Brignole, R. T. Kipp, D. E. Kopp, M. A. Leal, L. L. Eckhardt, J. M. Wright, K. E. Walsh, R. L. Page, and M. H. Hamdan. P-wave amplitude and pr changes in patients with inappropriate sinus tachycardia: Findings supportive of a central mechanism. *J Am Heart Assoc*, 7(9), 2018.

[129] F. Sessa, V. Anna, G. Messina, G. Cibelli, V. Monda, G. Marsala, M. Ruberto, A. Biondi, O. Cascio, G. Bertozzi, D. Pisanelli, F. Maglietta, A. Messina, M. P. Mollica, and M. Salerno. Heart rate variability as predictive factor for sudden cardiac death. *Aging (Albany NY)*, 10(2):166–177, 2018.

[130] A. E. Draghici and J. A. Taylor. The physiological basis and measurement of heart rate variability in humans. *J Physiol Anthropol*, 35(1):22, 2016.

[131] B. L. Henry, A. Minassian, and W. Perry. Effect of methamphetamine dependence on heart rate variability. *Addict Biol*, 17(3):648–58, 2012.

[132] Pavan K. V. Reddy, Tien M. H. Ng, Esther E. Oh, Gassan Moady, and Uri Elkayam. Clinical characteristics and management of methamphetamine-associated cardiomyopathy: State-of-the-art review. *Journal of the American Heart Association*, 9(11):e016704, 2020.

[133] S. M. Pikkujämsä, H. V. Huikuri, K. E. Airaksinen, A. O. Rantala, H. Kauma, M. Lilja, M. J. Savolainen, and Y. A. Kesäniemi. Heart rate variability and baroreflex sensitivity in hypertensive subjects with and without metabolic features of insulin resistance syndrome. *Am J Hypertens*, 11(5):523–31, 1998.

[134] E. Bazmi, F. Mousavi, L. Giahchin, T. Mokhtari, and B. Behnoush. Cardiovascular complications of acute amphetamine abuse: Cross-sectional study. *Sultan Qaboos Univ Med J*, 17(1):e31–e37, 2017.

[135] A. Sinha, O. Lewis, R. Kumar, S. L. Yeruva, and B. H. Curry. Amphetamine abuse related acute myocardial infarction. *Case Rep Cardiol*, 2016:7967851, 2016.

[136] Q. Wang, T. Michiue, T. Ishikawa, B. L. Zhu, and H. Maeda. Combined analyses of creatine kinase mb, cardiac troponin i and myoglobin in pericardial and cerebrospinal fluids to investigate myocardial and skeletal muscle injury in medicolegal autopsy cases. *Leg Med (Tokyo)*, 13(5):226–32, 2011.

[137] S. Ahnve. Correction of the qt interval for heart rate: review of different formulas and the use of bazett's formula in myocardial infarction. *Am Heart J*, 109(3 Pt 1):568–74, 1985.

[138] Liang Chih-Sung and Huang Yao-Chin. Methamphetamine-associated qtc prolongation in a dose-dependent and reversible manner. *The Journal of Neuropsychiatry and Clinical Neurosciences*, 25(2):E58–E58, 2013.

[139] P. Debonnaire, S. Katsanos, E. Joyce, Van Den Brink OV, D. E. Atsma, M. J. Schalij, J. J. Bax, V. Delgado, and N. A. Marsan. Qrs fragmentation and qtc duration relate to malignant ventricular tachyarrhythmias and sudden cardiac death in patients with hypertrophic cardiomyopathy. *J Cardiovasc Electrophysiol*, 26(5):547–55, 2015.

[140] L. M. Ryerson and R. M. Giuffre. Qt intervals in metabolic dilated cardiomyopathy. *Can J Cardiol*, 22(3):217–20, 2006.

[141] Y. H. Qu, K. P. Leung, D. F. Qiao, D. R. Li, C. Liu, X. Yue, and H. J. Wang. Remodeling of ion channel expression may contribute to electrophysiological consequences caused by methamphetamine in vitro and in vivo. *Biochem Biophys Res Commun*, 443(2):441–6, 2014.

[142] R. R. Shah. Drug-induced qt interval shortening: potential harbinger of proarrhythmia and regulatory perspectives. *Br J Pharmacol*, 159(1):58–69, 2010.

[143] S. Jayanthi, O. V. Torres, B. Ladenheim, and J. L. Cadet. A single prior injection of methamphetamine enhances methamphetamine self-administration (sa) and blocks sa-induced changes in dna methylation and mrna expression of potassium channels in the rat nucleus accumbens. *Mol Neurobiol*, 57(3):1459–1472, 2020.

[144] K. Sugimoto, K. Okamura, H. Tanaka, S. Takashima, H. Ochi, T. Yamamoto, and R. Matoba. Methamphetamine directly accelerates beating rate in cardiomyocytes by

increasing ca(2+) entry via l-type ca(2+) channel. *Biochem Biophys Res Commun*, 390(4):1214–20, 2009.

[145] R. Liang, Y. Zhou, F. Wu, C. Zhou, X. Zhao, M. Zhang, X. Tian, and B. Zhu. Effect of methamphetamine on potassium and l-type calcium currents in rat ventricular myocytes. *Toxicol Mech Methods*, 20(8):458–65, 2010.

[146] A. Scholz. Mechanisms of (local) anaesthetics on voltage-gated sodium and other ion channels. *Br J Anaesth*, 89(1):52–61, 2002.

[147] P. Sun, Y. Zhang, F. Yu, E. Parks, A. Lyman, Q. Wu, L. Ai, C. H. Hu, Q. Zhou, K. Shung, C. L. Lien, and T. K. Hsiai. Micro-electrocardiograms to study post-ventricular amputation of zebrafish heart. *Ann Biomed Eng*, 37(5):890–901, 2009.

[148] R. Dziaman, B. Kłyszejko, and G. Hajek. The effect of ms-222 on the cardiac and respiratory function and behaviour of common carp, cyprinus carpio l., during general anaesthesia. *Acta Ichthyologica et Piscatoria*, 35(2):125–131, 2005.

[149] J. P. Owen and R. N. Kelsh. A suitable anaesthetic protocol for metamorphic zebrafish. *PLoS One*, 16(3):e0246504, 2021.

[150] C. H. Kwon and S. H. Kim. Intraoperative management of critical arrhythmia. *Korean J Anesthesiol*, 70(2):120–126, 2017.

[151] I. Hoyer and P. A. van Zwieten. The centrally induced fall in blood pressure after the infusion of amphetamine and related drugs into the vertebral artery of the cat. *J Pharm Pharmacol*, 23(11):892–3, 1971.

[152] D. B. Vaupel, C. W. Schindler, S. Chefer, A. M. Belcher, I. Ahmet, K. B. Scheidweiler, M. A. Huestis, and E. A. Stein. Delayed emergence of methamphetamine's enhanced cardiovascular effects in nonhuman primates during protracted methamphetamine abstinence. *Drug Alcohol Depend*, 159:181–9, 2016.

[153] B. S. Muntean, C. M. Horvat, J. H. Behler, W. A. Aboualaiwi, A. M. Nauli, F. E. Williams, and S. M. Nauli. A comparative study of embedded and anesthetized zebrafish in vivo on myocardiac calcium oscillation and heart muscle contraction. *Front Pharmacol*, 1:139, 2010.

[154] M. Casanovas, I. Reyes-Resina, A. Lillo, J. Lillo, R. López-Arnau, J. Camarasa, E. Escubedo, G. Navarro, and R. Franco. Methamphetamine blocks adenosine a(2a) receptor activation via sigma 1 and cannabinoid cb(1) receptors. *Int J Mol Sci*, 22(5), 2021.

[155] M. Fehler, K. J. Broadley, W. R. Ford, and E. J. Kidd. Identification of trace-amine-associated receptors (taar) in the rat aorta and their role in vasoconstriction by -phenylethylamine. *Naunyn Schmiedebergs Arch Pharmacol*, 382(4):385–98, 2010.

[156] K. J. Broadley, M. Fehler, W. R. Ford, and E. J. Kidd. Functional evaluation of the receptors mediating vasoconstriction of rat aorta by trace amines and amphetamines. *Eur J Pharmacol*, 715(1-3):370–80, 2013.

[157] C. S. Abdullah, R. Aishwarya, S. Alam, M. Morshed, N. S. Remex, S. Nitu, G. K. Kolluru, J. Traylor, S. Miriyala, M. Panchatcharam, B. Hartman, J. King, M. A. N. Bhuiyan, S. Chandran, M. D. Woolard, X. Yu, N. E. Goeders, P. Dominic, C. L. Arnold, K. Stokes, C. G. Kevil, A. W. Orr, and M. S. Bhuiyan. Methamphetamine induces cardiomyopathy by sigmar1 inhibition-dependent impairment of mitochondrial dynamics and function. *Commun Biol*, 3(1):682, 2020.

[158] Hasitha Chavva, Daniel A. Brazeau, James Denvir, Donald A. Primerano, Jun Fan, Sarah L. Seeley, and Boyd R. Rorabaugh. Methamphetamine-induced changes in myocardial gene transcription are sex-dependent. *BMC Genomics*, 22(1):259, 2021.

[159] N. B. Miner, J. S. Elmore, M. H. Baumann, T. J. Phillips, and A. Janowsky. Trace amine-associated receptor 1 regulation of methamphetamine-induced neurotoxicity. *Neurotoxicology*, 63:57–69, 2017.

[160] K. Ravid, L. I. Smith-Mungo, Z. Zhao, K. M. Thomas, and H. M. Kagan. Upregulation of lysyl oxidase in vascular smooth muscle cells by camp: role for adenosine receptor activation. *J Cell Biochem*, 75(1):177–85, 1999.

[161] M. Grimm and J. H. Brown. Beta-adrenergic receptor signaling in the heart: role of camkii. *J Mol Cell Cardiol*, 48(2):322–30, 2010.

[162] P. D. Swaminathan, A. Purohit, T. J. Hund, and M. E. Anderson. Calmodulin-dependent protein kinase ii: linking heart failure and arrhythmias. *Circ Res*, 110(12):1661–77, 2012.

[163] D. M. Hedges, J. D. Obray, J. T. Yorgason, E. Y. Jang, V. K. Weerasekara, J. D. Uys, F. P. Bellinger, and S. C. Steffensen. Methamphetamine induces dopamine release in the nucleus accumbens through a sigma receptor-mediated pathway. *Neuropsychopharmacology*, 43(6):1405–1414, 2018.

[164] F. Limanaqi, S. Gambardella, F. Biagioni, C. L. Busceti, and F. Fornai. Epigenetic effects induced by methamphetamine and methamphetamine-dependent oxidative stress. *Oxid Med Cell Longev*, 2018:4982453, 2018.

[165] S. Hernandez-Lopez, T. Tkatch, E. Perez-Garci, E. Galarraga, J. Bargas, H. Hamm, and D. J. Surmeier. D2 dopamine receptors in striatal medium spiny neurons reduce l-type ca2+ currents and excitability via a novel plc[beta]1-ip3-calcineurin-signaling cascade. *J Neurosci*, 20(24):8987–95, 2000.

[166] Ellen Heber-Katz. Oxygen, metabolism, and regeneration: Lessons from mice. *Trends in Molecular Medicine*, 23(11):1024–1036, 2017.

[167] G. L. Semenza and G. L. Wang. A nuclear factor induced by hypoxia via de novo protein synthesis binds to the human erythropoietin gene enhancer at a site required for transcriptional activation. *Mol Cell Biol*, 12(12):5447–54, 1992.

[168] Patrick H. Maxwell, Michael S. Wiesener, Gin-Wen Chang, Steven C. Clifford, Emma C. Vaux, Matthew E. Cockman, Charles C. Wykoff, Christopher W. Pugh, Eamonn R. Maher, and Peter J. Ratcliffe. The tumour suppressor protein vhl targets hypoxia-inducible factors for oxygen-dependent proteolysis. *Nature*, 399(6733):271–275, 1999.

[169] O. Iliopoulos, A. P. Levy, C. Jiang, W. G. Kaelin, and M. A. Goldberg. Negative regulation of hypoxia-inducible genes by the von hippel-lindau protein. *Proceedings of the National Academy of Sciences*, 93(20):10595–10599, 1996.

[170] Neyda V. Gilman. Analyses of the 2019 nobel prize in physiology or medicine: Molecular machinery for cellular oxygen level response. *Science Technology Libraries*, 39(1):1–27, 2020.

[171] V. H. Haase. The vhl tumor suppressor: master regulator of hif. *Curr Pharm Des*, 15(33):3895–903, 2009.

[172] Demet Tekin, Ali D. Dursun, and Lei Xi. Hypoxia inducible factor 1 (hif-1) and cardioprotection. *Acta Pharmacologica Sinica*, 31(9):1085–1094, 2010.

[173] Chris Jopling, Guillermo Suñé, Adèle Faucherre, Carme Fabregat, and Juan Carlos Izpisua Belmonte. Hypoxia induces myocardial regeneration in zebrafish. *Circulation*, 126(25):3017–3027, 2012.

[174] Y. Nakada, D. C. Canseco, S. Thet, S. Abdisalaam, A. Asaithamby, C. X. Santos, A. M. Shah, H. Zhang, J. E. Faber, M. T. Kinter, L. I. Szweda, C. Xing, Z. Hu, R. J. Deberardinis, G. Schiattarella, J. A. Hill, O. Oz, Z. Lu, C. C. Zhang, W. Kimura, and H. A. Sadek. Hypoxia induces heart regeneration in adult mice. *Nature*, 541(7636):222–227, 2017.

[175] K. Wang, R. Ding, Y. Ha, Y. Jia, X. Liao, S. Wang, R. Li, Z. Shen, H. Xiong, J. Guo, and W. Jie. Hypoxia-stressed cardiomyocytes promote early cardiac differentiation of cardiac stem cells through hif-1/jagged1/notch1 signaling. *Acta Pharm Sin B*, 8(5):795–804, 2018.

[176] A. P. Mutvei, S. K. Landor, R. Fox, E. B. Braune, Y. L. Tsoi, Y. P. Phoon, C. Sahlgren, J. Hartman, J. Bergh, S. Jin, and U. Lendahl. Notch signaling promotes a hif2-driven hypoxic response in multiple tumor cell types. *Oncogene*, 37(46):6083–6095, 2018.

[177] A. Hiyama, R. Skubutyte, D. Markova, D. G. Anderson, S. Yadla, D. Sakai, J. Mochida, T. J. Albert, I. M. Shapiro, and M. V. Risbud. Hypoxia activates the notch signaling pathway in cells of the intervertebral disc: implications in degenerative disc disease. *Arthritis Rheum*, 63(5):1355–64, 2011.

[178] Donal MacGrogan, Juliane Münch, and José Luis de la Pompa. Notch and interacting signalling pathways in cardiac development, disease, and regeneration. *Nature Reviews Cardiology*, 15(11):685–704, 2018.

[179] J. Münch, D. Grivas, Á González-Rajal, R. Torregrosa-Carrión, and J. L. de la Pompa. Notch signalling restricts inflammation and serpine1 expression in the dynamic endocardium of the regenerating zebrafish heart. *Development*, 144(8):1425–1440, 2017.

[180] Long Zhao, Asya L. Borikova, Raz Ben-Yair, Burcu Guner-Ataman, Calum A. MacRae, Richard T. Lee, C. Geoffrey Burns, and Caroline E. Burns. Notch signaling regulates cardiomyocyte proliferation during zebrafish heart regeneration. *Proceedings of the National Academy of Sciences*, 111(4):1403–1408, 2014.

[181] Arnar B. Ingason, Andrew B. Goldstone, Michael J. Paulsen, Akshara D. Thakore, Vi N. Truong, Bryan B. Edwards, Anahita Eskandari, Tanner Bollig, Amanda N. Steele, and Y. Joseph Woo. Angiogenesis precedes cardiomyocyte migration in regenerating mammalian hearts. *The Journal of Thoracic and Cardiovascular Surgery*, 155(3):1118–1127.e1, 2018.

[182] Rubén Marín-Juez, Michele Marass, Sebastien Gauvrit, Andrea Rossi, Shih-Lei Lai, Stefan C. Materna, Brian L. Black, and Didier Y. R. Stainier. Fast revascularization of the injured area is essential to support zebrafish heart regeneration. *Proceedings of the National Academy of Sciences*, 113(40):11237–11242, 2016.

[183] D. M. Castilla, Z. J. Liu, and O. C. Velazquez. Oxygen: Implications for wound healing. *Adv Wound Care (New Rochelle)*, 1(6):225–230, 2012.

[184] H. D. Guo, G. H. Cui, J. J. Yang, C. Wang, J. Zhu, L. S. Zhang, J. Jiang, and S. J. Shao. Sustained delivery of vegf from designer self-assembling peptides improves cardiac function after myocardial infarction. *Biochem Biophys Res Commun*, 424(1):105–11, 2012.

[185] Yu-Ching Wu, Chao-Yuan Chang, Alex Kao, Brian Hsi, Shwu-Huey Lee, Yau-Hung Chen, and I. Jong Wang. Hypoxia-induced retinal neovascularization in zebrafish embryos: A potential model of retinopathy of prematurity. *PLOS ONE*, 10(5):e0126750, 2015.

[186] J. Muñoz-Sánchez and M. E. Chánez-Cárdenas. The use of cobalt chloride as a chemical hypoxia model. *J Appl Toxicol*, 39(4):556–570, 2019.

[187] X. Yu and Y. V. Li. Zebrafish as an alternative model for hypoxic-ischemic brain damage. *Int J Physiol Pathophysiol Pharmacol*, 3(2):88–96, 2011.

[188] Ziquan Cao, Lasse D. Jensen, Pegah Rouhi, Kayoko Hosaka, Toste Länne, John F. Steffensen, Erik Wahlberg, and Yihai Cao. Hypoxia-induced retinopathy model in adult zebrafish. *Nature Protocols*, 5(12):1903–1910, 2010.

[189] J. M. González-Rosa, V. Martín, M. Peralta, M. Torres, and N. Mercader. Extensive scar formation and regression during heart regeneration after cryoinjury in zebrafish. *Development*, 138(9):1663–74, 2011.

[190] M. Braile, S. Marcella, L. Cristinziano, M. R. Galdiero, L. Modestino, A. L. Ferrara, G. Varricchi, G. Marone, and S. Loffredo. Vegf-a in cardiomyocytes and heart diseases. *Int J Mol Sci*, 21(15), 2020.

[191] L. Iommarini, A. M. Porcelli, G. Gasparre, and I. Kurelac. Non-canonical mechanisms regulating hypoxia-inducible factor 1 alpha in cancer. *Front Oncol*, 7:286, 2017.

[192] Yong Zhang, Iossif Strehin, Khamilia Bedelbaeva, Dmitri Gourevitch, Lise Clark, John Leferovich, Phillip B. Messersmith, and Ellen Heber-Katz. Drug-induced regeneration in adult mice. *Science Translational Medicine*, 7(290):290ra92–290ra92, 2015.

[193] B. Deodato, N. Arsic, L. Zentilin, M. Galeano, D. Santoro, V. Torre, D. Altavilla, D. Valdembri, F. Bussolino, F. Squadrito, and M. Giacca. Recombinant aav vector encoding human vegf165 enhances wound healing. *Gene Ther*, 9(12):777–85, 2002.

[194] J. Li, L. F. Brown, M. G. Hibberd, J. D. Grossman, J. P. Morgan, and M. Simons. Vegf, flk-1, and flt-1 expression in a rat myocardial infarction model of angiogenesis. *Am J Physiol*, 270(5 Pt 2):H1803–11, 1996.

[195] Markus Räsänen, Ibrahim Sultan, Jennifer Paech, Karthik Amudhala Hemanthakumar, Wei Yu, Liqun He, Juan Tang, Ying Sun, Ruslan Hlushchuk, Xiuzheng Huan, Emma Armstrong, Oleksiy-Zakhar Khoma, Eero Mervaala, Valentin Djonov, Christer Betsholtz, Bin Zhou, Riikka Kivelä, and Kari Alitalo. Vegf-b promotes endocardium-derived coronary vessel development and cardiac regeneration. *Circulation*, 143(1):65–77, 2021.

[196] Richard L. Benton and Scott R. Whittemore. Vegf165 therapy exacerbates secondary damage following spinal cord injury. *Neurochemical Research*, 28(11):1693–1703, 2003.

[197] Traci A. Wilgus, Ahalia M. Ferreira, Tatiana M. Oberyszyn, Valerie K. Bergdall, and Luisa A. DiPietro. Regulation of scar formation by vascular endothelial growth factor. *Laboratory Investigation*, 88(6):579–590, 2008.

[198] Sarah A. Figley, Yang Liu, Spyridon K. Karadimas, Kajana Satkunendrarajah, Peter Fettes, S. Kaye Spratt, Gary Lee, Dale Ando, Richard Surosky, Martin Giedlin, and Michael G. Fehlings. Delayed administration of a bio-engineered zinc-finger vegf-a gene therapy is neuroprotective and attenuates allodynia following traumatic spinal cord injury. *PLOS ONE*, 9(5):e96137, 2014.

[199] Beth Han, Wilson M. Compton, Christopher M. Jones, Emily B. Einstein, and Nora D. Volkow. Methamphetamine use, methamphetamine use disorder, and associated overdose deaths among us adults. *JAMA Psychiatry*, 78(12):1329–1342, 2021.